UNIVERSITY OF SOUTHAMPTON

FACULTY OF ENGINEERING AND THE ENVIRONMENT

School of Engineering Sciences

Multi Parameter Computational and Experimental Investigations into the Robustness of Cementless Total Hip Replacements

by

Hatice Ozturk

Thesis for the degree of Doctor of Philosophy

May 2011

UNIVERSITY OF SOUTHAMPTON

ABSTRACT

FACULTY OF ENGINEERING AND THE ENVIRONMENT
SCHOOL OF ENGINEERING SCIENCES

Doctor of Philosophy

MULTI PARAMETER COMPUTATIONAL AND EXPERIMENTAL INVESTIGATIONS INTO THE ROBUSTNESS OF CEMENTLESS TOTAL HIP REPLACEMENTS

by Hatice Ozturk

Traditional computational and experimental assessments of implant performance are deterministic; each computational (usually finite element (FE) based) simulation or experiment describes a single situation. While useful information can be gained from these analyses, when the number of variables involved increases, experimental simulations becoming increasingly time consuming and complex. In these cases, computational simulations are increasingly relied upon to predict implant performance. However, even when employing computational simulations to look at the effect of a large number of variables via sweep simulations for example, the problem can become computationally expensive and unfeasible in terms of time required.

In the present work, stochastic computational methods are employed to assess the effect of multiple variables on the performance of the cementless hip replacement. To verify the computational simulations, at each stage of the project, selected scenarios were tested experimentally. To assess implant performance, the following metrics were used: (i) implant micromotion and migration; excessive micromotion and migration are believed to be related to the most common cause of implant failure, implant loosening, and (ii) bone strain; excessive bone strain can result in bone fracture. An initial study on a neutrally positioned stem showed good correlation between the experimental results and the computational predictions.

Mesh morphing techniques were employed to allow implant position to change throughout the simulations and assess how this altered the output metrics; it was observed that micromotion and strains generated in the cortex were most sensitive to varus/valgus angle. To further reduce computational expense, a surrogate modelling technique was used to assess the effect of both loading and implant positioning, on micromotion. The surrogate model was verified by selected FE models, placing confidence in the model, and again highlighted that in addition to vertical load, the varus/valgus angle affected the micromotion of cementless implant.

Experimental investigations were carried out to corroborate the results obtained computationally. The novelty of the experimental tests was in the use of an optical system, called digital image correlation (DIC), to measure implant motions and bone strains. This technique enabled non-contact three dimensional measurements to be made. While some qualitative relationships were obtained with FE outputs, good quantitative corroboration between the strain gauge and DIC suggests that DIC is a promising technique for the evaluation of implant performance in vitro.

Contents

List of Figures

List of Tables

DECLARATION OF AUTHORSHIP

I, **Hatice Ozturk**, declare that the thesis entitled:

"Multi Parameter Computational and Experimental Investigations into the Robustness of Cementless Total Hip Replacements"

and the work presented in the thesis are both my own, and have been generated by me as the result of my own original research. I confirm that:

- this work was done wholly or mainly while in candidature for a research degree at this University;
- where any part of this thesis has previously been submitted for a degree or any other qualification at this University or any other institution, this has been clearly stated;
- where I have consulted the published work of others, this is always clearly attributed;
- where I have quoted from the work of others, the source is always given. With the exception of such quotations, this thesis is entirely my own work;
- I have acknowledged all main sources of help;
- where the thesis is based on work done by myself jointly with others, I have made clear exactly what was done by others and what I have contributed myself;
- parts of this work have been published (listed in Appendix A).

Signed: .....

Date: .....

Acknowledgements

It is tradition to start the thesis with an acknowledgement section and I am quite happy to have this opportunity to thank the many people for their direct or indirect contributions to this PhD thesis.

My thanks go first to my main supervisor, Dr. Martin Browne, for being one of the best supervisors. I would like to thank you for your supervision, advice and support during this postgraduate degree. *Thanks Boss!* Along those lines, I would like to thank Dr. Prasanth Nair for his great supervision and support. *Thanks a lot!* I am also thankful to Dr. Mamadou Bah, who was also involved in the EPSRC project, for his advice and help with the computational work.

During the PhD project, I have been very fortunate to have had the opportunity to work with orthopaedic surgeons as it allowed me to understand the needs and difficulties faced during surgery. I would therefore like to thank Mr. Doug Dunlop for his valuable discussion on the total hip replacement and Mr. Andrew Jones for his help implanting the composite bones. I also extend my sincere thanks to Prof. Samuel Evans, for giving me the opportunity to use the equipment of his laboratory and for his help during the first experimental tests.

I would also like to acknowledge EPSRC for funding this project (Grant EP/E057705/1), Joint Replacement Instrumentation Ltd and Simpleware Ltd for their support. Special thanks go to Prof. Philippe Young for giving me access to Simpleware software.

While I was looking for a postgraduate project, Dr. Georges Limbert advised me to apply for a position at the University of Southampton, and I would like to thank him for that! Many thanks also to Dr. Nadia Butterlin, head of the Biomedical Engineering school (ISIFC) where I did my studies, and Prof. Jean-Marie Crolet for their support during the PhD degree.

I am also very grateful to all the researchers at the Bioengineering Research Group of the University of Southampton. I would specially like to thank my fantastic postgraduate colleagues for providing a fun environment to learn, and for making the work place one of the best... thanks to all the people I shared the office with: Pramod, Hamid, Pete, Meadhbh, Carolina, Catherine, Alex, Becky, Mike, Mav, Margaret, Francis, Orestis Sr., Faye, Lorenzo, Dario, Jonathan, Federico, Orestis Jr. and Gwen. More than officemates, we also had a great friendship, and I hope all of you succeed in your careers and personal life! I have already thanked you, but thanks again to Dr. Pramod Puthumanapully for proofreading my thesis and the time you spent on it!

Life in Southampton would simply not have been the same without the invaluable friendship: thanks to Aida, Gavin, Asa, Cesar, Luis, Rich, Maria, John, Diana, Tina, Kevin, Mari, Satveer and Amanda. Thanks also to Kedja and Rhamona for all their encouragement during these three years!

Last but certainly not the least, I would like to express my thanks to my family. To be honest, no words can really express my gratitude towards them. First thanks to my parents, *Annecim ve Babacim*, for their endless encouragement, support and patience during the past few years... And thanks to my sisters, Umran and Nuran, and my brothers, Erkan and Unal, for always being there, and for helping me, especially during the difficult times...

Glossary

Arthritis	Inflammation of a joint, usually accompanied by pain, swelling, and stiffness resulting from infection, trauma, degenerative changes, metabolic disturbances, or other causes.
Aseptic loosening	Loosening of prosthesis in absence of osteolysis and infection, with the proviso that bacteria may be present.
Avascular	Not associated with or supplied by blood vessels.
Body mass index	A person's weight in kilograms divided by their height in meters squared.
Bone cement	Usually an acrylic compound used in fracture repair and positioning of bone pins.
Bone remodelling	Life-long process where mature bone tissue is removed from the skeleton and new bone tissue is formed.
Cartilage	Firm, rubbery tissue that cushions bones at joints.
Cortex	Outer portion of an organ.
Cortical	Having to do with the cortex.
Finite Element Analysis or Method	Numerical technique for finding approximate solutions of partial differential equations (PDE) as well as of integral equations.
Gaussian distribution	Theoretical distribution (bell-shaped) with finite mean and variance.
Interference fit	Fastening between two parts which is achieved by friction after the parts are pushed together. Interference fit is aslo known as press fit.

Main Effect	Effect of the change in level of one factor in a factorial experiment measured independently of other variables.
Mean	Mathematical average for a group of data points.
Micromotion	Amplitude of the cyclic relative implant-bone displacement for a load cycle.
Migration	Permanent displacement of the implant with respect to the bone relative to the initial unloaded situation.
Monte Carlo Method	Any numerical method that employs statistical sampling to solve problems.
Osseointegration	Growth action of bone tissue, as it assimilates surgically implanted devices or prostheses to be used as either replacement parts or anchors.
Press fit	Cf. Interference fit.
Standard Deviation (SD)	Measure of the dispersion of a group of values around a mean, expressed in the units being measured.
Stereolithography (*.stl)	File format native to the stereolithography CAD software created by 3D Systems.
Stress shielding	Osteopenia (reduction in bone density) occurring in bone as the result of removal of normal stress from the bone by an implant
Synovial	A clear, viscid lubricating fluid secreted by membranes in joint cavities, sheaths of tendons, and bursae.
Valgus	Proximal stem positioned laterally.
Varus	Proximal stem positioned medially.

Nomenclature/List of Symbols

Nomenclature

Ant/Post	Anterior/Posterior
Ant/Ret	Anteversion/Retroversion
CAD	Computer Aided Design
CFD	Computational fluid dynamics
CT	Computerised or Computed Tomography
CTHR	Cementless Total Hip Replacement
DIC	Digital Image Correlation
E	Young's Modulus
FE	Finite element
FEA	Finite element Analysis
FEM	Finite element Method
GS	Grayscale
HU	Hounsfield Unit
LHS	Latin Hypercube Sampling
LVDT	Linear Variable Differential Transducer
MRI	Magnetic Resonance Imaging
SCVR	Standardized Cross Validation Residual
SD	Standard Deviation
STL	Stereolithography
THR	Total Hip Replacement
Var/Val	Varus/Valgus

List of Symbols:

α	Anteversion/retroversion angle
β	Varus/valgus angle
γ	Anterior/posterior angle
ρ	Density

Chapter 1

Introduction

1.1 Background

"Walking is man's best medicine" said Hippocrates, the father of medicine. Lee and Buchner [87] reviewed the benefits of walking on health in a paper and they explained its role in controlling and reducing chronic disease, such as diabetes. However, as a daily activity, walking can become very painful, especially for people suffering from joint pain. Millions of people suffer from joint diseases, i.e. from infections, degenerative disorders or injuries such as sprains (injuries to a ligament) or strains (injuries to a muscle or a tendon). However, the most common joint disease is osteoarthritis affecting more than 80 percent of those over 70 [9].

As the life span of the world population is increasing [7], see Table 1.1, there is a need to maintain quality of life and an active life style for elderly people. Table 1.1 shows that in 1950, 8.1% of the world's population were over the age of 60 and 0.6% was over the age of 80. However, in 2000, 9.9% were over 60 and 1.1% was over the age of 80. Statistics such as these highlight the importance of medical interventions that reduce the burden of suffering from joint diseases.

Although elderly people are more likely to suffer from degenerative joint disease, young people may also have problems in their joints. While osteoarthritis is often associated with advancing age, rheumatoid arthritis can occur in young adults. Treatment for aching joints have included rest, physical therapy sessions or anti-inflammatory medication. When pain is no longer relieved by medication, the most common treatment is joint replacement.

In hip replacement operations, there are two main types of implants: total hip replacement and hip resurfacing.

Table 1.1: Percentage of total population age 60 and 80, in 1950-2050, in 7 countries and within the world. Source: United Nations, *World Population Prospects: The 2008 Revision*

	Percentage age 60 and older			Percentage age 80 and older		
	1950	2000	2050	1950	2000	2050
Australia	12.5	16.7	29.5	1.1	3.1	9.0
Canada	11.3	16.7	31.9	1.1	3.0	9.7
France	16.2	20.7	32.6	1.6	3.8	11.3
Germany	14.6	23.2	39.5	1.0	3.5	14.1
Japan	7.7	23.3	44.2	0.4	3.8	15.6
United Kingdom	15.5	20.8	28.8	1.5	4.1	8.6
United States of America	12.5	16.2	27.4	1.1	3.3	7.8
World	**8.1**	**9.9**	**21.9**	**0.6**	**1.1**	**4.3**

To replicate a healthy hip joint, a total hip replacement implant has three parts: a stem, which fits into the femur, a ball, which replaces the spherical head of the femur and a cup, which replaces the worn out hip socket (Figure 1.1).

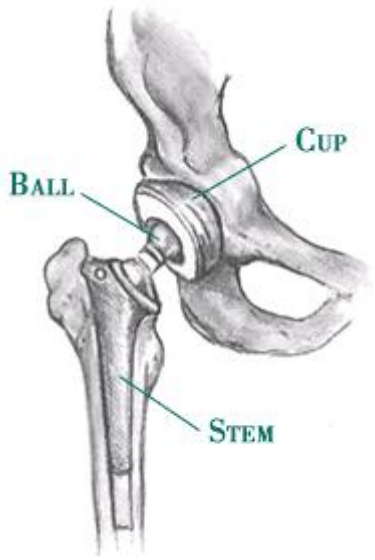

Figure 1.1: A total hip replacement[1]

To achieve good joint function, a total hip replacement must be fixed securely. This can be achieved by employing either a cemented or a cementless (uncemented) prosthesis. Cemented total hip replacement uses polymethylmethacrylate (PMMA) commonly known as bone cement as a grout, holding the implant in place almost immediately. Cementless designs can have a roughened, porous or coated surface, establishing fixation by rough frictional/mechanical interlock and bone ingrowth.

[1] http://www.toc-stl.com/info/totalhip.htm

In some cases, only one of the two components, i.e. the cup or femoral component, is cemented and the other is cementless; this is called a hybrid total hip replacement.

Many surgeons justify the choice of a cemented or cementless implant based on the patient's age and therefore quality of bone. In fact, cementless implants are used when good mechanical interlock and osseintegration are expected, which is more likely to happen with young patients with good quality bone; whereas cemented implants are most often used to treat older patients. The 7^{th} annual report of the national joint registry for England and Wales shows that in 2009 the mean age for cemented, cementless and hybrid THR respectively are 73, 66 and 70 years old [5], which points out again that cementless THR are used for younger patient compared to cemented THR. However, it has been noticed that the type of fixation used depends also on its popularity within the country. In Canada, in 2006-2007, cementless hip replacements were mostly used (71%) followed by hybrid (26%) and cemented implants (3%) but the patient's age were not specified [3].

Table 1.2 shows that, in Sweden, in 1992-2008, cemented hip implants were mostly used compared to the other type of implants. However, it should be noticed that cemented implants were used in more than 90 % of patients over 60 years old whereas cementless implants were used mainly to treat younger patients.

Table 1.2: The type of implants used for hip operations in 1992-2004. Source: The Swedish National Hip Arthroplasty Register - Annual Report 2008 [2]

	Cemented implants	Uncemented implants	Hybrid implants
Younger than 50 years	35.8%	31.8%	14.5%
Between 50-59 years	60.1%	17.4%	11.6%
Between 60-75 years	91.5%	3.0%	2.9%
Older than 75 years	98.0%	0.3%	0.7%

An alternative hip operation for young patients is hip resurfacing, which consists of relining the hip joint and replacing the diseased or damaged surfaces of the hip joint. The 7^{th} annual report of the national joint registry for England and Wales reported a mean age for hip resurfacing of 54 years old [5]. The hip-resurfacing implant consists mostly of a metal ball and a metal socket. The acetabular component used during the procedure is the same as for a total hip replacement. The advantages of this type of procedure are bone conservation, since the head and neck of the femur are preserved, and a low wear bearing due to a metal-on-metal bearing [16]. Moreover, the diameter of the head is larger than a conventional THR, hence the risk of dislocation is reduced [16]. Hip resurfacing is a procedure more suitable for young (below 55 years old) and active patients [47] because it requires high bone quality and an intact femoral neck.

1.2 Objectives and Scope

There are many different implants available in the market that differ in their sizes, geometries and materials. Surgeons can base their choice of implant on various factors such as the bone quality (from computerised or computed tomography (CT) scans or X-rays) and the activity level of the patient. However, these variables are subject to uncertainty. While a very experienced surgeon can select the most appropriate implant with some degree of confidence, there is no standard method for selecting the most appropriate implant for a particular patient which can account for these sources of uncertainty in a rapid, efficient manner. A further critical issue in the performance of the implant is how well positioned the implant is within the bone canal, since a malpositioned implant can lead to early failure. The combined effect of variability of the aforementioned factors (for example, a malpositioned implant subject to high activity levels in poor quality bone) is difficult to predict, and computational models are often needed to ascertain prospective behaviour.

The finite element method (FEM) is very popular in the biomechanical field to assess the behaviour of a structure under certain circumstances and predict strain and stress distributions throughout a structure. This has many advantages in studying joint replacement, such as testing different scenarios and predicting the implant performance before a clinical test. In FEM, geometry and material properties are defined allowing direct comparison between different situations, which can not be achieved in experimental or clinical testing; where the test specimens and environment can not be completely controlled [33]. However, it is evident that many parameters can influence the structural integrity (and thus the performance) of a total hip replacement construct and each of these parameters is subject to uncertainty. The FEM offers several advantages but if used alone to study different parameters, it will be very time consuming. The purpose of this project was to develop computational tools that would be able to discern how well a particular implant would perform for a specific patient in the presence of such uncertainty and in a rapid manner.

In this project, cementless total hip replacements were considered. In 2009, 39% of THR in England and Wales were cementless. In total, over 25,439 cementless stems have been implanted in England and Wales [5]. This trend is also seen in other countries with Canada and Australia recording 71% and 62.7% of cementless THR in 2009 [3, 8].

Predicting the robustness of an implant is potentially useful for surgeons, researchers and prostheses manufacturers as it could aid the choice of design and implant position in preoperative planning and allow virtual testing of implants to predict how well they will perform. The project consisted of developing a computational model of an

implanted synthetic femur (item 3406, Sawbones Europe AB, Sweden) and virtually testing the performance of a cementless femoral component (Furlong stem, model: 12mm diameter, JRI Instrumentation Ltd, London, UK) to investigate the effect of surgical technique variation. The computational study used finite element analysis and probabilistic methods to assess the implant stability. Experimental studies were then carried out on selected implant orientations to corroborate the computational model. To this end, a digital image correlation technique (DIC) was used for bone strain and implant motion measurements. Currently, this technique is very popular and is increasingly being used in the biomedical field. However, it has to be noted that this is one of the first systematic studies investigating the application of DIC to experimentally measure bone strain and implant motion.

1.3 Layout of the Thesis

This thesis is organized as fellows:

Chapter 2 presents background on total hip replacements. This chapter is divided into three sections: total hip replacements, computational investigations and experimental studies of the replaced hip.

Chapter 3 describes the materials used and the methodology employed for the computational study. It explains the steps used to generate a specific finite element model when the implant is in a neutral position and also its experimental validation.

Chapter 4 describes a method to assess the effect of implant positions on the stem micromotion and bone strain, at reduced computational cost. The outputs of the computational model was then used to design an experimental protocol: selected stem positions were defined and implanted by an orthopaedic surgeon for direct comparison with the predicted values.

Chapter 5 focuses on the use of the digital image correlation technique for biomechanical measurements. It describes in detail how to use the system and validate the measurements by using strain gauges. It also explains how to measure and compute the implant micromotion using an optical system and a custom made code.

Chapter 6 presents a surrogate modelling study assessing the effect of different loading scenarios and implant positions on the structural integrity of the total hip replacement. To this end, the computational model created and validated in chapter 3 was employed to asses the uncertainty of both the implant orientation and load.

Chapter 7 contains the discussion and conclusion of this project and outlines how this present work can be used in the future and what are the applications.

Chapter 2

Literature Review

2.1 The hip joint

This section focuses on the hip joint and contains a brief description of bones and their physical properties.

The human body is made up of more than 200 bones [24], which are classified into three main groups:

- long bones, such as the femur and tibia, are long in one direction
- short bones, such as the bones of the ankle, are bones that have approximately the same dimensions in all directions
- flat bones, such as the pelvis, are much smaller in one direction than the others

Bones are composed of hard living tissue that act as a scaffold, providing structural support to the body. They usually consist of a hard matrix of calcium salts deposited around protein fibres. The minerals make bone rigid with the proteins (collagen) providing strength and elasticity.

Bone consists of three main types of cells, with specific functions. They are the osteoblasts, osteocytes and osteoclasts [56] . Osteoblasts are the cells responsible for the formation and mineralization of the bone matrix (osteoid). Osteocytes, which are osteoblasts trapped in the bone matrix, maintain the structural and metabolic integrity of fully formed bone. Osteoclasts are responsible for the removal of bone.

Bone mass is maintained by a balance between the activity of osteoblasts which build or replace bone tissue, and osteoclasts which destroy or resorb bone. Until into the twenties, the skeleton grows and builds bone, so osteoblasts build more than osteoclasts resorb. However, after about age thirty-five, osteoclastic activity is more prominent,

with more bone removed than replaced, resulting in a gradual decrease in bone mass with age. The principle of bone remodelling in response to external mechanical forces is formulated as Wolff's law. In other words, bone mass and architecture changes with stresses acting on it [93].

Bone can either be compact or spongy, see Figure 2.1. Compact bone, also known as cortical or cortex bone is dense and forms the outer layer of bone. Eighty percent of skeletal bone mass is cortical bone. Spongy bone, also known as cancellous or trabecular bone, is an inner spongy structure, which accounts for the remaining twenty percent of bone mass. In long bones, it is located at the extremity of the bone.

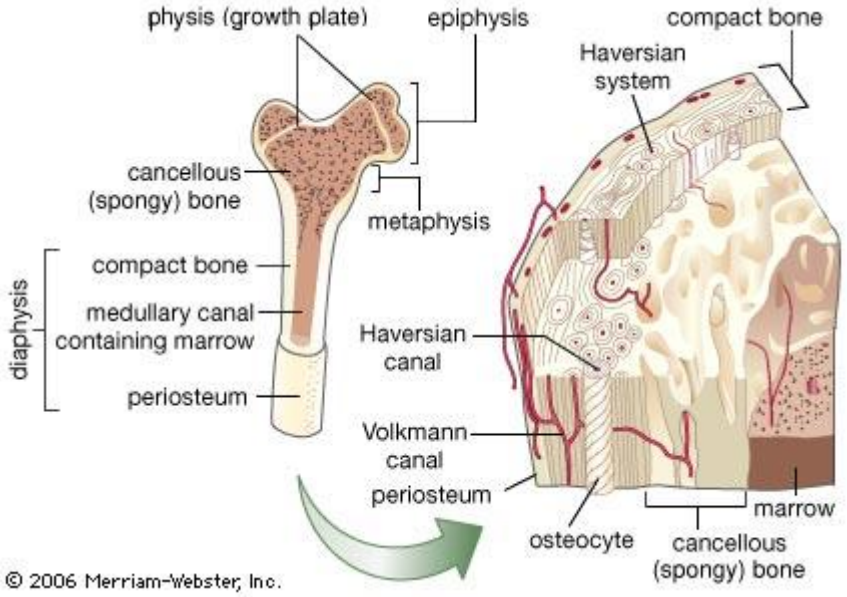

Figure 2.1: Human bone structure[1]

Bone tissue is non homogeneous and anisotropic. In other words, the mechanical properties are not the same in all directions and depend on the direction of loading [24]. Cancellous bone tissue has a lower Young' s Modulus and fatigue resistance than cortical bone [40].

The mechanical properties of bone vary as a function of location in the body [92, 120], disease [89], age [50] and sex [25] of the patient. These will be discussed later in the thesis (see section 2.3.2.3).

2.1.1 Anatomy of the hip joint

The hip joint is formed by the head of the femur and the acetabulum, as shown in Figure 2.2. It is classified as a ball and socket joint [24]. This arrangement gives the

[1] http://www.britannica.com/EBchecked/topic/72869/bone

hip a large amount of motion needed for daily activities such as walking, squatting and stair-climbing.

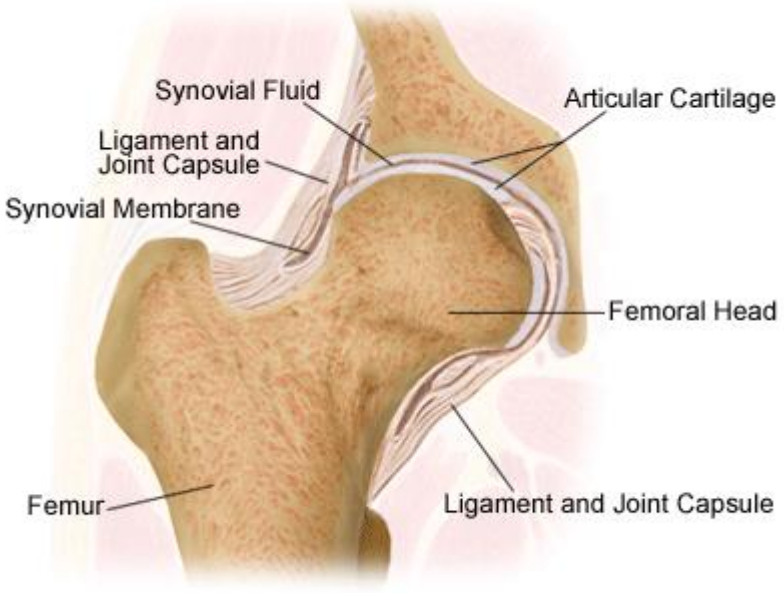

Figure 2.2: Healthy hip joint[2]

The main components of the hip joint are:

- the acetabulum
- the femoral head
- the cartilage covering the acetabulum and femoral head
- the joint capsule: flexible sack around the joint keeping the lubricating synovial fluid in place

The hip joint is a synovial joint, i.e. it is coated with articular cartilage which is a fibrous connective tissue and lubricated by synovial fluid, a viscous liquid. The lubricating properties of the synovial fluid is provided by hyaluronic acid, also known as hyaluronate [108]. Synovial fluid acts as a shock absorber, cushioning joints, and allows bones to move against each other. It also provides nutrients to the cartilage and helps remove waste from it as the cartilage is avascular [109].

During movement, the synovial fluid held in the cartilage is squeezed out into the joint cavity, separating the two cartilage surfaces. It is suggested that it is pressed out only in periphery and not at centre of pressure [161]. During the gait cycle, the contact area may vary with either injury or joint misalignment or disease. It increases with congruency of the mating surfaces and external loading and decreases with material

[2]http://www.reshealth.org

stiffness. In the hip joint, the acetabulum radius is greater than the femoral head radius which makes the contact area small around the periphery under low loads; when increased weight is borne by the hip joint, the contact area rapidly increases [13]. When the contact area increases, the stress remains approximately constant, which protects the cartilage.

The skeletal anatomy is different among populations and these variations are related to ethnicity, gender and age [117, 143]. For example considering the hip joint, the angles characterizing the hip joint, i.e. angles of inclination and anteversion, are not the same within the population.

The angle of inclination is the angle of the femoral neck in the frontal plane. The normal value of inclination angle for an adult is around 130° with respect to the femoral shaft. When this angle is bigger it is called coxa valga and when it is smaller it is called coxa vara, as shown in the Figure 2.3.

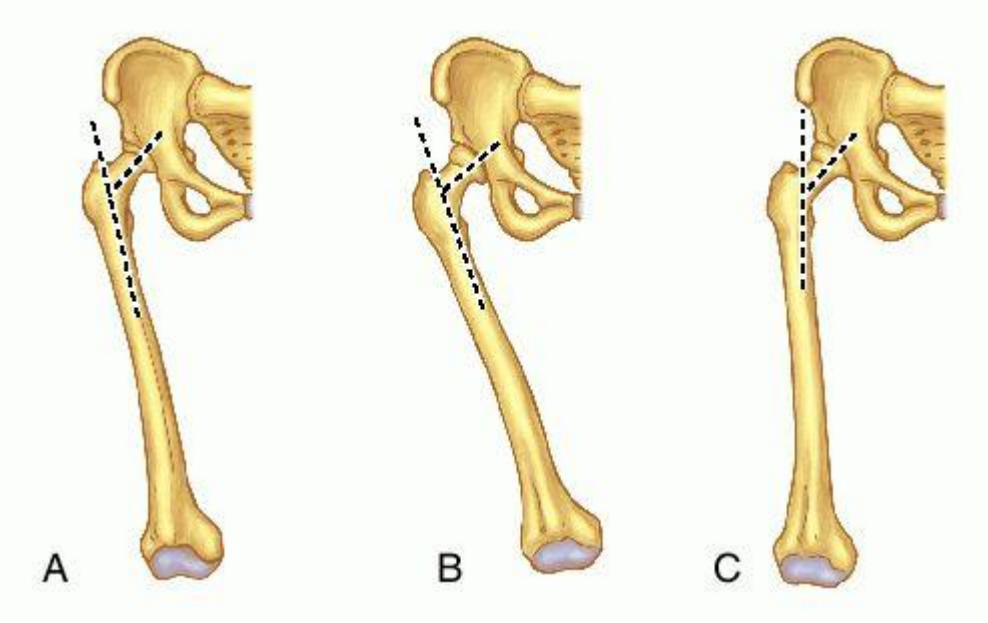

Figure 2.3: Angle of inclination: (A) normal femoral neck shaft angle; (B) coxa vara; (C) coxa valga[3]

The angle of anteversion is the angle of the longitudinal axis of the femoral neck to the line connecting the posterior aspect of both femoral condyles in the transverse plane. It is around 15° for a normal adult, see Figure 2.4. When this angle is bigger the femoral neck is anteverted and when it is smaller the femoral neck is retroverted.

The anatomy of the hip affects the rotation of the entire leg, in fact the toes turn in when femoral anteversion is too high and they turn out when femoral anteversion is too little.

[3]http://medical-dictionary.thefreedictionary.com

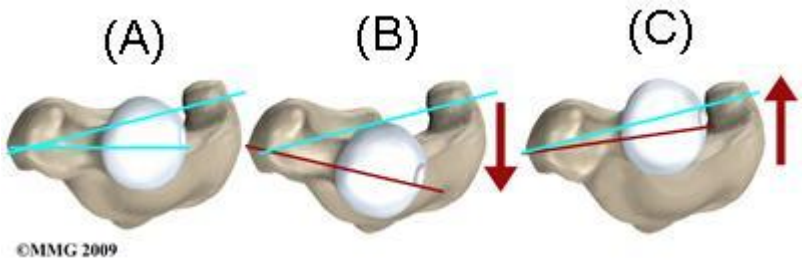

Figure 2.4: Femoral version: (A) Normal; (B) Anterversion; (C) Retroversion[4]

2.1.2 Kinematics of the hip

The hip is surrounded by strong ligaments and muscles. It allows three rotational degrees of freedom [112], as shown in the Figure 2.5: flexion-extension around a transverse axis, abduction-adduction around an anteroposterior axis and internal-external rotation around a vertical axis. In a standing position, hip movements can be described as followed:

- flexion: forward movement of the leg.
- extension: backward movement of the leg.
- abduction: movement of the leg straight out to the side.
- adduction: movement of the leg towards to other leg.
- internal rotation: foot rotation towards the other (toes pointing towards each other).
- external rotation: foot rotation away from the other (toes pointing outwards).

Circumduction, i.e. a circular movement which combines flexion, extension, abduction, and adduction, is also allowed.

The motion of the hip is limited and varies from one person to another. To get an idea to the range of motion, values are listed below [61]:

- 0 to 120 ° in flexion,
- 0 to 30 ° in extension,
- 0 to 45 ° in abduction,
- 0 to 25 ° adduction,
- 0 to 40 ° in internal rotation,
- 0 to 45 ° in external rotation.

[4] http://www.eorthopod.com

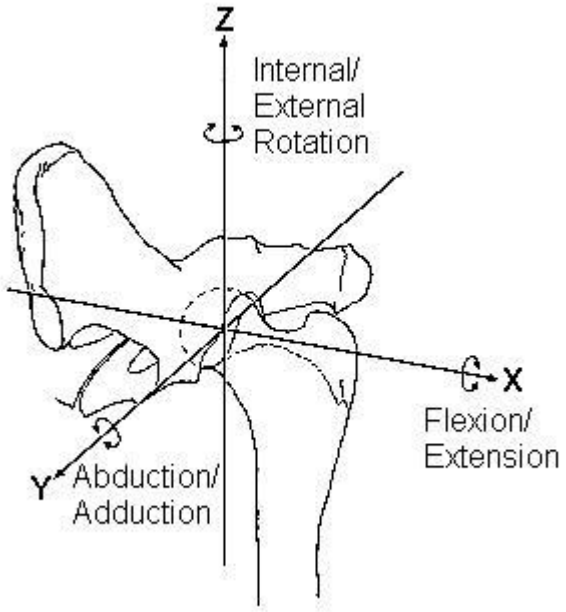

Figure 2.5: Diagram illustrating the three movements of the hip joint[5]

2.1.3 Hip joint degeneration

A degeneration of the hip joint can lead to a reduction in the range-of-motion of the joint. The reduced motion may be due to diseases or injuries of the joint and the treatment of hip degeneration focuses on relieving or reducing pain, preventing further degeneration and also maintaining or improving joint mobility. The degenerated hip can be cured in early stages by weight control, lifestyle changes, physical therapy, pain medications and as a last resort it can be treated by replacing the joint. The two main causes known for a hip operation are arthritis and osteonecrosis [5].

The term arthritis literally means inflammation of a joint, but is generally used to describe any condition in which there is damage to the cartilage. Figure 2.6 shows a normal hip joint compared to an arthritic hip joint.

The two main forms of arthritis are osteoarthritis and rheumatoid arthritis.

Osteoarthritis is the primary cause for painful hips. In 2009, it was the largest indication for surgery in England and Wales. Indeed, 93 % of patients for primary hip replacement suffered from osteoarthritis [5]. Osteoarthritis causes degeneration or wearing down of the articular cartilage which leads to a progressive erosion of the joint surface. Age is the strongest indicator of osteoarthritis but heredity, injury and obesity may also cause osteoarthritis.

Rheumatoid arthritis also causes degeneration of the joint, resulting in pain and disability of the joint. It is a disorder in which, for some unknown reason, the body's own

[5]http://www.pennhip.org

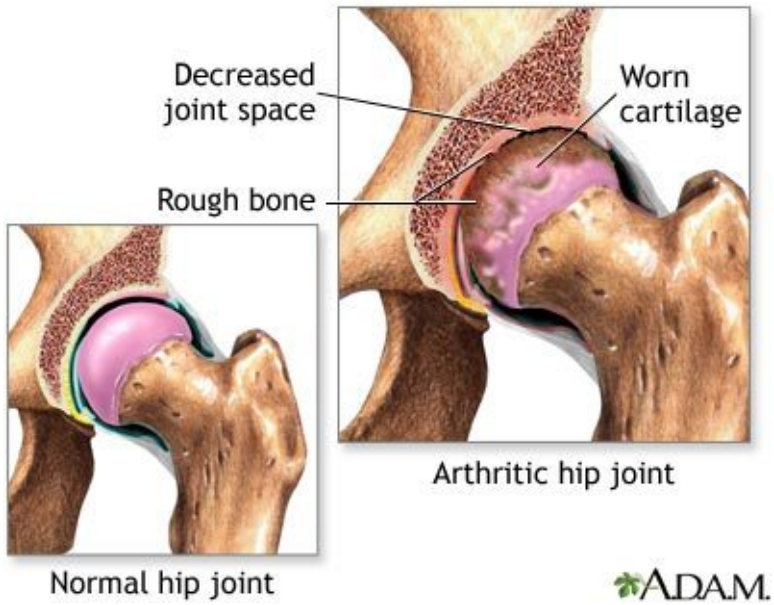

Figure 2.6: Arthritis in a hip - from left to right: normal and arthritic hip joint [6]

immune system starts to attack body tissues [149]. It occurs mostly in the younger patient aged twenty and above.

As stated previously, osteonecrosis, also known as avascular necrosis is another cause of hip joint degeneration. Literally, osteonecrosis means death of bone. As a living tissue, bone requires a certain amount of blood in order to function properly. In osteonecrosis, the femoral head looses a portion of its blood supply, dies and eventually collapses. It most commonly affects the ends of the femur and may occur after femoral neck fractures, dislocations of the hip, alcoholism and long term cortisosteroid treatment [90]. In 2009, in England and Wales, 2 % of patients for primary hip replacement suffered from avascular necrosis [1].

Other causes for hip pain are dislocation and fracture around the joint, which may both be a contributing factor in joint degeneration [36]. Dislocation is a joint injury that forces the end of a bone out of position. It is often associated with trauma, for example a fall. When a dislocation occurs, the joint is often immobile, swollen, very painful and visibly out of place.

2.2 Total hip replacements

This section presents an overview of total hip replacements. Various complications that arise during total hip replacements are also discussed.

[6] A.D.A.M. Images (A.D.A.M. Inc., Atlanta, Georgia)

2.2.1 Primary total hip operations

The aim of a hip replacement is to replicate the healthy hip joint and restore movement by replacing the diseased or damaged parts of the hip joint, see Figure 2.7.

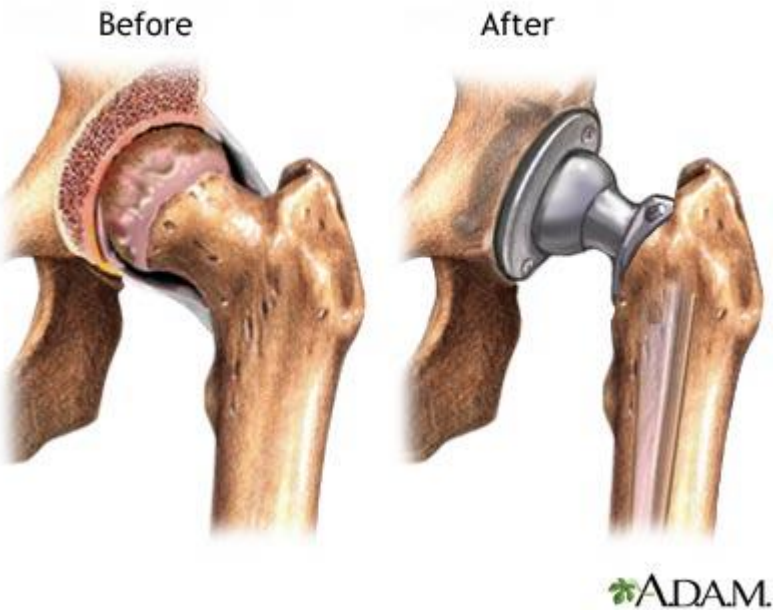

Figure 2.7: Hip replacement - from left to right: before and after surgery [7]

The prosthesis used has to be biocompatible, i.e. accepted by the body; and also resistant to corrosion, degradation and wear. The main stages of a total hip replacement operation are explained below.

The surgeon starts the operation by entering the hip joint. Note that, there are different surgical approaches, i.e. different surgical incisions used in hip surgery [70]. The choice is usually based on the surgeon's training and preference.

After making the incision, the ligaments and muscles are separated, and the surgeon can access the bones of the hip joint. Typically, hip operations are done in several stages, as follows:

- the femoral head is dislocated from the acetabulum and removed
- the cartilage is removed from the acetabulum and the hip socket is drilled so that it is a bit deeper to accommodate the implant
- the right size and shape of acetabular component is selected and inserted. This could be a cemented or uncemented component. In a cemented component, cement is used for the fixation whereas in a cementless component, screws through

[7] A.D.A.M. Images (A.D.A.M. Inc., Atlanta, Georgia)

the cup, spikes, pegs, or fins around the rim may be used to help hold the implant in place until the new bone forms.

- the femoral canal is prepared using rasps to shape and hollow out the femur to the shape of the stem. The correct size and shape is chosen and the surgeon will test the movement of the hip
- the ball is attached to the femoral head

An operation generally takes between one and two hours. The operation is hoped to relieve pain, restore the mobility of the joint, restore the leg length and give satisfying long-term results. The implant stability depends on the bone quality, implant geometry, alignment and level of activity of the patient.

2.2.2 Cementless total hip replacement

The principle of a cementless joint replacement is based on the bone growth into or onto the implant surface. Press fit or interference fit cementless implants allow the stem and the prosthetic cup to be anchored to the bone. Some cementless stems incorporate a structure on the surface such as a porous coating or a fibre mesh. Through biologic fixation, bone can grow into and through the pores of the coating, thereby securing it firmly in place. Cementless implants can also have an additional surface coating surface applied that encourages new bone growth. This is carried out by spraying the femoral stem with a biologically attractive surface layer. This layer is usually applied by plasma spraying, and can be made of materials such as titanium-alloy [115] or hydroxyapatite [55, 81, 99]. Hydroxyapatite is a calcium phosphate ceramic that is used as a biomaterial to improve implants' fixation within the bone.

In the 1970s, many researchers carried out experimental studies on bone ingrowth into porous surfaces such as titanium porous-coatings [60]. Galante et al. [60] carried out tests on rabbits and dogs. After implanting a titanium fibre composite into the trochanteric and supracondylar region of the femora of each animal, the rabbits and dogs were sacrificed at different stages after the operation to assess the bone growth into the samples. It was found that bone formation started within ten days, bone ingrowth within two weeks and penetration into the implant in three weeks. It has been suggested a minimum pore size of 50-300 μm is optimal for the growth of bone into the implant surface [39].

Bone preparation is very important in a cementless hip replacement. Gaps between the implant and the bone should be reduced to allow new bone growth. The diameter of a cementless stem is generally larger than that of a cemented stem for the same bone in order to better fill the femoral canal. Because they depend on new bone growth

for stability, cementless implants require a longer healing time than cemented designs. Implant fixation into the bone needs six to twelve weeks. During this period, the patient can protect his joint by employing walking aids, such as a walking stick or crutches. Andersson et al. [17] and Taunt et al. [144] studied immediate weight bearing after cementless total hip replacement. Andersson et al. [17] studied two groups of patients; one was allowed early weight bearing and the other late weight bearing. They showed that there was no difference in functional recovery after 24 weeks between these two groups.

Stem geometry design should avoid edges and sharp changes, as they generate stress concentrations. Moreover, if the implant is stiffer than bone, stress shielding is the direct consequence. If the material is too elastic, high interfacial motions discourage bone ingrowth.

Cementless THR is most often recommended for younger, more active patients and patients with good bone quality [155]. In young patients, the long term use of cement could produce problems, often associated with structural integrity and damage.

2.2.3 Advantages and disavantages of cementless total hip replacement

Implantation has traditionally been carried out in the past using bone cement but complications for young patients have been reported and therefore cementless implants became a promising alternative.

In fact, cemented implant can be problematic even in the preparatory stages, where the presence of air bubbles during mixing, and during the insertion of the cement into the femoral canal [59], can lead to weakening or failure [106]. Other problems associated with the use of a cemented implant is that its position may vary while the bone cement is setting and the bone cement layer can be subjected to shrinkage cracks during cure, which can lead to disintegration years after the operation [121]. Moreover, other risks such as a fall in blood pressure [147] and even heart failures [51] can occur and revisions of the cemented hip replacement are mostly due to infections [69].

Despite the fact that cementless implants avoid these issues, they may also present complications. In fact, there is a risk of fracture of the femur during the operation [72] that can occur when the implant is inserted into the femur [69]. Other complications such as dislocation of the implant [72] and failure of bone ingrowth [123] have also been reported. Another risk associated with a cementless device is that metallic balls or fibres can also be separated from the porous coated surface of the implant and this debris may cause osteolysis [14].

However, in comparison with cemented implants, cementless replacements tend to be more expensive [69] but are easier to revise [123].

2.2.4 Complications following total hip replacement

The hip operation is one of the most successful orthopaedic operations, however failure can occur. Reasons of failure are diverse and can be linked to the biology of the hip, the type of implant used and the accuracy of the surgery achieved. This section summarises the complications that can occur post operatively.

2.2.4.1 Complications due to hip degeneration

Patients diagnosed with knee osteoarthritis are usually obese patients [65] whereas hip osteoarthritis is usually associated with elderly patients [145] and the effect of obesity on osteoarthritis of the hip is unclear. Some papers suggested that bilateral hip osteoathritis may be associated with obesity [145] and some papers have rejected the fact that overweight patients will suffer from osteoathritis [64]. However, excessive loads are applied post-operation on their artificial implant, which may increase the risk of implant loosening.

The marrow cavity of the femoral component of patients suffering from rheumatoid arthritis is larger [137], which makes the bone softer and increases the risk for fracture [73]. The risk of fracture of the femur increases also during a corticosteroid treatment [150]. Hip operations of patients suffering from rheumatoid arthritis may also lead to a malpositioning of the implant [122] due to the size of the cavity.

Complications after a total hip replacement can also arise for people with developmental hip dysplasias, such as fracture of the femoral component during the operation, dislocation or aseptic loosening of the cup [114].

Total hip replacements for congenital hip dislocation are very difficult. Patients are at risk of sciatic nerve damage after the operation and the operation may also lead to dislocation and the cup may loosen [75].

Patients suffering from blood disorders such as hemophilia may risk postoperative implant infection or loosening [79, 91]. These complications mostly occurred with seropositive patients for the human immunodeficiency virus [79, 91]

2.2.4.2 Aseptic loosening

Aseptic loosening is the most common complication following surgery, and is generally accepted as being loosening in the absence of infection; however, it has been suggested that this may not always be the case. For example, Gristina and Costerton [63] have hypothesized that in some instances, bacteria persist in biofilms on implant surfaces. In the present work, the term aseptic loosening is considered in its original concept, i.e. as occurring without clinical signs of infection, with the proviso that bacteria may be present. In 2009, 56% of hip revision in England and Wales were due to aseptic loosening [5]. The causes of an aseptic loosening may be biological or mechanical. The main biological cause is osteolysis due to the degeneration of wear debris that contribute to an inflammatory reaction, which promotes bone resorption [130]. Osteolysis is a process in which the bone around the prosthesis is reabsorbed by the body, which can cause the joint to become weakened and unstable.

One of the main mechanical causes of aseptic loosening is stress shielding of the bone [26], which can be explained by the fact that when the bone is implanted, the load applied is borne by the bone but also by the implant [71]. The other main mechanical cause of aseptic loosening is due to the movement at bone-implant interface, also known as micromotion. As defined by Westphal et al. [157], micromotion is "the amplitude of the cyclic relative stem-bone displacement for a load cycle" and migration is "the permanent displacement of the implant with respect to the bone relative to the initial unloaded situation". To illustrate this, Figure 2.8 shows what the implant micromotion and migration are for a cyclic test. For each cycle, the implant moves and the implant micromotion corresponds to the dynamic or reversible elastic motion of the implant, whereas the implant migration corresponds to the total or irreversible motion of the implant.

Bone ingrowth can occur if the relative stem/bone micromotion is between a value of 30 and 150 μm [119]. However, osseointegration might take place above micromotion of 30 μm, while a fibrous differentiation can take place at the interface when micromotion is above 150 μm [76]. It has also been suggested that an implant migration higher than 1.2 mm per year during the first two years after implantation can lead to aseptic loosening [58].

2.2.4.3 Other causes

After a hip operation, the hip joint becomes less stable and this may lead to a dislocation, which is a painful complication. Dislocation of the artificial hip joint occurs when the ball comes out of its socket. In most cases, a second operation is not needed, an

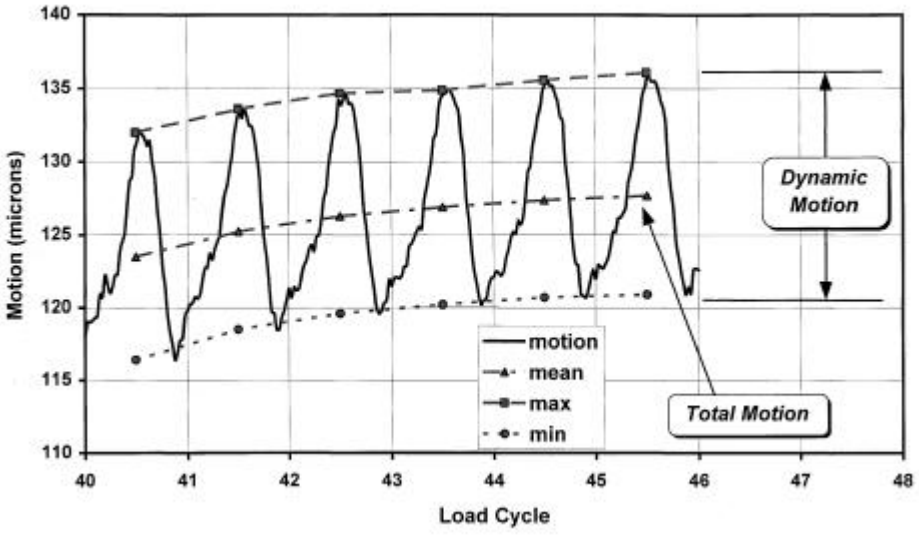

Figure 2.8: Implant dynamic and total motions within a cyclic loading [135]

orthopedic surgeon can push the joint back into place while the patient is sedated. In their study, Ali Khan et al. [15] reported that dislocation occurred in about 2 percent of patients and in more than half the cases was due to malposition of the acetabular cup. On the femoral component, excessive anteversion or retroversion was identified as being the greatest problem of stem positioning.

Other complications such as infection of the wound or around the new joint can occur following hip replacement or years after the operation. A second operation to treat or replace the joint can be carried out if the infection is deep. In 2009, 56% of hip revisions in England and Wales were due to infection [5].

Leg length discrepancy can also occur after an operation. In their study, White and Dougall [158] assessed 200 (200 hips) patients undergoing total hip operation. They measured leg length from radiographs after six months after the surgery. They reported leg length differences within 10 mm in 143 THR of all patients, with the operative leg longer in 41 patients and shorter in 16 patients. They highlighted that radiographic evidence of leg length discrepancy did not correlate with patient function, comfort or satisfaction.

As mentioned by Kessler and Kafer [80], many doctors believe that obesity and being overweight can affect the early outcome after total hip replacement. That is why they studied three groups of patients (normal-weight, overweight and obese patients) to assess how patient weight can affect the early postoperative results. The outcome of each patient was analysed at 10 days and 3 months after the operation based on a self-administrated assessment chart, the Western Ontario and McMaster Universities (WOMAC) Osteoarthritis Index. Other parameters such as the age, sex and affected

size were used to build a statistical model to assess the effect of the body mass index on the initial outcome. The authors suggested that being overweight or obese does not have an impact on the initial outcome of total hip replacement or hospital length stay after the operation. This also agreed with other studies based on different methods [98, 103, 138].

2.2.5 Revision total hip replacement

As explained in section 2.2.4, complications may occur after a primary total hip replacement and in some cases, such as implant loosening, wearing out or breaking, the implant needs to be replaced. The 7^{th} annual report of the national joint registry for England and Wales reported a revision rate of 4.4% and 4.0% respectively for cemented and cementless total hip replacement at five years [5].

For the revision procedure, the primary implant needs first to be removed; therefore, compared to the primary operation, it is more difficult to conduct a revision operation. The operating time and hospital stay are usually longer [32]. In comparison with primary operations, Bozic et al. [32] reported a longer mean operative time of 41% and a longer mean hospital stay length of 16% for revision operations.

Revision operations may also lead to complications and the complications reported following a primary operation can also not be ruled out after the revision operation. However, it should be noted that complication rates after a revision operation is higher that after a primary operation [32, 96]. Bozic et al. [32] reported a mean complication rate of 32% higher than after primary operations. Therefore, one of the challenges of bioengineers and surgeons are to avoid revision due to low success rate.

2.3 Computational investigations of the replaced hip

2.3.1 Finite element analysis of the replaced hip

2.3.1.1 Development of the Finite Element Method

A finite element model (FEM) describes the physical behaviour of a structure under loading. The structure is divided into a number of discrete elements. The elements can be one-dimensional, two-dimensional (for example: triangular) or three-dimensional (for example: tetrahedral or hexahedral) and they can be linear or non-linear. These elements are connected at specific points, called nodes. From each element, a stiffness matrix is derived, which reflects the material and geometric characteristics.

Computational modelling consists of different steps: modelling of the geometry, meshing, defining of material properties and boundary conditions. In FEM, the mesh of the model influences the accuracy, convergence and speed of the solution. However, there is a compromise between mesh size and the accuracy and time taken to compute the solution.

One of the advantages of using FEM is to study the variables under well-controlled conditions. Huiskes and Hollister [71] explained the different roles of finite element analysis in orthopaedics; they explained that it can be used as a "method of data-evaluation" i.e. integrate data from experiments into the models; a "method of data-extrapolation" i.e. to estimate variables that cannot be measured physically and a "method of numerical experimentation" i.e. to test different factors of a system.

In biomechanical and orthopaedic research, finite element analysis (FEA) became widely used as computational resources became more powerful and finite element software more elaborate. Because of limited resources, previous modelling was restricted to two-dimensional analyses whereas recent advances have had a huge impact in modelling and made possible the generation of multiple parts in three dimensions.

Modelling different parts of the body often involves the creation of a three-dimensional model of the joint from medical imaging [12, 127, 152]. Modalities such as CT-scans or magnetic resonance imaging (MRI) can be used; the main requirement being images enabling differentiation of the anatomy. Images are defined by pixels (picture element) and each pixel has an intensity of gray level or Hounsfield unit (HU). The HU scale is a quantitative scale of x-ray attenuation used for CT scans [38] and the reading in HU is also called the CT number. The HU of a material is:

$$HU = \frac{\mu - \mu_{water}}{\mu_{water}} * 1000, \tag{2.1}$$

where μ is the linear attenuation coefficient of the material and μ_{water} the linear attenuation coefficient of water.

As an example, the CT-value of water and air at standard pressure and temperature is defined respectively as 0 HU and as -1000 HU, see Table 2.1.

In previous studies such as those carried out by Reggiani et al. [127] and Abdul-Kadir et al. [12], the bone material properties were assigned based on the grayscale value (or Hounsfield unit) of CT data. For this purpose, BoneMat software (Instituti Ortopedici Rizzoli, Bologna, Italy) is often used, which is a mapping software that allows material properties to be assigned to the elements of the mesh.

[8] http://www.medcyclopaedia.com

Table 2.1: Hounsfield Unit of substances[8]

	Hounsfield Unit
bone	1000
muscle	10 40
water	0
fat	-50 ..... -100
air	-1000

As already explained, each slice of a CT-scan consists of pixels and the pixels intensity (or greyscale) is related to the density. However, the greyscale can vary from one type of CT-scan to another; in fact, it is highly dependent on the parameters set by the radiologist when the images were taken [142].

The relationship between the grayscale (GS) and the density ϱ is assumed to be linear:

$$\varrho = a + b * GS \tag{2.2}$$

From the density, the Young's Modulus (E) is calculated using the equation:

$$E = c + d * (\varrho)^e \tag{2.3}$$

The parameters a, b, c, d and e are specific to the patient; and the user can choose them. Usually, the Young's Modulus varies with density: $E = d * (\varrho)^e$.

In finite element software, many parameters are defined but some do not have a physical meaning, which means that they cannot be estimated experimentally, which makes the specification of a value more difficult. However, they may have an impact on the outcome of the analyses, as identified by Bernakiewicz and Viceconti [28]. In their computational model, they simulated the same scenario as an experimental test, employing similar mechanical properties and loading. CT scans of an implanted sawbone were used to create the three-dimensional model and two contact pairs (stem-cancellous bone and stem-cortical bone) were defined. In their contact analyses, they pointed out that contact stiffness and convergence tolerance influence the accuracy of the finite element results.

2.3.1.2 Primary stability studies

The primary stability of an implant is associated with the early postoperative stage before osseointegration of the implant has occurred. It is very crucial for the long

term success of a cementless joint replacement, and depends on factors such as implant design, bone quality and surgical technique.

Viceconti et al. [152] studied the primary stability of an implanted sawbone computationally using different contact scenarios between the cementless stem and the bone: frictionless contact, frictional contact and press-fitted frictional contact. They also assessed different contact elements: node-to-node, node-to-face and face-to-face. They showed that modelling based on face-to-face elements, simulating a frictional contact at the bone-stem interface and the press-fit load were accurate at predicting micromotion. For face-to-face contact, they used a normal contact stiffness of 6000 N/mm and a convergence tolerance of 0.5% for the force.

In another study, Viceconti et al. [153] assessed the effect of a soft tissue layer around a cementless total hip replacement using finite element analysis. The three-dimensional model was based on a CT-scan of a synthetic bone implanted by a surgeon. In the finite element study, the thickness of the layer was changed and the micromotion of the implant was measured at different locations. A stair-climbing load was applied and the resultant torque applied to the implant was 19.8 Nm. They noticed that when the thickness of the soft tissue layer increased, the torsional stability of the implant reduced. For the FEA, they described the three-dimensional motion as sliding tangential to the contact interface, and the detachment or gap normal to the contact surface. Results from the computational study were validated by the experimental tests.

Duda et al. [54] showed the effect of applying muscle forces to a finite element model on femoral strain distribution. It was shown that tensile and compressive strains were overestimated when muscle forces were applied, while torsional effects were underestimated.

In another study including the muscle forces, Bitsakos et al. [31] investigated bone resorption following a hip operation using different boundary conditions. They showed the importance of modelling muscle loads in computational studies.

Abdul-Kadir and Hansen [11] also investigated the effect of including the muscles forces in a FEM but on the predicted micromotion. Their study looked at three phases of the gait cycle: heel-strike, mid-stance and toe off of two loading scenarios: walking and stair-climbing, which is known as the critical loading case. In the stair-climbing case, the model estimated the micromotion at the interface to be ten times higher in the model including the muscles than the other model. In other words, they claimed that the implant primary stability is overestimated in models without muscles. They also showed that during the walking case, the toe-off phase may be as critical as the stair-climbing case to the micromotion.

In some computational studies, researchers such as Orlik et al. [111] and Viceconti et al. [154] have varied the coefficient of friction at the implant bone interface. When bone grows into the surface of the implant, this coefficient increases and implant micromotions decrease. Orlik et al. [111] changed the coefficient of friction between 0.1 and 0.6 and the normal contact stiffness between 100 and 10000 GPa/m. To define laws describing the change of the effective normal contact stiffness and effective coefficient of friction, they suggested that further experimental data on bone ingrowth and mineralisation processes were needed.

Abdul-Kadir et al. [12] carried out a combined computational and experimental study to assess the micromotion at the bone-implant interface. They explained that the cavity made experimentally in the femur was larger than the nominal interference of 0.3-0.5 mm. They showed that it is important to consider the interference fit for predicting micromotion. In their study, they compared the results from finite element analysis with experimental tests. They identified that if interference fit is not taken into account for the FEA, the stem stability will be underestimated. Micromotion at the distal and proximal ends of the stem were higher than micromotion at the stem mid-section. Comparing results between FEA and experiments, they suggested that surgeons introduce 1-2 μm of interference fit. They explained that the measurements were carried out by linear variable differential transducers (LVDTs) and so the motion measured corresponds to the motion between the LVDT fixation point on the bone and the point of the peg insertion on the implant. This lead to an overestimated micromotion and so small levels of interference fit. However, they pointed out that surgeons are more likely to introduce 50-100 μm of interference fit and from their analyses, an optimal interface fit of 50 μm was predicted to achieve good primary fixation.

Pancanti et al. [113] used finite element analysis to study the relative micromotion of the bone-cementless hip implant in four patients performing nine different tasks. They showed that stair climbing is the more critical activity for primary stability for some patients. For all activities, the highest value of micromotion was found in the distal-posterior part of the stem. The micromotion found in their computational work was within the threshold of 40 and 150 μm. They noted that the implant was perfectly fitted into the bone in their modelling, which is not always the case in clinical practice.

Reggiani et al. [127] studied the relative micromotion at the interface of a cadaveric bone and cementless implant using FE. They used BoneMat to apply the material properties to the bone. The implant was positioned in the bone by a surgeon. The purpose of their study was to create numerical models to predict primary stability during the pre-operative planning session. They used asymmetric face-to-face contact elements at the bone-implant interface to create a model of frictional contact. A

maximum internal rotation of 11.4 Nm was applied to the stem. The results from the computational study was validated by the results from the experimental tests. The error for the maximum predicted micromotion was 12%. They also generated a new model from the CT-scan, in order to get the same stem position and found a difference of 20 μm between the two models. They showed the possibility of creating a patient-specific FE model using a pre-operative CT scan and pre-operative planning to evaluate the primary stability of a cementless stem.

2.3.2 Probabilistic methods in biomechanics

2.3.2.1 Limitation of a deterministic finite element analysis

Computer simulation is used more and more in biomechanics to predict, for example, the success or failure of a total hip replacement by taking into account different parameters. Thereby, deterministic or probabilistic methods can be employed to the analysis and the main difference between these two methods is that solving a deterministic model will always give the same results if the same parameters and equations are used to solve the problem.

Although finite element analysis alone can give a qualitative idea of the system behaviour for a specific scenario and can also be used to compare different cases, the analyses can become very tedious and time consuming when several scenarios need to be assessed. Moreover, analysing multiple parameters simultaneously can become very difficult. Therefore, the use of probabilistic methods has become popular to study multivariable problems as computers are becoming powerful.

2.3.2.2 Uncertainties

Probabilistic methods are widely used to predict the distribution of performance, especially in aerospace. In biomechanics, in particular in hip and knee arthroplasty, uncertainty is related to the patient, implant geometries, material properties, component alignment and loading conditions [86]. Probabilistic methods would therefore appear to be well suited for the analysis of these constructs. In their paper, Laz and Browne [85] reviewed the use of these techniques in the biomechanical field.

There are two types of random variables (RVs): discrete and continuous. Discrete random variables take on one of a set of specific values, each with some probability greater than zero. Continuous random variables can be realized with any of a range of values (e.g., a real number between zero and one), and so there are several ranges (e.g. 0 to one half) that have a probability greater than zero of occurring. A random

variable has either an associated probability distribution (discrete random variable) or probability density function (continuous random variable).

Uncertainties encountered in computational modelling can be classified into two groups: aleatory and epistemic uncertainty. Aleatory uncertainty refers to randomness of "events or [modelling] variables" and epistemic uncertainty refers to "a lack of knowledge" of a physical system and the capability to measure and model it [19, 160]. In other words, the aleatory uncertainty cannot be reduced by improved measurements and the epistemic uncertainty can be reduced by increasing knowledge.

Table 2.2 summarizes the different expressions used by different authors to define uncertainty, and is taken from the book "Risk and uncertainty in dam safety" [66].

Table 2.2: Expressions used to describe uncertainties

Terms pertaining to uncertainty due to naturally variable phenomena in time or space: "uncertainties of nature"	**Terms pertaining to uncertainty due to lack of knowledge or understanding: "uncertainties of the mind"**
Natural variability	Knowledge uncertainty
Aleatory uncertainty	Epistemic uncertainty
Random or stochastic variation	Functional uncertainty
Objective uncertainty	Subjective uncertainty
External uncertainty	Internal uncertainty
Statistical probability	Inductive probability
Chance [Fr]	Probabilité [Fr]

2.3.2.3 Uncertainties in orthopaedic biomechanics

Bioengineering systems are subjected to uncertainties, and this can be explained by the fact that their responses to a specific condition depends mainly on the living tissue, environment and material used. To fully assess a biomedical model, the variables have to be carefully defined and estimated. In the case of a hip operation, its success depends on several factors such as the patient, implant design, surgical variation. Some of these variables are described in Table 2.3.

Table 2.3: Variables affecting the success of a THR

Implant Design	**Surgical Variation**	**Patient**
Geometry of components	Surgeons' skills	Sex
Material properties	Surgical approaches	Level of activities
Fixation method		Bone quality
Wear couples		

Based on the literature review, the distribution of some of these variables can be estimated and the main methods used to solve the stochastic model are described in the following section.

2.3.2.4 Probabilistic uncertainty analysis

Probabilistic methods have become more widely used with advances in computational sciences. The key idea of probabilistic uncertainty analysis is to compute uncertainty in the outputs of interest as a function of uncertainty in the inputs. In a typical uncertainty analysis problem, the following metrics may be of interest: (1) the first few statistical moments of the outputs, (2) probability density functions of the outputs and (3) the probability of the output exceeding a critical value (reliability estimation).

Some commonly used methods for uncertainty analysis are described below:

Monte Carlo methods are stochastic techniques and are useful for investigating problems with significant uncertainty in inputs, such as calculation of the failure of an implant. However, it requires large numbers of samples to be run as it takes sample points from throughout the sample space. It is a method for iteratively evaluating a deterministic model using sets of random numbers as inputs. The term refers to games of chance in Monaco famed for its casinos. The aim of this method is to assess how random variation and a lack of knowledge affects the sensitivity, performance or reliability of the modelling. As the inputs are randomly generated from probability distributions, Monte Carlo simulation is a sampling method. The following steps summarize how to use this method:

- create a quantitative model
- generate a set of random inputs from their probability distributions
- evaluate, solve the model and store the results
- repeat the 2 previous steps for each realization of the parameters
- analyze the results

Latin Hypercube Sampling is a sampling method that uses a "stratified sampling scheme to improve the coverage of the input space" [74]. The cumulative curve is divided into intervals of equal probability where the intervals are the number of iterations performed on the model. One random value from each interval is selected and randomly paired or correlated to the input variables. The whole region is sampled providing a higher accuracy. This technique reduces the number of trials compared to the Monte Carlo simulation [110].

Response surface method (RSM) is a "collection of mathematical and statistical methods that are used to develop, to improve, or to optimize a product or process" [104]. The method was introduced in 1951. The main idea of this method is to use a set of designed experiments to obtain an optimal response. This method requires two steps: generating sufficient experiment sets and then define a relationship between the random variables; i.e. a training dataset and a quadratic response surface model are first defined. The undetermined coefficients of the polynomial model are then estimated by substituting the experimental outputs into the model. For a robust estimation of the coefficients, training points must be greater than the number of undetermined coefficients. RSM can be time consuming for problems with more than ten design variables and the polynomial approximation has some limitations for models with complex input-output relationships.

In this thesis, the **Bayesian Gaussian process modelling** is employed. The aim of Gaussian process is to generate a computationally cheap emulator, which is a statistical approximation of the simulator instead of the original code [83]. The simulator is a function that maps inputs X into an output [107]. The results obtained from the analysis would be close to the one produced by the original simulator if the approximation is good enough. The Bayesian approach consists of building the emulator and then using it in lieu of the computationally expensive finite element solver to accelerate probabilistic analysis and sensitivity studies.

2.3.2.5 Previous studies

Although relatively recently introduced into orthopaedic biomechanics, probabilistic methods are increasingly being used to investigate the replaced construct, in particular cemented THR [20, 105, 100]. Bah and Browne [20] studied the probability of cement fatigue failure in a cemented total hip replacement by measuring the cement maximum Von Mises stress. In their analysis, a response surface method was used. A three-dimensional model of a cylindrical cemented hip stem in the bone was created and meshed for finite element analysis. The distal ends of the bone and cement were constrained. The bone-cement and stem-cement interfaces were bonded and the material properties of the bone, cement and implant were assumed to be linearly isotropic and homogeneous. They investigated 11 parameters and sensitivity analyses showed that bone diameter and length, cement thickness and axial joint loading affected cement fatigue failure.

Nicolella et al. [105] studied the effect of joint and muscle loading, bone and cement material properties on a cemented total hip replacement. Probabilistic methods were used to investigate the effect of shape optimization of the stem on the predicted prob-

ability of failure. In their study, the modelling was more sensitive to the joint loading, cement strength and implant-cement interface strength. A shape-optimised implant was generated to improve the long-term performance of the implant.

Mehrez [100] assessed different parameters, such as the mechanical properties and geometry of the bone, prosthesis and cement and their effect on the performance of the cemented total hip replacement using statistical analysis combined with finite element analysis. In this study, the bone-cement interface was fully bonded and contact elements were used at the implant-cement interface in order to allow a sliding displacement of the stem. The axial inducible displacement, a mechanism thought to be related to loosening, was investigated as a failure criterion. The most sensitive parameter was the material properties of the cement, followed by the implant geometry, load and bone material properties. It should be noted that the particularity of this work is its investigation into geometrical effects, which is rare in the field.

Kayabasi and Ekici [78] assessed the performance of cemented total hip replacement and the aim was to design a shape-optimised stem from the Charnley stem. In their study, Kayabasi and Ekici [78] investigated the effect of joint and muscle loading and implant, cement and bone material properties and strengths on the integrity of implant. To this end, design optimization methods were used to assess probability of failure of the cement, bone-cement and implant-cement interface and the stem and the newly designed stem was compared with the initial shape-stem. The optimised hip stem design provided promising results with a lower probability of failure than the Charnley design. The main conclusion of this work is that the implant performance can be assessed preclinically using probabilistic methods.

These two studies show how bone cement may affect the biomechanical responses of the integrity of hip operation, but it should be noted that cementless devices are also subjected to uncertainties. Dopico-González et al. [52] investigated the magnitude and the direction of the applied load, and the Young's modulus of the bone and the implant to assess their impact on a cementless total hip replacement. Monte Carlo simulations were used to randomly assign values to these parameters using a normal distribution function for the magnitude and direction of the load, and a logarithmic normal distribution for the Young's Modulus of the bone and implant. The implant and bone were assumed to be fully bonded and the distal part of the bone was constrained. Two sampling methods were compared: the Latin Hypercube Sampling (LHS) and the Direct Sampling (DS). For the LHS, the results obtained from 1,000 samples were compared to results from 10,000 samples. In their study, the LHS method with 1,000 simulations appeared sufficient, giving similar results in a shorter time. According to their results, bone stiffness and magnitude of the load affected the maximum bone strain.

2.4 Mechanical testing of the replaced hip

The aim of this section is to review experimental tests that have been carried out to study the primary stability of a hip prosthesis. In most cases, implant performance has been determined by investigating the implant micromotion and/or migration, or bone deformation. Furthermore, computational methods need experimental validation and to this end, the section also covers some relevant examples of such work.

2.4.1 Implant motion measurement

Implant motion can be measured either *in vivo* or *in vitro*. However, it is very difficult to measure the micromotion *in vivo* as it requires the measurement of the implant position when it is loaded and then unloaded whereas it is easier to measure the migration as it corresponds to the permanent implant motion. Roentgen stereophotogrammetric analysis (RSA) is an *in vivo* technique which provides three-dimensional measurements based on radiographs and is the most commonly used technique for assessing orthopaedic implants. Verdonschot et al. [151] measured the implant migration using the RSA technique and they claimed a of $40\mu m$; on another study, Kiss et al. [82] investigated implant migration during four year post-operation and they estimated the accuracy of the measurements of 0.25 to 0.50 mm/year. However, this range of accuracy may present problems in assessing implant alignment; therefore, in vitro techniques can be a good alternative to measure the implant position with a better accuracy.

In vitro tests have been widely used to measure implant motion and these tests were carried out either on human cadaver bones or synthetic bones, which have been shown as a good alternative to cadaver bones [43]. In an *in vitro* test, the bone is prepared by removing the femoral head and readying the cavity inside the bone for implantation. The distal part of the bone is then rigidly fixed. In some studies, the end of the bone was clamped within the condyles [95, 102, 140] but in most cases, the femur was sectioned at two-thirds of its length from the femoral head and the distal part of the diaphysis potted using a resin [11, 29, 34, 45, 48, 88, 116, 118, 135]. When the distal end of the femur is sectioned, the bone is aligned according to standards for testing total hip prostheses such as the British Standard (BS 7206: Part4: 2002). In terms of loading the implant, load is usually applied to the top of the femoral head [29, 34, 45, 48] but it can also be applied to the shoulder of the stem [11].

The stem micromotion/migration can be measured using measurement tools such as LVDTs and extensometers. Figure 2.9 shows the test set-up of the experiments carried out by Cristofolini et al. [46]. An implanted femur was first embedded in a pot and cyclic force was applied at the top of the femoral head as an axial force F, a bending moment

M_B and a torque M_T. The implant motions were measured using an extensometer and four LVDTs. The extensometer measured the axial motion and the LVDTs measured the rotational interface shear motion. The accuracy of their measurement technique was $\pm 2.3 \mu m$.

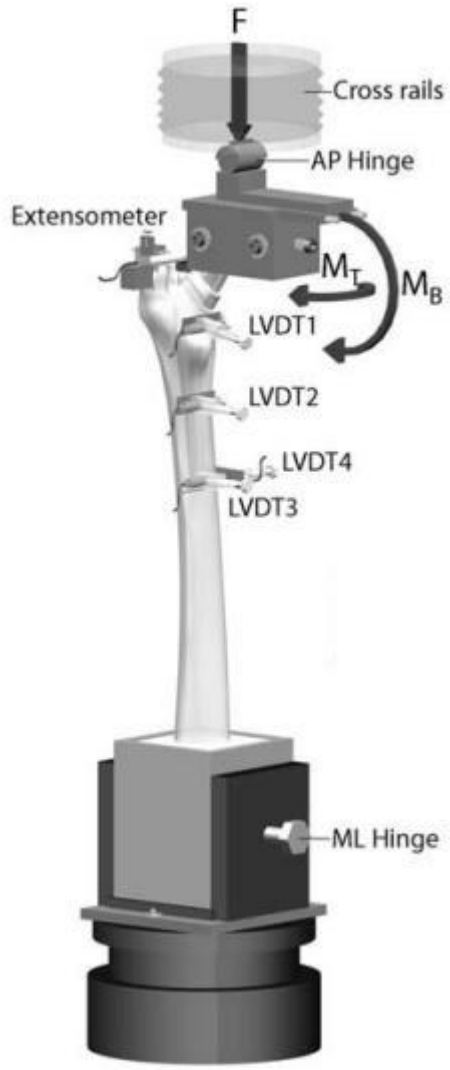

Figure 2.9: Implant motion measured using four LVDTs and a extensometer - image from Cristofolini et al. [46]

An LVDT is an electromechanical transducer that can convert linear displacement of an object (that it is in mechanical contact with) into an electrical signal. It consists of a cylindrical array of primary and secondary windings with a separate cylindrical ferromagnetic core that is attached to the object which passes through the axis of the tube. The primary winding is energized by alternating current of appropriate amplitude and frequency, known as the primary excitation. The LVDT's electrical output signal is the differential alternating current voltage between the two secondary windings, which varies with the movement of the core within the LVDT coil. This electrical output can then be converted to a dimensional output. It is notable that LVDTs are widely used

compared to the other techniques [11, 29, 34].

The LVDT can be in direct contact with either the stem or a target device which is in contact with the stem. Some test setups require a hole through the cortical wall to access the implant [11, 29, 45]. However, drilling holes in the bone introduces a mechanical weakening of the bone as mentioned by Pettersen et al. [118]. Therefore, to avoid this, they attached a yoke with six LVDTs at the shoulder of the implant and a ring with three hemispherical ceramic ball probes at the outside of the femur to measure the implant micromotion, see Figure 2.10. In this study, the implant was considered as a rigid body compared to the bone, however the cross section of bone where the ring was attached was assumed as a rigid body.

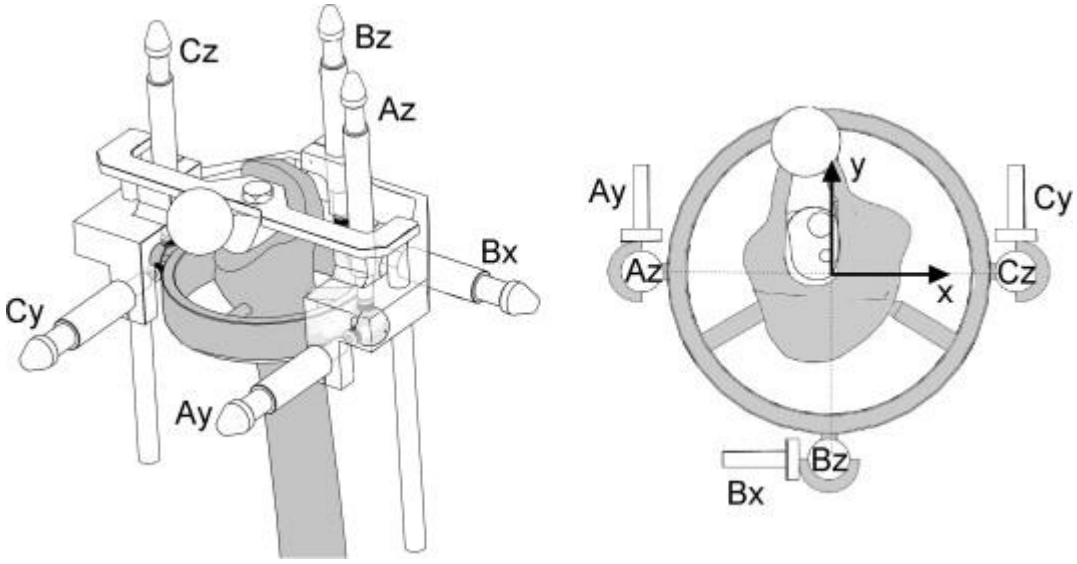

Figure 2.10: Implant motions measured using six LVDTs - image from Pettersen et al. [118]

The following paragraphs summarise a few important studies that have employed LVDTs to measure implant motion.

Monti et al. [102] studied the relative shear motion at the bone-cementless implant interface using synthetic femurs and four LVDTs. The anchorage of each LVDTs was fixed with cyanoacrylate. The implanted femur was subjected to a cyclic load simulating the physiological load for stair climbing: an axial compressive force (275-1683 N), a torque (5000-26180 Nmm) and a bending moment (3795-23225 Nmm) were applied. Before starting the tests, each implanted femur was also subjected to 1000 cycles in order to stabilize the stem in the bone. Three 100 cycle tests were conducted on three specimens. Relaxation times were set at 0, 7.5 and 15 s. They showed that the frequency of the load and the strain distribution across the cortical bone influenced the relative shear motion. They explained that the introduction of a relaxation time during the test made the experimental test more physiologically relevant for primary

stability studies and a relaxation time of 7.5 s allowed the specimens to recover most of the elastic strain; this generated higher shear motions at the interface, resulting in a more severe loading condition.

Baleani et al. [22] carried out experimental tests on implanted synthetic bone. They compared three stems: AnCAFit size 9.5, AnCAFit size 14 and CLU (Cremascoli Ortho, Italy). The AnCAFit 9.5 stem is a collarless cemented stem, the AnCAFit 14 collarless cementless and the CLU has the same shape of the AnCAFit 14, except for lateral pockets and canals, which are filled with cement, making it a partially cemented stem. In total, they used six implants of each type and implanted 18 femurs. They measured the stem micromotion at four locations using LVDTs: three on the medial side and one on the anterior side of the femur. An extensometer was fixed on the proximal tip of the femur and in contact with a pin attached to the implant and aligned with the femur, was used to measure the axial relative micromotion. They applied a pure torque sinusoidally cycled between 0.1 and 18.9 Nm for 1,000 cycles at a frequency of 0.06 Hz simulating a month of patient activity to assess the stems primary stability. They found that immediately after implantation, the partially cemented CLU stem may be as stable as the cemented stem. They believed that the use of a hybrid fixation method to maintain the stem would reduce stem loosening.

Claes et al. [41] carried out tests on femoral components implanted on cadaveric bones. They used an Option 3000 (Mathys,Orthopaedics, Bettlach, Switzerland) partially cemented stem and a fully cemented Weber Shaft stem (AlloPro, Baar, Swizerland) and measured implant micromotion using six LVDTs. Two LVDTs were mounted at about two-third of the stem length and two LVDTs were mounted at the distal end of the stem. Holes were drilled on the bone to allow direct contact of the LVDTs with the stem surface. The two other LVDTs were mounted proximally. A hip joint force of 2.2 times the body weight was used, i.e. 1.6 kN. The maximum micromotion measured in the axial direction at the bone-implant interface for both stem was 43 μm. They found that in terms of micromotion measurements, the partially cemented performed as good as the fully cemented stem.

Britton et al. [35] measured implant micromotion using six LVDTs mounted on a rigid frame. They were in contact with a target device attached to a pin press-fitted to the femoral component. Six Omnifit cementless femoral components (Stryker Howmedica Osteonics Corp., Mahwah, NJ, USA) were implanted in synthetic bones. The implanted bones were subjected to a sinusoidal load of mean 1.0 kN and amplitude 0.8 kN during 10,000 cycles with a frequency of 3 Hz. They noticed that all implants translated medially, posteriorly and distally. A rotation into varus was mainly observed. During their experimental tests a change of 2.5 $^{\circ}C$ of temperature was measured. They carried out static tests to determine the effect of this temperature change and found a maxi-

mum error of 5 μm for translation and 0.004° for rotations were measured which was negligible. However, for a longer cyclic test, the temperature variations may affect the measurements. Implants are often considered as rigid bodies but elastic deformations may have an effect on the micromotion measurement.

Motion analysis systems have also been used to measure implant movement. Westphal et al. [157] used this technique to measure the migration of an uncemented stem, the $Proxima^{TM}$ (DePuy; Leeds, UK). Load was applied at a frequency of 2 Hz, and was increased as shown in Table 2.4. However, the use of this technique has been limited and less popular compared to other techniques.

Table 2.4: Amplitude of the load increasingly applied

cycles	0-19	20-1000	1001-2000	2001-3000	3001-15000 or failure
load applied (N)	50-200	50-800	50-1200	50-1600	50-2100

Westphal et al. [157] did not include muscles in their experimental tests and the bone ingrowth was not considered, which could explain why migration measured experimentally was higher than in a clinical test. They reported that a cyclic motion of 290-430 μm at 15000 cycles was measured and that the stem migrated into varus position.

2.4.2 Bone strain measurement

As mentioned earlier, primary stability can also be assessed by measuring the bone strain when a load is applied, mainly because a high strain can lead to fracture. The most popular and widely used sensor for strain measurement is the strain gauge. It is a passive transducer that uses electrical resistance variation in wires. It consists of a grid of strain-sensitive metal foil bonded to an elastic backing material. Its fundamental principle is based on the fact that when the wire is subjected to a mechanical deformation, its electrical resistance changes proportionally. For example, if a wire is held under tension, it gets slightly longer and its cross-sectional area is reduced. The equation relating the length change to the resistance change is:

$$R = \rho \frac{L}{A},$$

where R is the resistance, ρ the resistivity (material property of the conductor), L the length of the conductor and A the cross-sectional area of the conductor.

This changes its resistance in proportion to the strain sensitivity of the wires resistance: $\frac{dR}{R} = S.\varepsilon$, where S is the strain sensitivity factor of the gauge material (also called

gauge factor) and ε the strain. As the gauge factor S is provided by the manufacturer, the strain ε where the sensor is attached can be obtained by measuring the change in electric resistance of the strain gauge.

A wire strain gauge can effectively measure strain in only one direction. To determine the three independent components of plane strain, strain rosettes may be used to determine the principal strains. As an example, gauges of a three-gauge rosette can have their axes at either 45 ° or 60 ° to each other. A two-gauge rosette can be used when the principal strain directions are known in advance otherwise a three-gauge rosette is required.

In most biomechanical studies, triaxial rosettes have been employed for bone strain measurements [30, 42, 48, 62, 128, 140, 148]. Strain gauges were usually used to measure the strains on the surface of the bone to compare different devices or verify a computational model. Before fixing the strain gauges, the bone surface was usually smoothened with sandpaper and then bonded following the standard technique with cyanoacrylate glue. Then, the gauges are connected to a data logger to record data over time such as the system 6000, Vishay Micro-Measurement, USA (45 Channels, up to 10 kHz) [62].

In their study, Bessho et al. [30] created a FE model based on CT images to predict the bone strains, strength and fracture sites, and to verify their model, they carried out experimental tests using strain gauges. They used eleven femurs and measured the strains at twelve locations: 4 at the femoral neck, 2 at the anterior, 2 at the posterior, 2 at the medial and 2 at the lateral of the femur. In their experimental work, a quasi-static compression load was applied at the femoral head. They observed fractures at the subcapital region of the femur.

In another study, Decking et al. [48] compared a stemless femoral implant, a conventional and anatomical stem. The strain measurements were carried out on intact and implanted femurs. In their study, six strain gauges were used for the measurements. They noted that the longitudinal strains decreased with the conventional and anatomical femoral stem, whereas the strain on the lateral side of the greater trochanter increased with stemless implant. The bone implanted with the stemless prosthesis provided more similar medial strains of the physiological bone than the bone implanted with the other devices.

In their study, Umeda et al. [148] used a cementless femoral component with interchangeable necks implanted in composite bone. During the experiment, they used the same bone and stem but changed the neck of the femoral component to assess its effect on the bone by measuring the bone stress. They fixed 25 rosettes to the bone surface; 5 laterally, 5 medially, 5 anteriorly and 5 posteriorly. They pointed out that the bone

strain measured in implanted bone was lower than the strain measured in intact bone and they also noted that the neck version of the femoral component affected the strain on the bone. They also identified higher value of strain around the distal tip of the stem with increasing anteversion or retroversion angles. However, as the same bone was used in the test, the results may be affected by the mechanical failure of the bone.

2.4.3 Motion and strain measurements in biomechanics using digital image correlation

Most recently, there has been a move towards measuring optically (i.e. non contact methods). Digital image correlation (DIC) is an optical technique that can analyse digital images of a two or three dimensional surface using a mathematical correlation method. Its principle is based on tracking the movement of natural or artificial patterns that are on the sample surface.

The DIC system uses one or two cameras to undertake measurements. Two-dimensional measurements require a single camera while three-dimensional measurements require two. The deformations and strains calculations can be carried out using a commercial or custom-made software. Figure 2.11 shows the test set-up using two cameras and a computer to analyse the data (image from Limess website, http://www.limess.com).

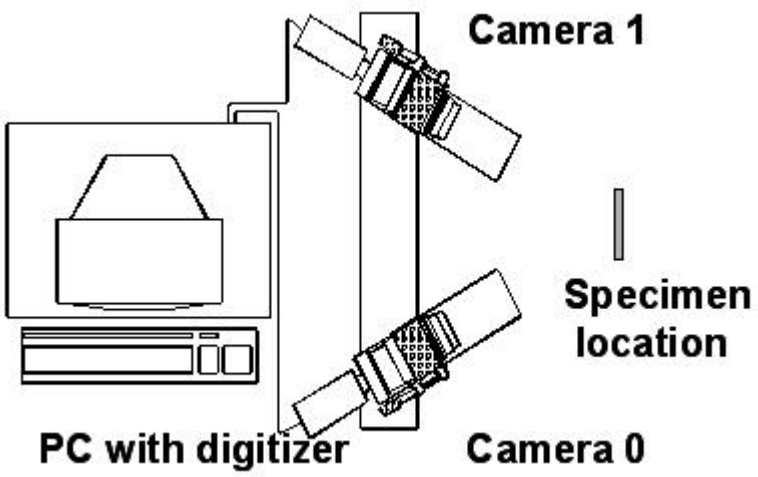

Figure 2.11: Test set-up - image from Limess website, http://www.limess.com

The use of the DIC system is becoming more and more popular in biomechanics. Evans et al. [57] used the DIC technique to measure skin mechanical properties. To this end, the medial forearm of a volunteer was prepared for testing by the application of random dot patterns to the skin. A force was applied using a fine wire attached with adhesive tape to the skin in the centre of field of view of the cameras. This study was the first attempt for measuring skin properties using an optical system and it was observed

that the DIC has great potential to measure deformation or strain of the skin and the combination with finite element analysis provided good measurements.

In another study, Mann et al. [97] used the DIC system to investigate the micromechanics of the cement-bone interface in cemented total hip replacement. The study was carried out on cadaveric bone. The distal part of the bone was potted and the femoral head was removed. The femur was then prepared for cementation and to replicate the natural environment, the bone was placed in a blood analogue solution warmed to $37°C$. The cement was introduced into the femur followed by the stem. Cement-bone specimens were prepared by sectioning the femur transversely prior to mechanical testing. The deformation was therefore measured on the surface and not through the structure. They identified that 83% of the total motion occurred at the cement-bone interface, but the accuracy of the technique was not mentioned. They also showed that the crack was more located in the cement than the bone when the sample was loaded to failure.

Sztefek et al. [141] studied bone strain in mouse tibias under an axial compression load. Measurements were carried out using both strain gauges and DIC techniques and the results were compared. The particularity of this work is that cadaveric bones were used for the tests, and it showed the capability of the DIC system to measure strains on living tissue. However, the measurement required patterns on the bone surface and this may have affected the bone mechanical properties. In their test, a good correlation of the strain measurements was observed: from 0.1 to 0.2%. They also investigated the load-induced adaptive changes in bone and they noted that after bone adaptation, the strains measured were more uniform on the bone surface that the non-adapted bone, and peak strains decreased from 0.5 to 0.3%.

Although the DIC has been used in some biomechanical studies, it has been observed that its application has not been investigated for implant motion measurements. The section 5.2 of this thesis introduces a methodology to measure the implant micromotion. To enable these calculations a custom-made code was written in Matlab to postprocess the DIC measurements and calculate the implant motions.

2.5 Summary of the literature review

Total hip replacement is one of the most successful operations in orthopaedic surgery; however the long-term success of the femoral component depends mainly on its primary stability. There are different kinds of implants, and the fixation method varies between them. Cementless total hip replacement is more often recommended for young, active patients and patients with good bone quality [155]. In this procedure, the femoral

component is embedded in the host femur using a press-fit fixation.

The primary stability achieved during the operation, in other words the stability at the early post-operation stage, has an impact on the long-term stability, also known as secondary stability. The secondary stability is related to the osseointegration, i.e. bone in- and ongrowth to the implant surface, which is in turn affected by a number of factors including the relative motion between the implant and the bone, or the implant micromotion. Therefore, it has been hypothesized that the implant micromotion can be used to predict the outcome of cementless total hip replacement. When micromotion is above $150\mu m$, a fibrous differentiation can take place at the bone-implant interface [119, 76] which can lead to aseptic loosening. Loosening of the implant can also occur when permanent movement of the stem, also known as implant migration, is higher than 1.2 mm per year during the first two years after implantation [58]. To this end, experimental investigations have used these metrics as failure criteron. A number of in vitro tests were carried out on human cadaver bones or synthetic bones, which are a good alternative to cadaver bones. Different measurement techniques are available to measure the implant motion, such as LVDT, extensometers and roentgen stereophotogrammetric analysis. However, it is worth noting that LVDTs have been the most widely used method [12, 44, 118]. Other methods of assessing implant performance focus on bone strain measurement. These are often measured through the use of strain gauges fixed to specific locations on the bone [48, 140]. Kopperdahl and Keaveny [84] suggested that the yield strain of bone is $0.78 \pm 0.04\%$ in tension and $0.84 \pm 0.06\%$ in compression. This may therefore be also considered as a failure criterion in biomechanical studies.

In previous studies, finite element analysis has been widely used to give an indication about how an implant would perform in a specific scenario and also to predict the implant micromotion [152, 127, 113, 12, 111, 154]. A single FE study will help to predict the performance of the total hip replacement on a single implant position; however, it is possible that other implant positions will lead to a different outcome regarding the stability. Probabilistic methods offer the option of looking at many scenarios in a single analysis. Despite the fact that the stem position is known to affect the primary stability, there are only few studies on the effect of stem misalignment on the integrity of cementless THR [53]. Moreover, it is worth mentioning that many probabilistic analyses have not been experimentally validated.

This project aims to use probabilistic methods and finite element analysis to assess the effect of implant positions on implant stability, and also validate the results from the computational study by carrying out experimental tests on selected scenarios. The originality of this project is the use of probability based computational model to assess the implant performance and also its validation with experimental tests using an optical

analysis based system, digital image correlation. The novelty of the computational study is the use of the mesh morphing technique and Bayesian Gaussian process model to investigate the effect of implant orientations and load case scenarios. The novelty of the experimental study is the use of the DIC system, which has been used widely in maritime, civil and aerospace engineering and has become increasingly popular in biomechanics based studies. However to the author's knowledge, its potential has not been greatly exploited in the arthroplasty field.

Chapter 3

Computational Modelling and Experimental Validation

This chapter presents an introduction to the computational modelling and experimental testing methodologies adopted in the present research. The computational model predictions are validated for the case of neutral implant position against experimental data.

3.1 Materials

The implant model selected for this programme was a 12 mm diameter Furlong collar cementless total hip arthroplasty (JRI Ltd, Sheffield, UK, Figure 3.1).

Figure 3.1: The femoral component used in this study: the Furlong hydroxyapatite coated (HAC) stem [10]

This implant is made of titanium alloy and its surface is coated with a $200\mu m$ layer of plasma-sprayed hydroxyapatite [133]. According to the national joint registry for

England and Wales, the Furlong stem was the second most implanted cementless stem, and has an orthopaedic data evaluation panel (ODEP) rating of 10A[1][6] with a revision rate of 2.7 % at 3 years (for data collected between 1st April 2003 and 30th November 2008) [4]. This stem has a successful clinical history, the implant survivorship of patients with a mean age of 71.2 years (31.1 to 89.8) at a mean of 17 years was 97.4 % with no cases of aseptic loosening of the femoral component [125]. In another study, Shah et al. [131] reported no case of aseptic loosening at 16 years for patients below the age of 50 years.

Although fracture of the stem is very rare, three cases of fracture have been reported at two main locations: neck-shoulder (Figure 3.2) or conical-distal junctions (Figure 3.3) and in all cases the fracture was due to fatigue [67].

Figure 3.2: Radiograph of the fracture at the neck-shoulder junction [67]

It was noted that the size of the stem chosen to treat the patients was not appropriate; in fact, these cases of failure were observed for patients with a body mass index exceeding 25 and in each case, a femoral component of size 9 or 10 was used.

As shown in Figure 3.1, the femoral component has a cylindrical stem with a collar and the proximal section is rectangular and tapered to resist torsion.

The bone model used in this study was a large size left synthetic composite femur (item 3406, fourth generation sawbones, Sawbones Europe AB, Sweden, Figure 3.4).

[1]10A benchmark designs strong clinical evidence of prosthesis survival available for at least 10 years [6]

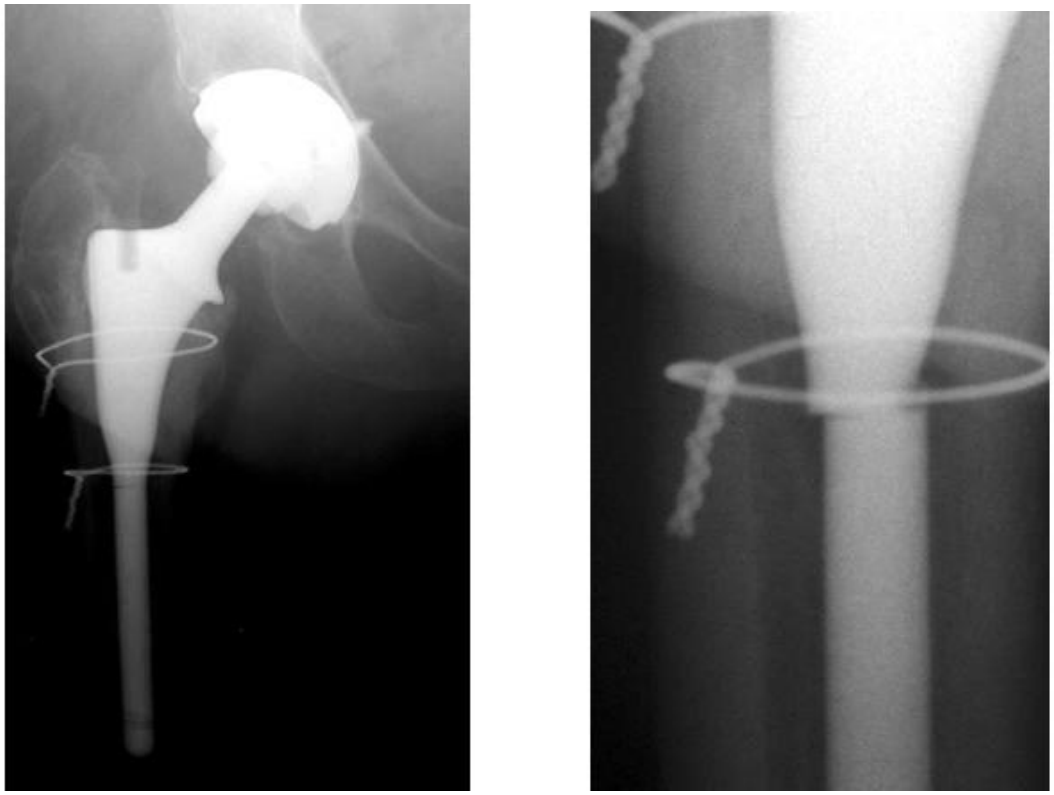

(a) Radiograph of the fracture (b) Zoomed-in radiograph of the fracture

Figure 3.3: Radiograph of the fracture at the conical-distal junction [67]

Sawbones were developed as an alternative to cadaveric bone for bone testing. Their material properties are close to natural bone and they consist of two main parts; one simulating the cortical bone and the other simulating cancellous bone. The cortical bone is made of a mixture of short glass fibres and epoxy resin and the cancellous bone is made of rigid polyurethane[2]. However, there are significant differences compared to real bone. The bone is living and can adapt to load, which in comparison, sawbones cannot do. Sawbones were selected as they were readily available and cheaper than real bone, while offering consistent geometry and material properties. The consistent properties were particularly useful for the experimental verification study where the number of variables were kept low. Moreover, modelling of many types of bone would have been too exhaustive. In this study, large size synthetic femur was used to enable large degrees in orientation variability for the verification study.

The following sections describe the methodology used for both the experimental and computational studies.

[2]http://www.sawbones.com/products/bio/composite.aspx

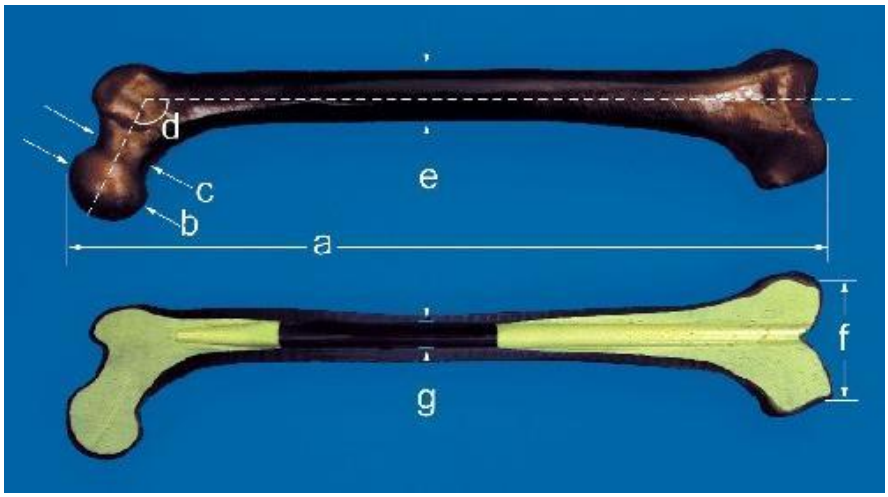

Figure 3.4: Synthetic composite femur (Size: a. 455 mm, b. 45 mm, c. 31 mm, d. 135°, e. 27 mm, f. 74 mm, g. 13 mm)[3]

3.2 Implantation and Experimental Setup

A synthetic femur was initially implanted with the Furlong stem in a neutral position by an orthopaedic surgeon. The sawbone was first rigidly fixed by a clamp and the resection line was defined using a head resection guide, as shown in Figure 3.5. The femoral head was then removed using a surgical cutting implement and the implant bed prepared using a set of rasps of increasing size. The implant was then hammered home in as close to neutral orientation as possible by the surgeon, as shown in Figure 3.6.

The femur was subsequently sectioned at two-thirds of its length below the femoral head, i.e. about 250 mm distal to the lesser trochanter. The distal end of the sawbone was embedded in a metal cup using a resin based on methyl-methacrylate (Technovit 3040, Heraus Kulzer GmbH, Wehrheim, Germany). The femur was then positioned in a pot at 9° flexion and in 10° abduction (conforming to the British Standard for testing total hip replacement BS 7206: Part 4: 2002) and was fully constrained, see Figure 3.7. The implanted bone was subjected to a compressive load of 1.6 kN which corresponds to two times body weight using an Instron servo-hydraulic test machine (Instron Ltd., High Wycombe, UK).

Two LVDTs (Solartron, RS Components Ltd, Corby, UK) were positioned to measure the longitudinal movement of the stem in the bone. The LVDTs were attached to the bone, and the tips were located against landmarks on the prosthesis: one LVDT was fixed inside the medullary canal and was directly in contact with the tip of the stem; the other was fixed on the proximal lateral aspect of the bone and was in contact with

[3]http://www.sawbones.com/products/product.aspx?1936

(a) Sawbone rigidly fixed by a clamp

(b) Use of the head resection guide

(c) Resection line drawn on the bone

Figure 3.5: Sawbone preparation

a target device attached to the shoulder of the stem, see Figure 3.8.

In the following sections "LVDT inside" refers to the LVDT in contact with the implant distal end and "LVDT outside" the LVDT in contact with the implant shoulder. Before starting the measurement, a conversion factor (Volts to millimetres) was measured for each LVDT. A micrometer was used to measure the voltage corresponding to the displacement from 0.1 mm to 1 mm with a step of 0.1 mm. Thereby, a conversion factor was calculated (Table 3.1).

The movement of the stem was monitored continuously using the two LVDTs. The stem micromotion was calculated in Matlab as the peak-to-peak amplitude of the stem movement; as shown in Figure 3.9.

(a) Cutting the femoral head

(b) Femoral head removed and implant bed prepared

(c) Implant insertion

Figure 3.6: Implantation of the stem

Three-dimensional deformation and strain measurements over the sawbone surface were undertaken using a digital image correlation (DIC) system (Limess GmbH, Pforzheim, Germany). The reader is referred to the DIC procedure detailed in chapter 5; however, to summarize, the system consists of two cameras and Vic3D software to process the recorded data. For the testing, 28 mm lenses were used and calibration was performed using a 5 mm calibration grid. The outer surfaces of the sawbones were prepared by

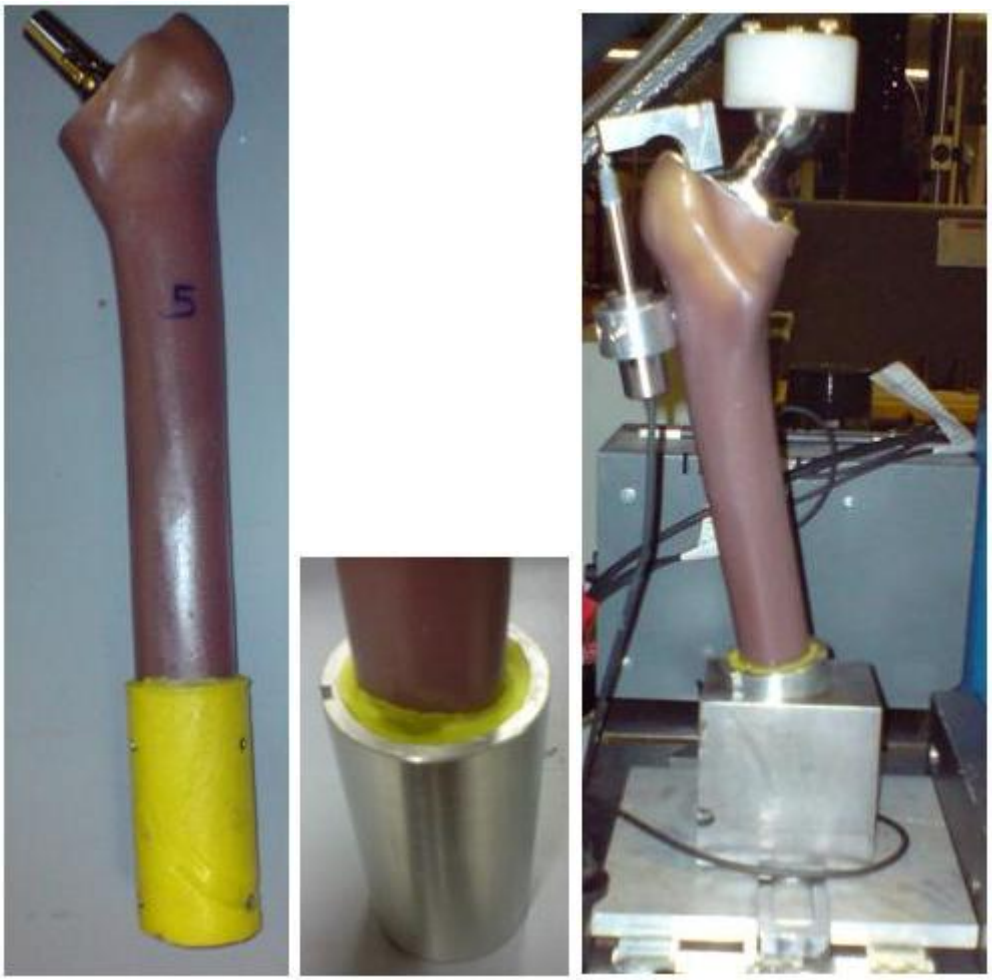

(a) (b) (c)

Figure 3.7: Distal end preparation of the implanted sawbone: (a) Femur sectioned at two-thirds of its length; (b) Distal end of the femur embedded in a cup and (c) Femur at 9° flexion and in 10° abduction (BS 7206: Part 4: 2002)

applying random dot patterns to measure the surface strain. To improve the contrast, a white paint was applied on the surface of the sawbone then a black speckle pattern was applied. The DIC measurement process consisted of applying a ramp load gradually raised in 100 N increments from 0 to -1.6 kN and taking images of the sample loaded at each stage.

3.3 Computational modelling

3.3.1 3D model construction

Prior to the experimental test, a computer tomography (CT) scan of the implanted sawbone was taken at the Southampton General Hospital using a Siemens Sensation

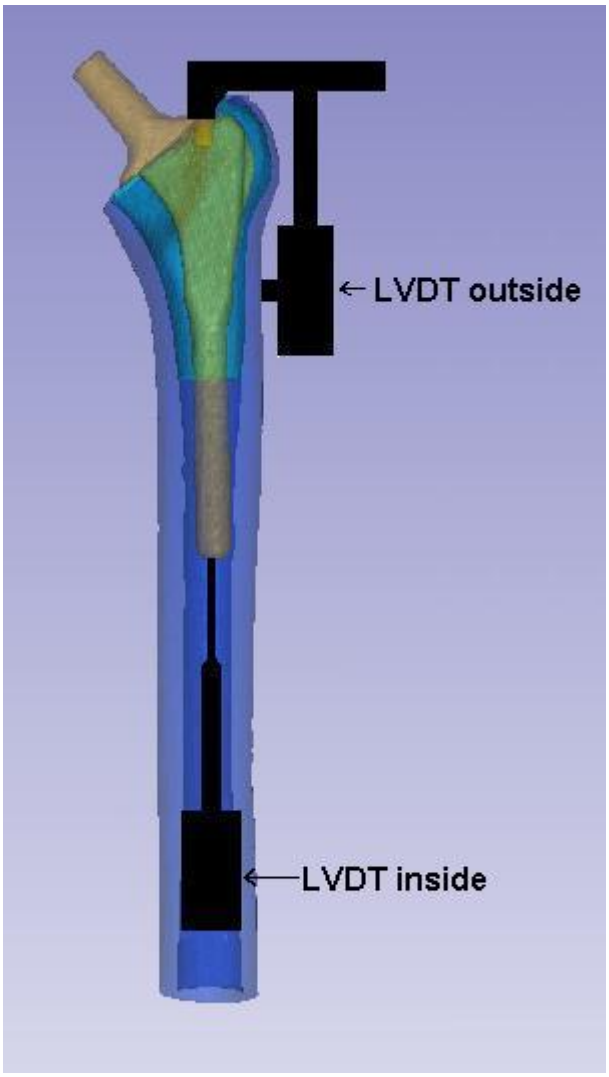

Figure 3.8: Fixation of the LVDTs

scanner (64-slice) with a fine resolution of 0.3 mm x 0.3 mm x 0.7 mm. These images were used to generate a three-dimensional model of the implanted sawbone using Simpleware software (Simpleware Ltd, Exeter, UK, packages are briefly presented in Appendix B). The images were resampled to $1mm^3$ in order to minimise the size of the model.

It should be noted that the quality of the CT images were affected by the metallic implant, which caused artefacts on the images. These artefacts are circled in red in Figure 3.10. As a result, the simulated cancellous bone could not be clearly delineated on the images as it was in contact with the implant.

The stages involved in model generation of the implanted bone is illustrated below:

1. The cortical bone and the implant were generated as masks in ScanIP (Simpleware Ltd, Exeter, UK). In ScanIP, a mask is the result of a segmentation algorithm applied on a given volume, and the segmentation tools used for the

Table 3.1: Conversion factor (V/mm) of the LVDTs

	Micrometer	**LVDT inside**	**LVDT outside**
	Displacement in mm	Displacement in Volt	Displacement in Volt
	0.1	0.085	0.081
	0.2	0.170	0.168
	0.3	0.255	0.238
	0.4	0.341	0.338
	0.5	0.426	0.421
	0.6	0.516	0.505
	0.7	0.598	0.600
	0.8	0.681	0.671
	0.9	0.768	0.765
	1.0	0.854	0.854
Conversion factor	**1 mm**	**0.853 V**	**0.837 V**

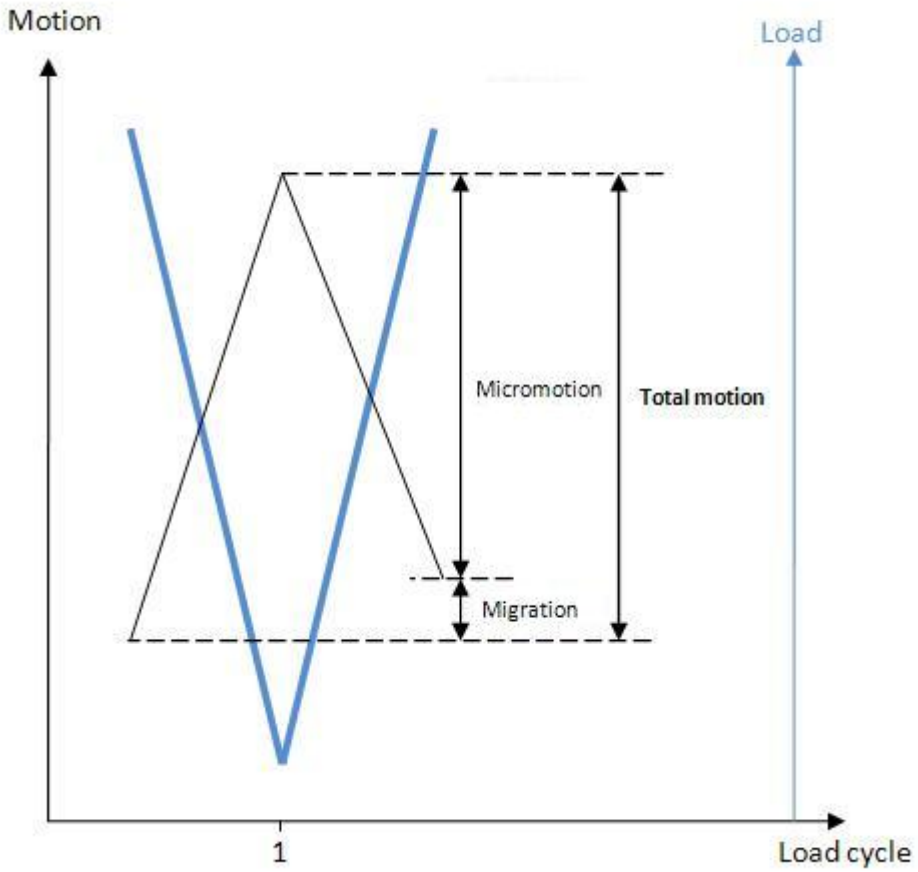

Figure 3.9: Definition of micromotion

creation of the masks were: threshold, floodfill, paint and unpaint. Figure 3.10 shows the model generation in the 3 views (plane xy, yz and xz) and the metal

artefacts due to the implant were circled in red.

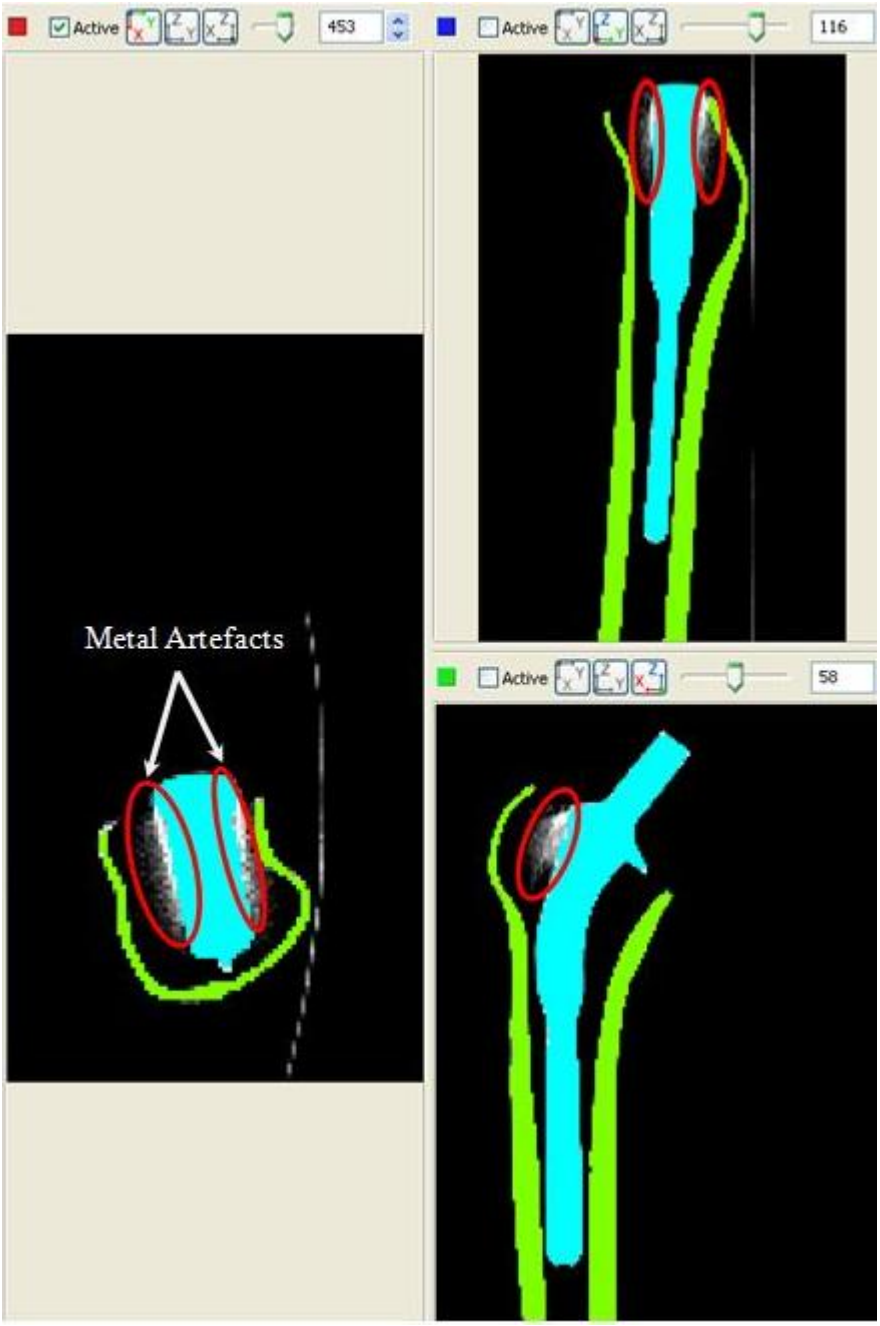

Figure 3.10: Generation of the simulated cortical bone and implant

2. A custom designed cutter was created and positioned at the cut of the femoral head, in ScanCAD (Simpleware Ltd, Exeter, UK) (Figure 3.11a), which shows the 3D model of the simulated cortical bone and implant, and Figure 3.11b, which shows the implanted bone with the cutter.

3. The contrast of the images was adjusted to enhance the quality of the implant and the simulated cortical bone. However, the simulated cancellous bone was not visible in the images. As its length was provided by the manufacturer, the

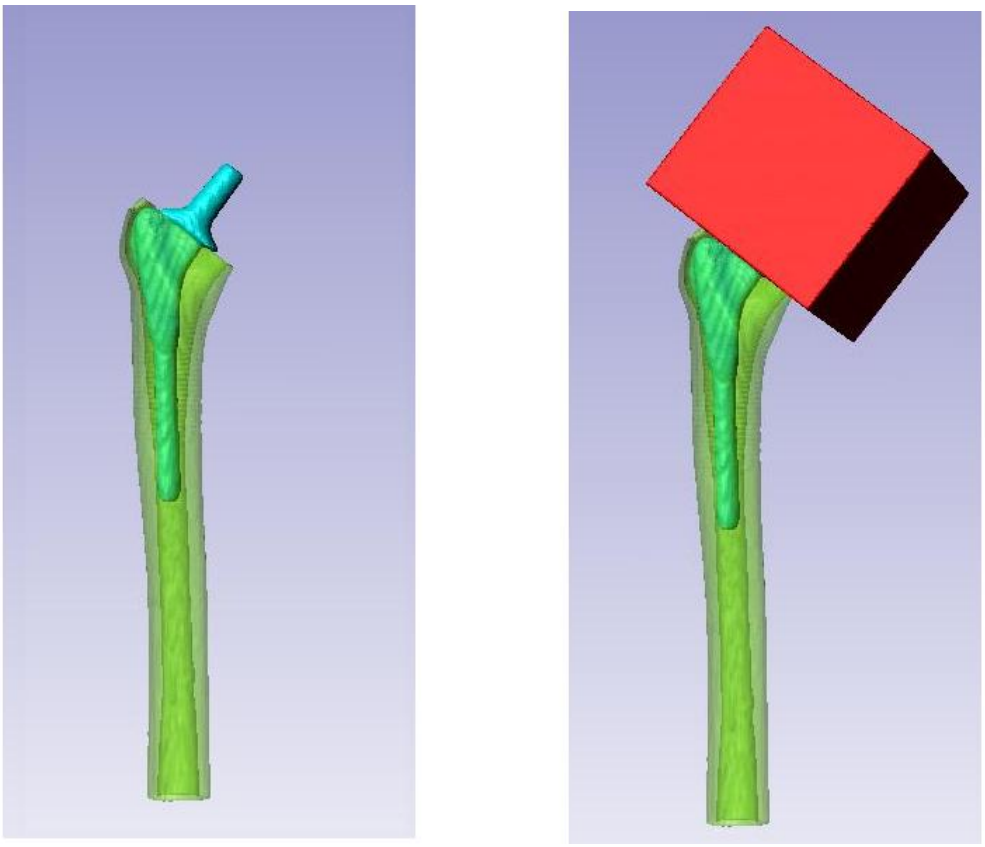

(a) (b)

Figure 3.11: 3D model of the implanted bone creation: (a): 3D model of the simulated cortical bone and implant; (b): Cutter at the cut of the femoral head

simulated cancellous bone was created manually: it corresponded to the volume between the cortical bone and cutting surface (Figure 3.12).

4. The entire model of the implanted synthetic bone is shown in Figure 3.13, in which the 3 views (plane xy, xz and yz) and the 3D model are also visible.

3.3.2 Mesh generation and convergence studies

A convergence study was carried out to assess the effect of mesh size on selected outputs. The three-dimensional model was meshed three times using four-node tetrahedral elements in Ansys Icem (Ansys INC, Canonsburg, PA) with a global mesh maximum size of either 3, 5 or 6 mm and a minimum size of 1 mm in all cases. Tetrahedral elements were used as this reduced the number of elements and nodes. Reduction in model complexity enables significant reductions in the computational cost of probabilistic analysis which involves running the model at several points in the parameter space (see Chapter 4).

The convergence study was based on the micromotion values obtained at the bone-

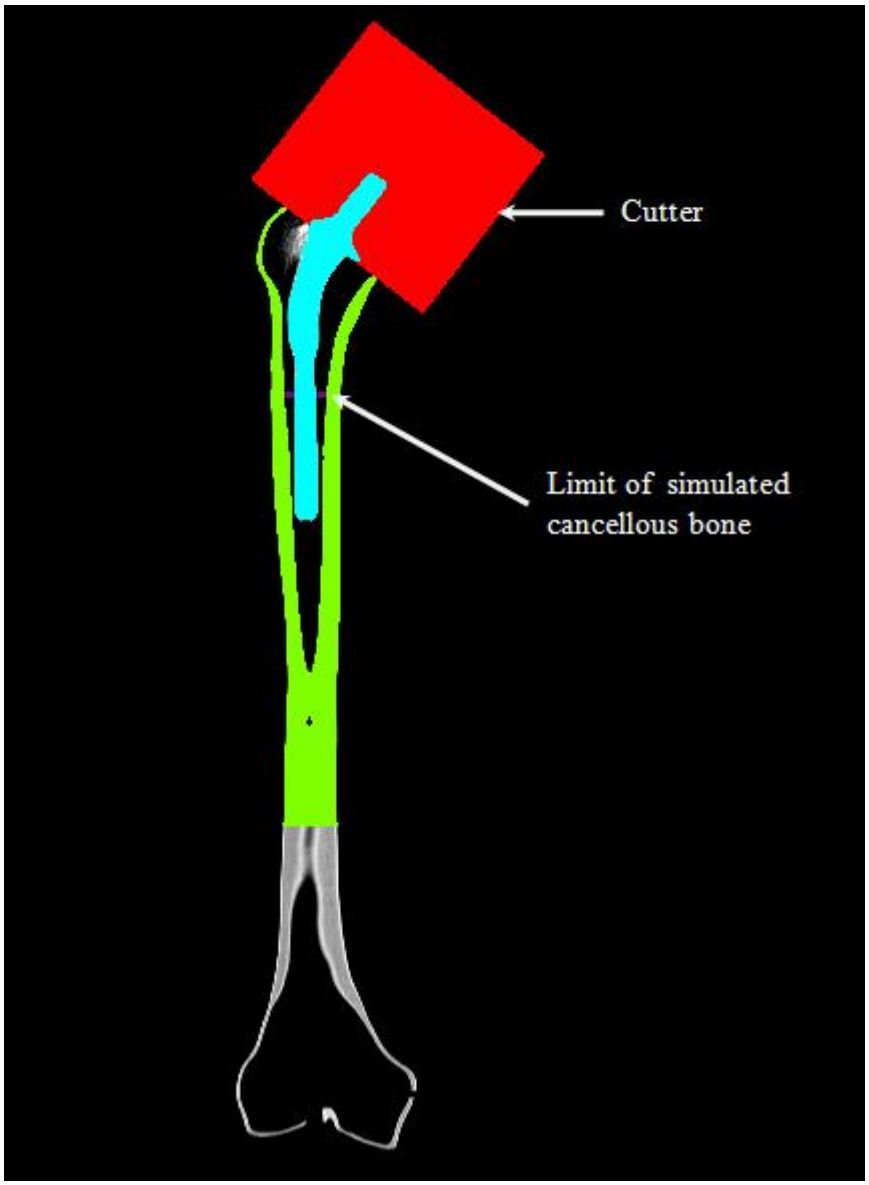

Figure 3.12: Limitation of the simulated cortical bone

implant interface and bone strain, as they were both identified as failure criteria. Table 3.2 details the metrics computed in the study. As the implant micromotion and bone strain are suggested as good indicators for assessing implant primary stability; they were both computed to assess the model mesh size.

From the convergence study, it was seen that the model with a maximum mesh size of 6 mm provided satisfactory results, therefore that model was used for the computational study. The entire mesh consisted of approximately 145,000 elements and 32,600 nodes, see Figure 3.14.

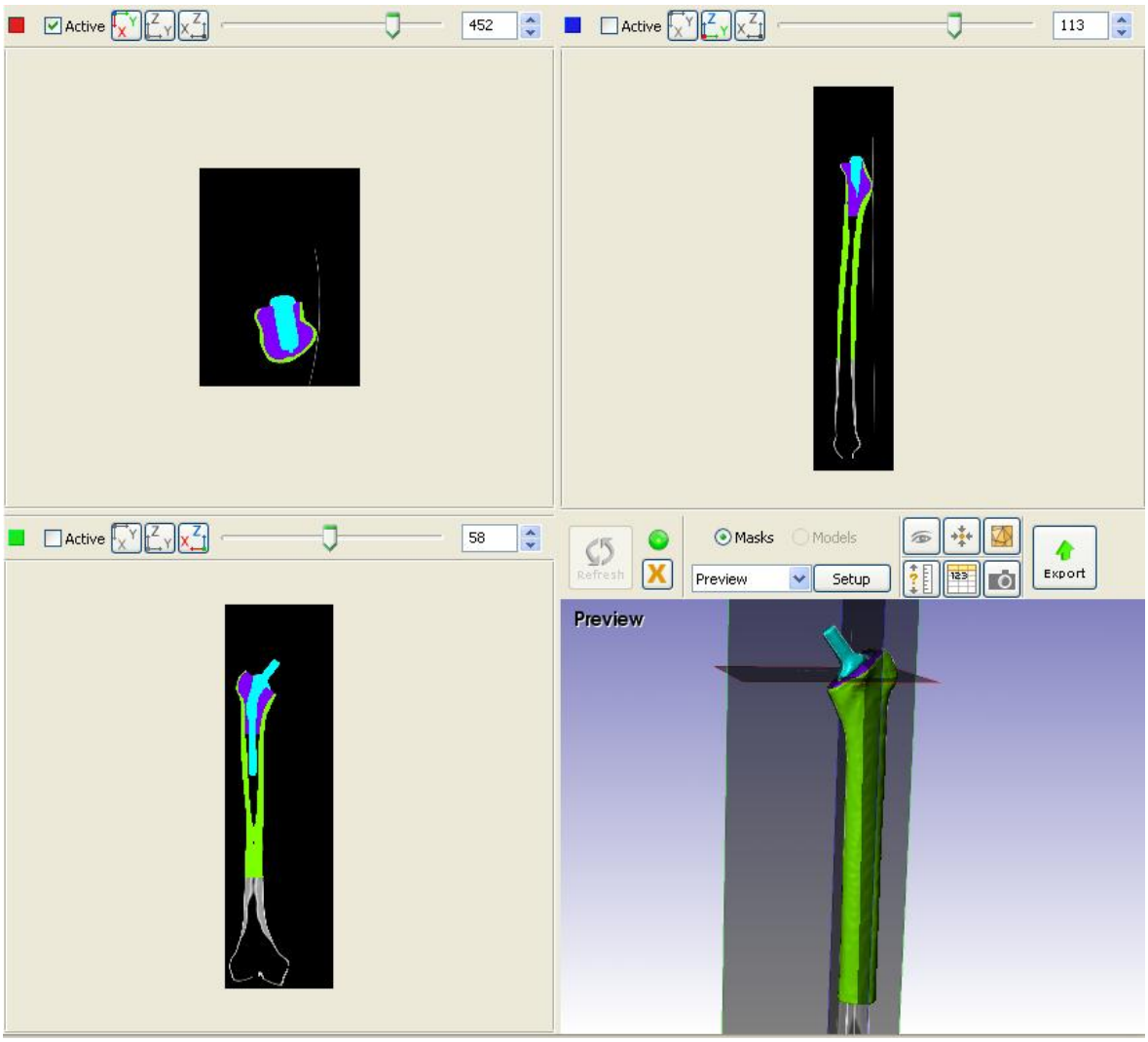

Figure 3.13: Screenshot of the entire model of the implanted bone: simulated cortical and cancellous bones and implant.

Table 3.2: Convergence study

	Maximum mesh size		
	3 mm	5 mm	6 mm
average micromotion (in μm)	3.19	2.55	2.40
micromotion lower than $50\mu m$ (in %)	99.72	99.95	99.93
average maximum strain on the bone surface(in %)	0.06	0.06	0.06
average minimum strain on the bone surface(in %)	0.003	0.004	0.004
average Von Mises strain on the bone surface(in %)	0.1	0.1	0.1
average bone volume strain (in %)	0.09	0.09	0.09

3.3.3 Boundary conditions, loading and contact analysis

The Young's modulus, density and Poisson' ratio of the implant and the bone were provided by the manufacturers, see Table 3.3.

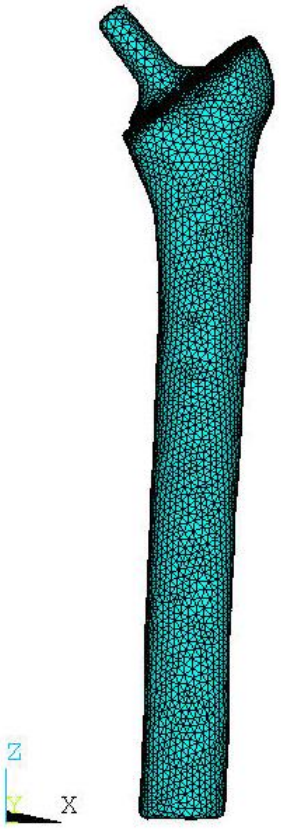

Figure 3.14: Mesh of the implanted synthetic bone in Ansys

Table 3.3: Sawbone and stem material properties

	simulated cortical bone (short fiber filled epoxy)	simulated cancellous bone (rigid polyurethane bone)	Furlong stem
Young' s modulus	16.0 GPa	0.155 GPa	105 GPa
Density	1.64	0.27	8.28
Poisson' ratio	0.3	0.3	0.3

In this study, the distal end of the proximal femur (8 cm) was fully constrained, to match the experimental test set-up. As stated in subsection 3.2, the bone should be at 9° flexion and 10° adduction according to the British Standard for testing total hip prostheses (BS 7206: Part4: 2002). For the computational analysis, the load was applied at the corresponding angles rather than positioning the bone at these angles, i.e instead of tilting the femur to achieve this configuration; three forces Fx, Fy and Fz with a resultant of the load were applied at the top of the stem. A 1,600 Newtons load corresponding to two times body weight was applied, in accordance with the experimental tests. The load applied corresponds to a representative ambulatory load after hip replacement and it was decided to not apply excessive load at the pot/bone

interface as fracture occurred at hole stress concentrations. It should also be noted that this configuration introduces torsion into the implanted construct.

Referring to the coordinate system shown in Figure 3.15, the hip adduction corresponds to the rotation angle around the y-axis and the hip flexion corresponds to the rotation angle around the x-axis.

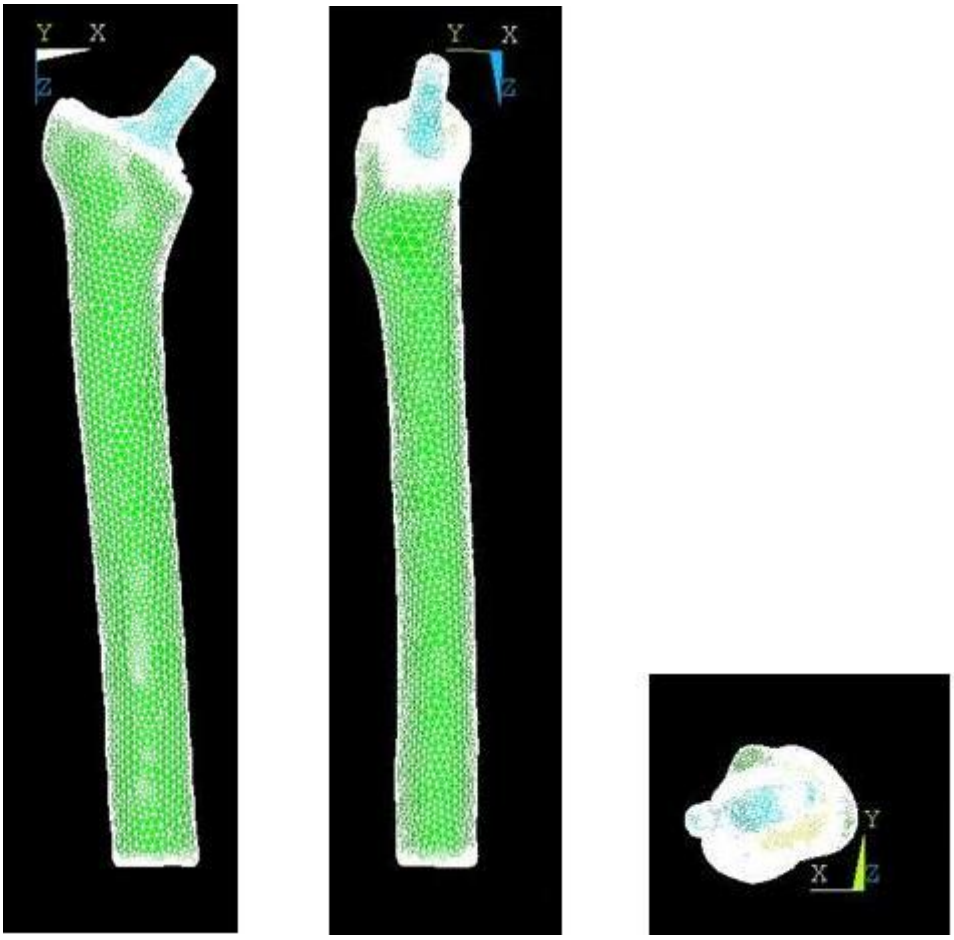

(a) (b) (c)

Figure 3.15: Coordinate system of the implanted bone in Ansys: (a): x-z plane; (b): y-z plane; (c): x-y plane

Let θ and ψ denote the angle of flexion and adduction of the femur, respectively.

The y-z plane was tilted by the angle θ, see Figure 3.16, and hence the new coordinate system can be written as:

$$\begin{bmatrix} x' \\ y' \\ z' \end{bmatrix} = \begin{bmatrix} 1 & 0 & 0 \\ 0 & cos(\theta) & sin(\theta) \\ 0 & -sin(\theta) & cos(\theta) \end{bmatrix} \begin{bmatrix} x \\ y \\ z \end{bmatrix},$$

where the rotation matrix Rx is given by:

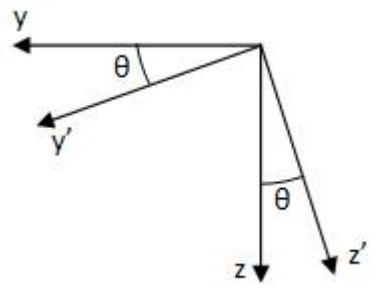

Figure 3.16: y-z plane and the angle θ

$$Rx = \begin{bmatrix} 1 & 0 & 0 \\ 0 & cos(\theta) & sin(\theta) \\ 0 & -sin(\theta) & cos(\theta) \end{bmatrix}$$

The y-z plane was tilted by the angle ψ, see Figure 3.17.

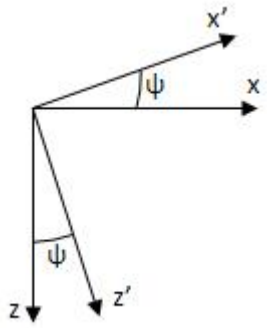

Figure 3.17: x-z plane and the angle ψ

The coordinate system can be written as:

$$\begin{bmatrix} x' \\ y' \\ z' \end{bmatrix} = \begin{bmatrix} cos(\psi) & 0 & -sin(\psi) \\ 0 & 1 & 0 \\ sin(\psi) & 0 & cos(\psi) \end{bmatrix} \begin{bmatrix} x \\ y \\ z \end{bmatrix},$$

where the rotation matrix Ry is given by:

$$Ry = \begin{bmatrix} cos(\psi) & 0 & -sin(\psi) \\ 0 & 1 & 0 \\ sin(\psi) & 0 & cos(\psi) \end{bmatrix}$$

The total rotation matrix R_{tot} can be either RxRy or RyRx. In 3D, the rotation matrices are commutative only for infinitesimally small angles, in this case, for the

angles θ and ψ, $R_{tot} = RxRy = RyRz$ RxRy = RyRx to two decimal places.

$$R_{tot} = \begin{bmatrix} -0.17 \\ 0.15 \\ 0.97 \end{bmatrix}$$

Consider that F is the load applied at the top of the stem: $F = \begin{bmatrix} 0 \\ 0 \\ F \end{bmatrix}$. Therefore Fx, Fy and Fz are equal to:

$$\begin{bmatrix} Fx \\ Fy \\ Fz \end{bmatrix} = \begin{bmatrix} -0.17F \\ 0.15F \\ 0.97F \end{bmatrix}$$

Contact analysis was carried out within Ansys using the Penalty method with surface-to-surface elements and contact detection at the Gauss points [152]. A stiffness of 6,000 N/mm was used and the force convergence tolerance was set to 0.5 %. An unsymmetric stiffness matrix was used to enable the solution to converge. Based on section 14.174 of Ansys Documentation, frictional contact analyses produce non-symmetric stiffness. If frictional stresses have an effect on the displacement field and the magnitude of the frictional stresses is solution dependent, the use of an unsymmetric stiffness matrix is more computationally efficient; as in such cases, any symmetric approximation to the stiffness matrix may result in a poor convergence rate.

3.3.4 Coefficient of friction

The literature review has demonstrated that the appropriate value of coefficient of friction to assign is not known although most studies suggest that a value between 0.1 and 0.5 [132, 152] is suitable. A parametric study was hence conducted to study the effect of the coefficient of friction on the finite element model predictions. In the present study, 30 values of the coefficient of friction were sampled within the range of 0.1 to 0.5.

The analysis was carried out using the mesh, boundary conditions, loading scenario and contact analysis employed previously. To enable comparison, the same failure criteria were studied to assess the effect of the friction value; i.e. the stem micromotion and bone strain. It should be noted that these investigations were carried out to obtain an appropriate friction value for the model and therefore the results are reported in this

section. As expected when the coefficient of friction was increased from 0.1 to 0.5, the maximum micromotion at the bone-implant interface decreased (Figure 3.18).

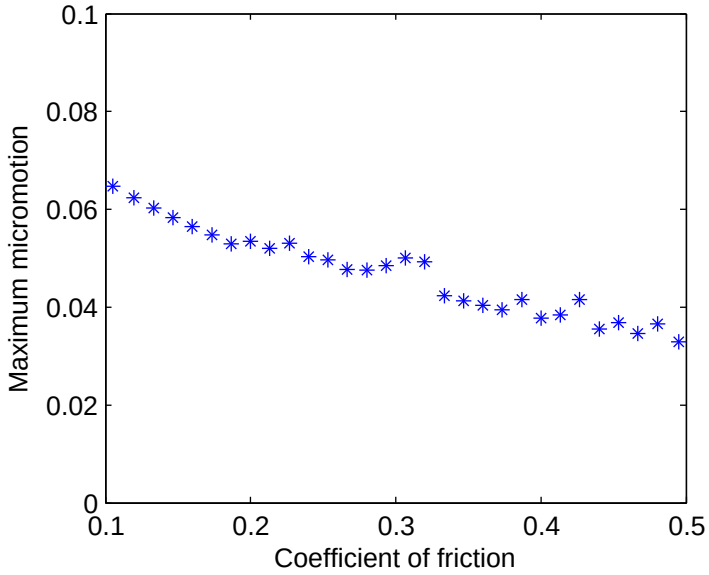

Figure 3.18: Maximum micromotion predicted at the bone-implant interface when the coefficient of friction varies from 0.1 to 0.5

The Von Mises bone strain volume was also computed. Figures 3.19 and 3.20 show that the average and maximum bone strain volume decreased as the coefficient of friction increased.

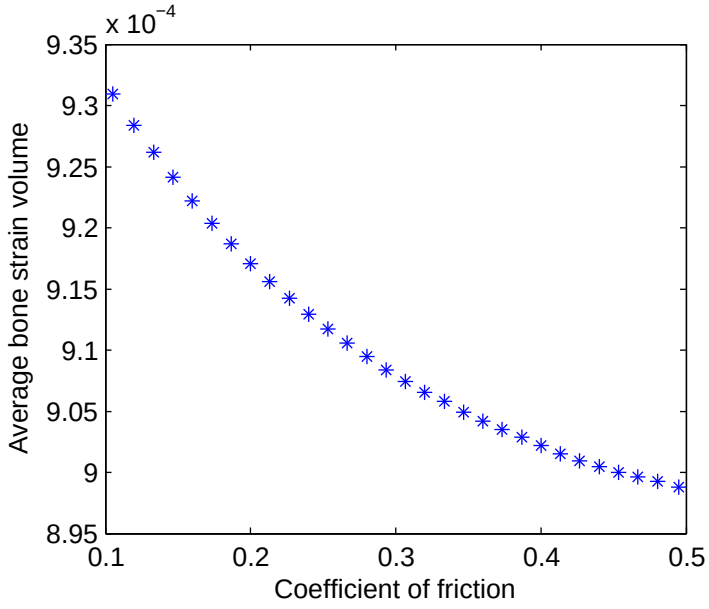

Figure 3.19: Average Von Mises bone strain volume measured at the bone-implant interface when the coefficient of friction varies from 0.1 to 0.5

The biomechanical responses at the implant-bone interface and within the bone depend strongly on the coefficient of friction applied at the bone-implant interface. It is clear

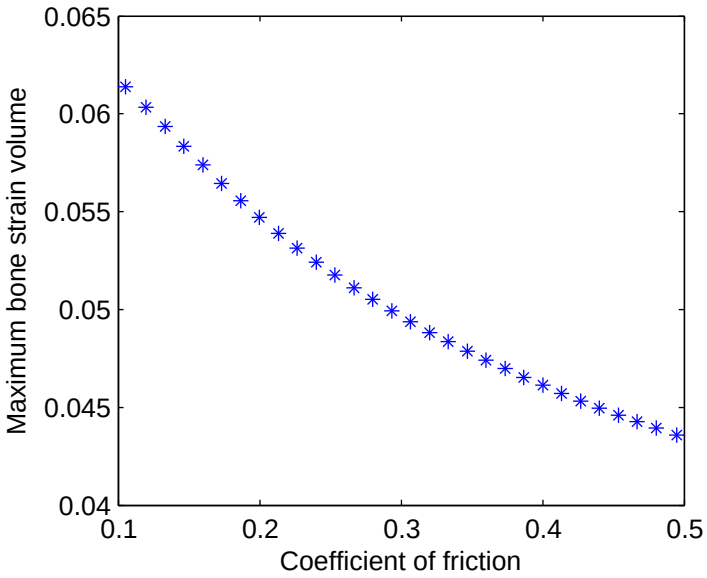

Figure 3.20: Maximum Von Mises bone strain volume measured at the bone-implant interface when the coefficient of friction varies from 0.1 to 0.5

that the variability is such that a single value of the coefficient of friction would be difficult to assign. However, there is a need of a single value for probabilistic studies where too many variables make the problem more complex. Therefore, the choice of the friction value was based on the literature review; for instance, a value of 0.3 was applied between the implant and the composite bone [49]. This study aimed to show that the use of such a value should be taken with caution.

3.3.5 Summary of modelling assumptions

In computational work it is often necessary to make some assumptions as all parameters cannot be considered or accurately modelled; for example, physiological loads such as muscles and ligaments are sometimes not included. This is usually related to a lack of computational resources. In addition, despite the terminology of "total hip replacement" used, the study was carried out only on the femoral component whereas the cup of the total hip replacement was not taken into account, even though it also suffers complications. In FEM, a number of common assumptions are regularly applied, in this project these include:

- the implant bed (hole made in the bone for the implant) had the same shape as the external surface of the stem
- the size of the mesh is subject to a compromise between a fine mesh density and computational cost
- an approximation of materials properties (Young's modulus, density, Poisson's

ratio)

- the boundary conditions can vary, in particular the distal part of the femur is normally fully constrained
- a point load is applied through the centre of the top of the stem as three forces: Fx, Fy and Fz
- all materials were assumed to be homogeneous, isotropic and with linear elastic behaviour
- the coefficient of friction at the bone-implant interface was constant

3.4 Comparison of computational and experimental results

The axial motion of the implant was measured at the proximal shoulder and at the distal tip of the implant. Figure 3.21 shows the implanted bone for both the experimental and computational tests.

For the first cycle, implant micromotion calculated proximally using finite element analysis was $61.3\mu m$ compared to the experimental value of $59.6\mu m$. At the distal end, the implant micromotion from FEA was $168.9\mu m$ compared to $170\mu m$ experimentally.

Bone strain was measured experimentally and predicted computationally. As an example, the maximum principal strain over the bone surface was variable and the strain value varied from 0 to 0.05% for both the experimental test and computational study. It is worth mentioning that the digital image correlation system identified qualitatively similar strain patterns (Figure 3.22).

3.5 Concluding remarks

Implant micromotion and bone strain have been identified as good indicators of implant performance with respect to loosening [53]. This chapter consisted of analysing a single implant orientation while a static load was applied at the top of the femoral head. The aim of this study was to define and assign parameters for the contact analysis and verify them by conducting experimental tests.

In order to create the three-dimensional meshed model, several techniques and methods were used, such as image processing, computer-aided design, mesh and finite element software. The choice of software was based on either availability within the School of

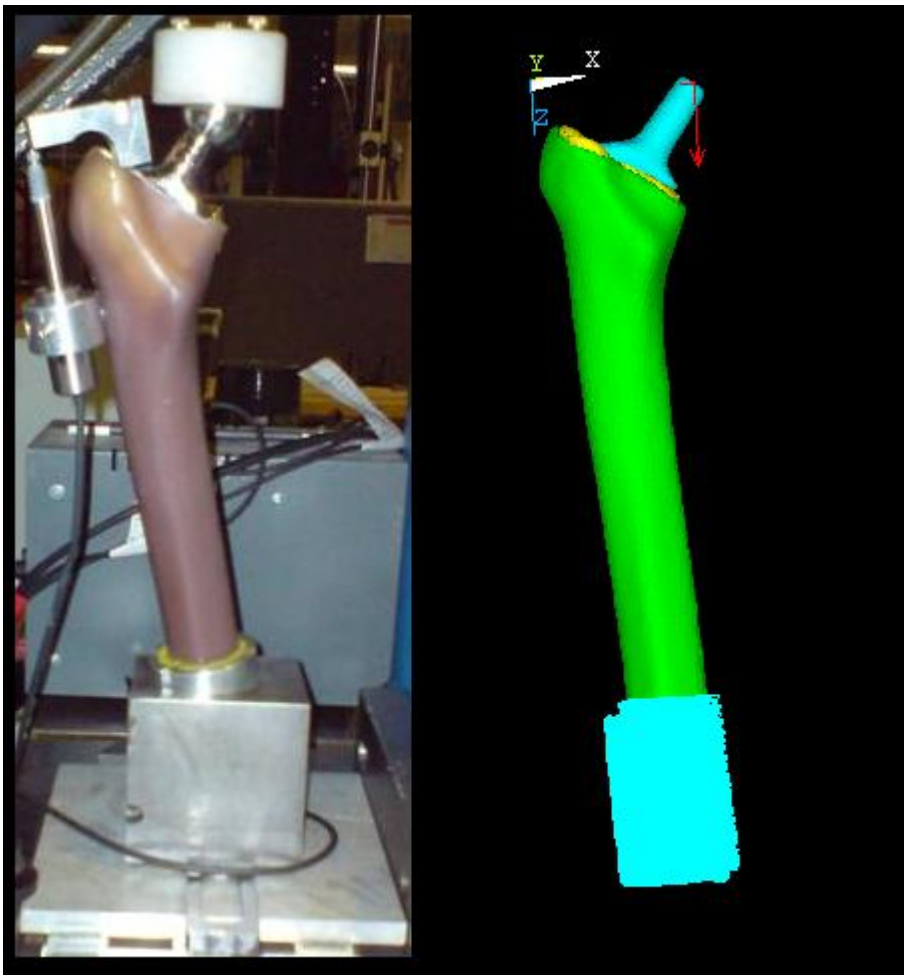

Figure 3.21: Tests of the implanted synthetic bone: experimental test (left) and "virtual" test (right)

Engineering Sciences (University of Southampton, UK) or familiarity with the software or the one that was most appropriate for the project. For instance, Rhinoceros software was first used to carry out Boolean operations to implant the stem into the bone. Even though, its use was successful with other projects [53], it has been noted that many problems occurred with an *.stl model while using boolean operations; as an example, if one element of the bone was aligned with one element of the implant, the intersection between the two components would not be found which failed the boolean operation. To avoid this, Simpleware software were used to first create the three-dimensional model and then carry out the boolean operations. The use of these software offered the advantage of creating the implanted bone in one single package avoiding problems due to compatibility between software. However, it should be noted that the software is based on voxelisation and so if the voxel size is bigger than the volume mesh size, i.e. if the pixel size of the CT data and the spacing are bigger, the implant geometry would be modified, which would affect the implant geometry. In other words, if the voxel size is smaller than the volume mesh size, it is believed that it would not affect

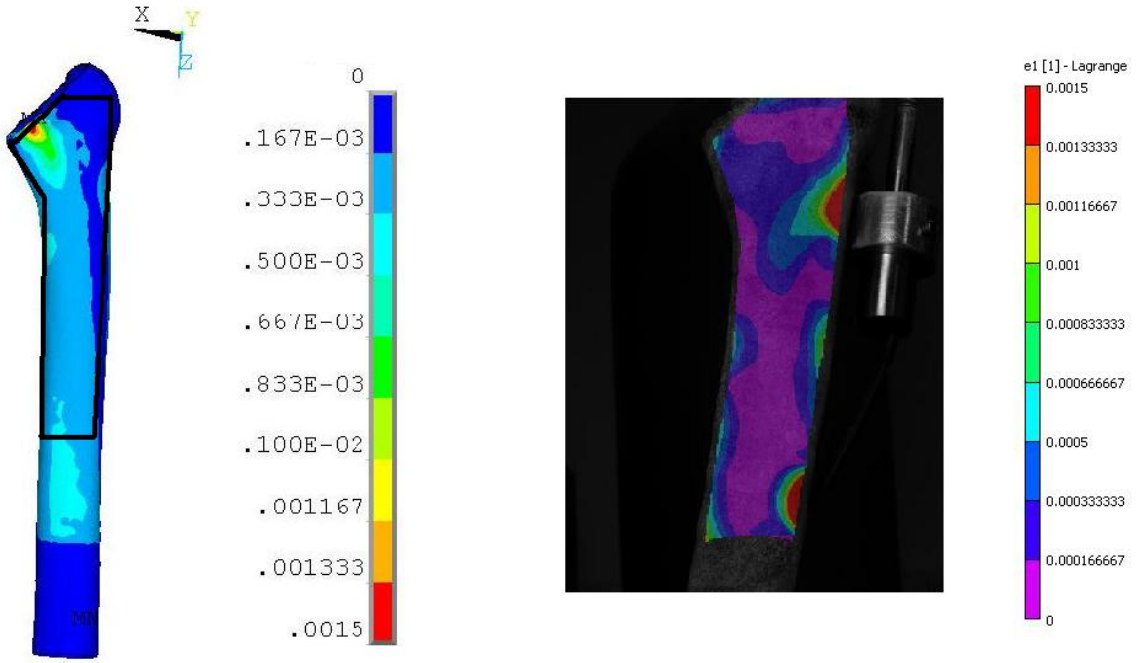

Figure 3.22: Maximum principal strain - from left to right: FEA and DIC results

the final results. Once the 3D model was created, its mesh was then generated in Ansys Icem and different mesh size was assigned to each component. In the present study, four-noded tetrahedral elements were used, which approximated well the model [126]. In their study, Ramos and Simões [126] compared tetrahedral and hexahedral elements of the proximal part of the femur, and they observed that the model consisting of tetrahedral linear elements provided results close to experimental ones. However, they also noted that the biomechanical responses were less affected by the mesh refinement when using hexahedral quadratic elements.

After creating the meshed model, Ansys was used to solve the finite element analysis. For the contact analysis, the Penalty Method was used in which virtual springs are applied to surfaces in contact to minimize interpenetration but some interpenetration is allowed. This method is a spring-damping system; it results in oscillatory behavior and considerable penetration. It is reliable and fast for computing contact and friction forces [23]. This method was used in previous work for modelling an implanted composite bone by Viceconti et al. [152]. In this present work, a contact stiffness of 6000 N/mm and a coefficient of friction of 0.3 were used, which were also used previously by Viceconti et al. [152]. In their work, they showed that 6000 N/mm of contact stiffness produced a maximum compenetration of 7 μm. These parameters fitted well the model as a good correlation with the experimental test was demonstrated during the static test.

In the computational work, a number of assumptions were applied, in particular:

(i) the surrounding soft tissue was not considered

(ii) the synthetic bone was elastic and isotropic

(iii) the implant bed (hole made in the bone for the implant) had the same shape as the external surface of the stem (in common with other studies)

(iv) the distal part of the femur was fully constrained at 9° flexion and 10° adduction to recreate a standard set up (BS 7206: Part4: 2002)

(v) the mesh consisted of linear tetrahedral elements [12, 53, 21]

(vi) the coefficient of friction at the bone/implant interface was constant [12]

In the experimental study, the implant micromotion was measured along the longitudinal axis of the implant and the measurement was carried out relative to the bone as the LVDT was attached to the bone and in contact with the implant. It was observed that the axial motion of the stem was quite small when a force equivalent to two body weight load was applied, which could be explained by the fact that the collar of the stem may prevent high micromotion. In a study assessing the effect of a collared stem, Whiteside and Easley [159] compared the primary stability of collared and collarless cementless implant by measuring implant micomotion and migration. Cadaveric bones were implanted and axial cyclic tests were performed. In their study, they observed that the collared femoral component did not migrate distally and the fixation did not fail, however there was no record on the effect of the collar on micromotion. Nevertheless, they noticed that tight distal fit minimises micromotion.

The technique employed to measure implant motion consisted of two LVDTs. One of them was fixed inside the medullary canal and was directly in contact with the tip of the stem, the other one was fixed on the proximal lateral aspect of the bone and was in contact with a target device attached to the shoulder of the stem. The tip of the stem was more constrained to axial movement, and therefore the LVDT measuring the motion at the tip of the stem was more likely to produce realistic results. However, this configuration may lead to a slippage of the tip of the stem against LVDT; but this would not be observed while carrying out the experimental test as the LVDT was fixed inside the medullary canal. The shoulder of the stem was far less constrained; but the test set-up allowed only measurements along the axial direction. Therefore, if the motion at the shoulder of the stem occurred in other directions, whole information on implant movement would be not complete. However, it should be noted that most of the bone surface needed to be kept free as an optical system was used for bone strain measurements.

The strain over the bone surface was measured using a DIC system. To the authors' knowledge there has been no study using the DIC technique on an implanted cementless

total hip replacement to date. In previous studies, strain gauges have been widely used to measure the bone strain [30, 42, 48, 140]. These provide excellent resolution, but are limited to area specific measurements and rely heavily on the correct choice of gauge and surface preparation. DIC can provide a map of strains and is a non-contact technique. However, the bone surface has to be prepared carefully to get a good contrast; for instance, white paint and black speckle patterns need to be applied on the bone surface and the specimen needs to be lit with a standard white light source to get a good image acquisition. Notwithstanding these limitations, the experimental test demonstrated the ability of the DIC technique for synthetic bone testing and the measurement of small deformations. The good correlation with experimental results imparts confidence on the computational model, which formed the basis of the study presented in Chapter 4 that considered implant angle variability. It should be noted that this technique has been rarely correlated with strain gauges and therefore the present study focussed on DIC approach for bone strain measurements. Validation of this technique is investigated later in chapter 5.

Chapter 4

Computational and Experimental Investigations into Effect of Implant Orientation

Chapter 3 introduced a computational method to assess the primary stability of the implant for a single orientation along with experimental validation. This chapter contains computational and experimental results for various implant orientations. In this study, the mesh created in chapter 3 was used as a baseline mesh to generate new implant orientations. The computational study used a mesh morphing technique to automatically update the baseline mesh for each new implant position. The data generated via design of computer experiments is used to construct a Bayesian Gaussian process model which can be thought of as a computationally cheap emulator or approximation model. The emulator is subsequently postprocessed to estimate: (1) the sensitivity of the biomechanical response to implant orientation variables and (2) orientations that lead to worst-case values of the response quantity of interest. Experimental studies were conducted for worst-case implant positions estimated using the Bayesian Gaussian process model and the results are compared to those obtained for the neutral implant position presented earlier in Chapter 3. LVDTs were used to measure implant motions and the DIC technique was employed for bone strain measurements.

4.1 Automatic model construction using mesh morphing

The computational method used in chapter 3 would be a very laborious and time consuming task to study the effect of various implant orientations; as it requires (i) the

creation of a 3D model of the implanted bone for each implant position, (ii) generation of the mesh of each implanted bone, and (iii) finite element analysis of each implanted bone. Therefore, a mesh morphing strategy was employed to automatically create a mesh for each new implant position.

4.1.1 Mesh morphing approach

The following paragraphs summarize the main steps of the mesh morphing technique. The implant and bone were first fully bonded in order to produce common nodes at the interface. After reading the mesh of the implanted bone, the implant was debonded from the bone to virtually test the performance of the stem shortly post implantation. A local reference system was defined at the distal end of the stem. The z axis was aligned to the longitudinal axis of the stem pointing towards the proximal end of the stem; this axis was the axis of rotation of the retroversion/anteversion angle; the y axis, which was in the transverse plane was the axis of rotation of the varus/valgus angle and the x axis was orthogonal to the two previous axes and was the axis of rotation of the flexion/extension angle. A rigid body transformation matrix TM was applied to each node's coordinates of the implant to modify its position according to the angles α, β and γ which were rotations around the z, y and x axis respectively.

$$TM = \begin{bmatrix} \cos(\alpha)\cos(\beta) & \cos(\alpha)\sin(\beta)\sin(\gamma) - \sin(\alpha)\cos(\gamma) & \cos(\alpha)\sin(\beta)\cos(\gamma) + \sin(\alpha)\sin(\gamma) \\ \sin(\alpha)\cos(\beta) & \sin(\alpha)\sin(\beta)\sin(\gamma) - \cos(\alpha)\cos(\gamma) & \sin(\alpha)\sin(\beta)\cos(\gamma) - \cos(\alpha)\sin(\gamma) \\ -\sin(\beta) & \cos(\beta)\sin(\gamma) & \cos(\beta)\cos(\gamma) \end{bmatrix}$$

The nodes at the bone-implant interface were subjected to the displacements prescribed by the new orientation of the implant, but the nodes at the outer surface of the bone were allowed to move only tangentially to the surface; the displacements along the normal directions were constrained to zero. The nodes at the cutting plane of the femoral head were also allowed to move only in-plane and the displacements along the normal direction are constrained.

A linear elasticity analysis was carried out to estimate the vertices of the morphed mesh [21]. Equations governing a linear elastic boundary value problem are based on three equations: equation of motion (an expression of Newton's second law), Cauchy stress tensor and strain-strain equations. The equations are described as follows:

$$\nabla.\sigma + \mathbf{F} = \mathbf{0} \quad \text{on} \quad \mathbf{\Omega}, \tag{4.1}$$

where ∇ is the Laplacian operator (differential operator), σ is the Cauchy stress tensor, $\mathbf{F}$ is the external body force vector and Ω corresponds to the domain of interest. In

linear elasticity, the Cauchy stress tensor is given by:

$$\sigma = \lambda Tr(\varepsilon(\mathbf{y}))\boldsymbol{I} + 2\mu\varepsilon(\mathbf{y}), \tag{4.2}$$

where λ and μ are the Lamé constants, Tr() is the trace operator, $\mathbf{y}$ is the displacement, $\mathbf{I}$ is the identity tensor and $\varepsilon(\mathbf{y})$ is the strain tensor defined as:

$$\varepsilon(\mathbf{y}) = \frac{1}{2}(\nabla\mathbf{y} + (\nabla\mathbf{y})^T)$$

The following Dirichlet and Neumann boundary conditions were used with the governing equations:

$$y = g \ \text{ on } \ \Gamma_g \text{ and } \ n.\sigma = h \ \text{ on } \ \Gamma_h, \text{ where n is the surface normal.} \tag{4.3}$$

The integrals that appear in FE analysis can be written in general form as:

$$\int_{\Omega} [.]\mathrm{d}\Omega = \sum_{e} \int_{\Xi} [.]^e J^e \mathrm{d}\Xi, \tag{4.4}$$

where $[.]$ is the term being integrated, Ω is the spatial domain, Ξ is the FE parent domain and J^e is the Jacobian for element e defined as: $J^e = det(\delta\mathbf{x}/\delta\xi)^e$. $\mathbf{x}$ and ξ are the vectors of physical and local coordinates.

Equation (4.4) can be also written as:

$$\int_{\Omega} [.]\mathrm{d}\Omega = \sum_{e} \int_{\Xi} [.]^e \left(\frac{J^0}{J^e}\right)^{\chi} \mathrm{d}\Xi, \tag{4.5}$$

where J^0 is an arbitrary scaling factor and χ is a positive stiffening power parameter.

The process used consists of applying a virtual high Young's modulus EX to each element of the bone by using the volume of the element VOL:

$$EX = k\left(\frac{1}{VOL}\right)^{\chi}, \tag{4.6}$$

where k is a constant arbitrarily chosen and χ dictates the degree for mesh morphing. χ was defined by analysing the mesh of the extreme positions of the stem, limiting the distortion of the morphed elements. When the element volume was smaller, the virtual Young's modulus assigned was higher in order to consistently deform the mesh. It is worth noting here that linear elasticity analysis was carried out only to compute the

vertices of the morphed mesh. After the mesh has been morphed, contact analysis is carried out to predict the biomechanical response of the bone-implant construct.

4.1.2 Effect of implant pivot position on micromotion and strain

In the previous analysis (Section 4.1.1), the distal tip of the femoral component was set as a pivot point to rotate the implant in three degrees of freedom. To justify the choice of this reference point, a statistical analysis was carried out on the impact of the pivot point on the micromotion and strain outputs. In this study, two logical points were assessed: the distal tip (see Figure 4.1a) and the centre of the stem (see Figure 4.1b). In Figure 4.1, 'Ant/Ret' stands for anteversion/retroversion angle, 'Var/Val' stands for varus/valgus angle and 'Ant/Post' stands for anterior/posterior angle.

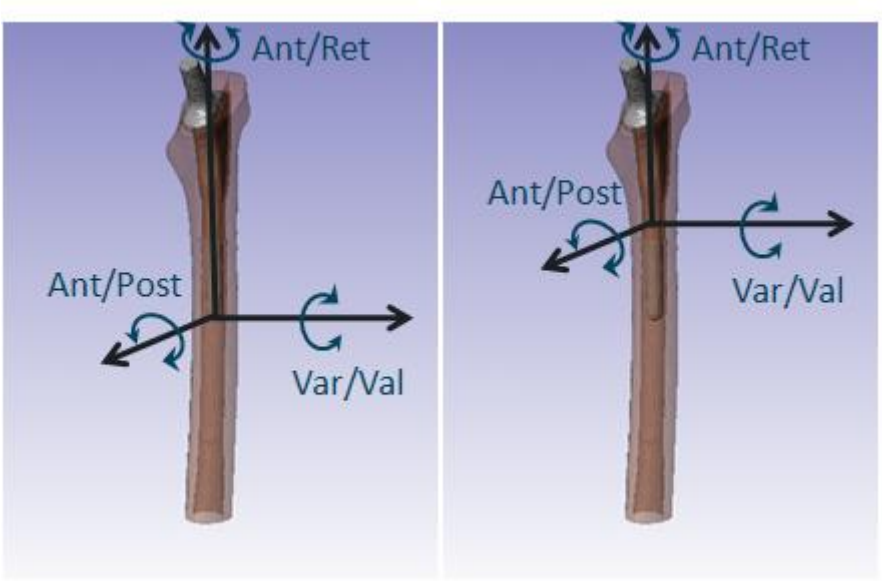

(a) (b)

Figure 4.1: Pivot point rotation: (a): at the distal tip of the femoral component; (b): in the middle of the femoral component

The generated mesh was used as a baseline mesh and the implant position was modified using these two different pivot points for the three rotational degrees of freedom of the implant. When the tip of the stem was the pivot point, the implant could rotate within these ranges[1]:

- anterversion/retroversion angle = $[-15\,°; 8\,°]$
- varus/valgus angle = $[-2\,°; 3.6\,°]$
- anterior/posterior angle = $[-1.8\,°; 1.2\,°]$

[1]Note that if the implant rotates outside this range then it will move outside the bone

When the middle of the stem was the pivot point, the implant could rotate within these ranges:

- anterversion/retroversion angle = $[-15\,°; 8\,°]$
- varus/valgus angle = $[-6\,°; 6.6\,°]$
- anterior/posterior angle = $[-5.5\,°; 4\,°]$

A computational design of experiments was used to define a set of implant positions for these two configurations and the mesh morphing technique was employed to automatically update the baseline mesh. As explained in Section 4.1.1, a contact analysis was run in Ansys (Ansys INC, Canonsburg, PA) for each implant position and face-to-face elements were used to generate a contact pair between the synthetic bone and the implant. The Penalty method was used to solve the analysis with a contact stiffness of 6000 N/mm and a friction coefficient of 0.3 [152]. The analysis simulated a load of -1.6 kN, i.e. two times body weight, applied to the head of the implant.

Two biomechanical metrics were investigated: the bone-implant micromotion and bone strain and a statistical t-test was carried out in Matlab to compare the mean value of each metric for both pivot positions.

It was observed that although the outputs varied slightly, the difference was not statistically significant at the p=0.05 level. As an example, see Figures 4.2a and 4.2b, which shows the box plots of two outputs: maximum nodal micromotion and maximum volume strain of the bone.

Thus, the position of the reference point for implant movement in probabilistic analyses of the implanted hip does not appear to affect the response of the construct in terms of implant micromotion and bone strain. Thereby, it was fixed in the distal tip of the femoral component.

4.2 Gaussian process modelling

This section outlines the Bayesian Gaussian process modelling approach on the studies carried out by Kolachalama et al. [83]. In the present project, the computational model consisted of the implant orientation as input, i.e. rotational degrees of freedom of the implant, and the implant micromotion and bone strains were computed for each implant orientation as scalars. For clarity this section considers a model with an input vector $\mathbf{x} \in \mathbb{R}$ and a scalar output $\omega(x)$.

A design of computer experiments was employed to define the inputs of the model, i.e. the ante-retoversion, varus-valgus and ante-posterior angles of the implant po-

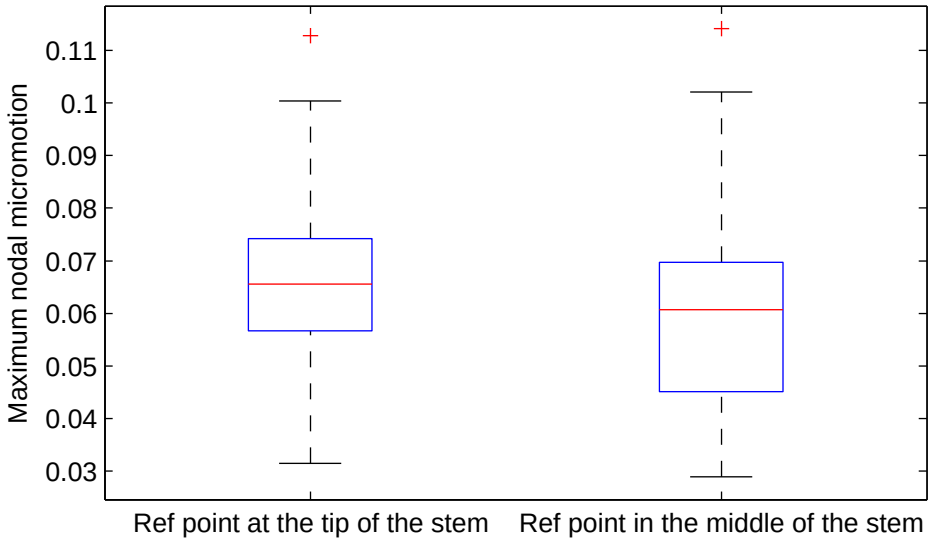

(a)

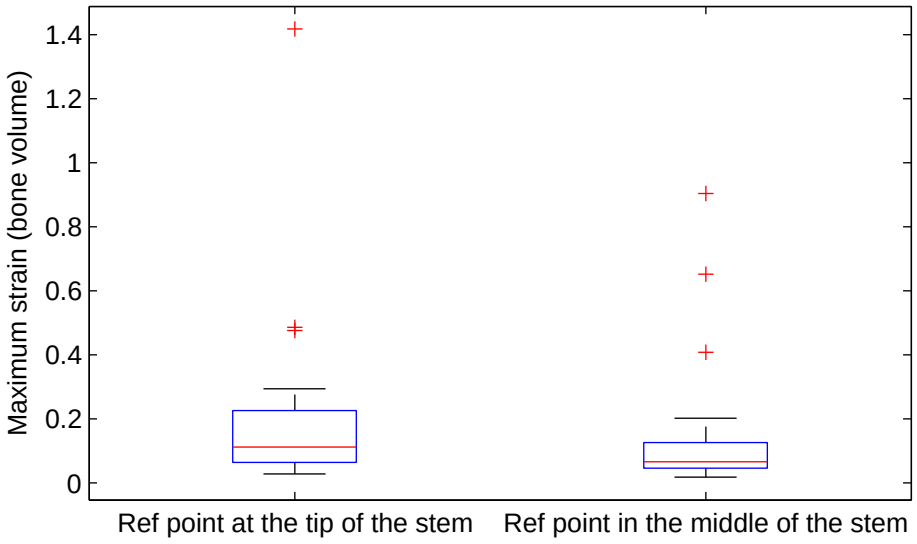

(b)

Figure 4.2: Box plots comparing the two references points for two outputs: (a): Maximum nodal micromotion; (b): Maximum volume strain of the bone

sition. To this end, a Latin Hypercube Sampling was used to define random input implant orientation within a selected range of angles from the neutral position. The datasets can be written as: $\mathscr{D} = \{X, y\}$, where $X = \left\{\mathbf{x}^1, \mathbf{x}^2, \ldots, \mathbf{x}^l, \right\} \in \mathbb{R}^{p \times l}$ and $y = \left\{\omega^1, \omega^2, \ldots, \omega^l\right\} \in \mathbb{R}^l$. Here, p denotes the number of input variables and l denotes the number of observations used to construct the Bayesian Gaussian process model.

The assumption made is that the outputs $\omega^1, \omega^2, \ldots, \omega^l$ are considered the realization of a Gaussian random field with parameterized mean and covariance functions. The model for the emulator can be written as:

$$Y(\mathbf{x}) = \beta + Z(\mathbf{x}), \tag{4.7}$$

where β is an unknown hyperparamater to be estimated from the data and $Z(\mathbf{x})$ is a Gaussian stochastic process with zero-mean and covariance:

$$Cov(Z(\mathbf{x}), Z(\mathbf{x}')) = \sigma_Z^2 R(\mathbf{x}, \mathbf{x}'), \tag{4.8}$$

where $R(\mathbf{x}, \mathbf{x}')$ is a correlation function that can be tuned to the training dataset and σ_Z^2 is the process variance which is another parameter to be estimated from the data. By definition, R must be positive-definite. A commonly used choice of correlation function is the stationary family which obeys the product correlation rule:

$$R(\mathbf{x}, \mathbf{x}') = \prod_{j=1}^{p} exp(-\theta_j |x_j - x_j'|^{p_j}), \tag{4.9}$$

where $\theta_j \geq 0$, $2 \geq p_j > 0$, $j = 1, 2, \ldots, p$ are the hyperparameters. θ is then used to denote the vector of hyperparameters. p_j was chosen to be equal to 2 to reflect the belief that the underlying function being modelled is smooth and infinitely differentiable.

The Bayesian approach involves two steps of inferencing. The first step of inferencing aims to estimate the unknown hyperparameters from the given dataset $\mathscr{D}$, using the Bayes theorem:

$$P(\theta, \beta, \sigma_Z^2 | \mathscr{D}) = \frac{P(\mathscr{D} | \theta, \beta, \sigma_Z^2) P(\theta, \beta, \sigma_Z^2)}{P(\mathscr{D})}, \tag{4.10}$$

where $P(\theta, \beta, \sigma_Z^2 | \mathscr{D})$ is the posterior probability of the hyperparameters, $P(\mathscr{D} | \theta, \beta, \sigma_Z^2)$ is the likelihood, $P(\theta, \beta, \sigma_Z^2)$ is the assumed prior for the hyperparameters and $P(\mathscr{D})$ is a normalizing constant called the evidence.

The second step of inferencing uses the estimated hyperparameters to estimate the value of the unkown function $\omega(x)$ at a new implant orientation x. The prediction of the emulator at $\mathbf{x}$ can be written as : $Y(x) = \mathscr{N}(\hat{Y}(x), C(x, x'))$. The posterior mean and covariance can therefore be written as:

$$\hat{Y}(\mathbf{x}) = \beta + \mathbf{r}(\mathbf{x})^T \mathbf{R}^{-1} (\mathbf{y} - \mathbf{1}\hat{\beta}), \tag{4.11}$$

and

$$C(\mathbf{x}, \mathbf{x'}) = \sigma_Z^2(R(\mathbf{x}, \mathbf{x'}) - \mathbf{r}(\mathbf{x})^T\mathbf{R}^{-1}\mathbf{r}(\mathbf{x'})), \tag{4.12}$$

where $\mathbf{R} \in \mathbb{R}^{l\times l}$ is the correlation matrix computed using the training points whose ijth element is computed as $\mathbf{R}_{ij}$ is the correlation between the new point x and the training points, and $\mathbf{1} = \{1, 1, \ldots, 1\} \in \mathbb{R}^l$:

$$\mathbf{R}_{ij} = \mathbf{R}(\mathbf{x}^{(i)}, \mathbf{x}^{(j)}) \text{ and } \mathbf{r}(\mathbf{x}) = \left\{\mathbf{R}(\mathbf{x}, \mathbf{x}^{(1)}), \mathbf{R}(\mathbf{x}, \mathbf{x}^{(2)}), \ldots, \mathbf{R}(\mathbf{x}, \mathbf{x}^{(l)})\right\} \in \mathbb{R}^l \tag{4.13}$$

For the computational efficiency, the Cholesky decomposition of R is computed, which allows the posterior mean to be computed at any implant orientation of interest using a vector-vector product, i.e., $\hat{Y}(\mathbf{x}) = \beta + \mathbf{r}(\mathbf{x})^T\mathbf{w}$, where $\mathbf{w} = \mathbf{R}^{-1}(\mathbf{y} - \mathbf{1}\hat{\beta})$.

In the Bayesian approach, the hyperparameters $\theta = \{\theta_j\}$, $j = 1, 2, \ldots, p$, and $P(\theta, \beta, \sigma_Z^2)$ in the correlation function defined in equation 4.12 are estimated by maximizing the likelihood function, which provides the values of the hyperparameters most likely to have generated the training dataset. The likelihood function is given by:

$$P(\mathscr{D}|\theta, \beta, \sigma_Z^2) = \frac{1}{(2\pi\sigma_Z^2)^{l/2}|\mathbf{R}|^{1/2}} \times \exp(-\frac{(\mathbf{y} - \mathbf{1}\beta)^T\mathbf{R}^{-1}(\mathbf{y} - \mathbf{1}\beta)}{2\sigma_Z^2}), \tag{4.14}$$

The negative log-likelihood function to be minimized is:

$$L(\theta, \beta, \sigma_Z^2) = -\frac{1}{2} \times (l \ \ln\sigma_Z^2 + ln|\mathbf{R}| + \frac{(\mathbf{y} - \mathbf{1}\beta)^T\mathbf{R}^{-1}(\mathbf{y} - \mathbf{1}\beta)}{\sigma_Z^2}), \tag{4.15}$$

To estimate the unknown parameters, numerical optimization techniques are required for the maximization of equation 4.15.

Once the emulator is constructed, the next step consisted of validating the model.This was carried out, by running additional finite element code for extra implant orientation and checking the values predicted by the emulator by the finite element outputs. This method was found to be time consuming as each contact analysis required approximatively 45 minutes. Therefore, another method was used to assess the accuracy of the emulator. The accuracy of the prediction error estimate, i.e. the posterior variance $C(x, x)$ depends on the validity of the assumptions made in creating the emulator. The standardized cross validation residual (SCVR) can be used for model diagnostics.

$$SCVR_i = \frac{\omega(\mathbf{x}^{(i)}) - \hat{Y}_{-i}(\mathbf{x}^{(i)})}{\sqrt{C_{-i}(\mathbf{x}^{(i)}, \mathbf{x}^{(i)})}}, i = 1, 2, \ldots, l \tag{4.16}$$

where $\hat{Y}_{-i}(\mathbf{x})$ and $C_{-i}(\mathbf{x},\mathbf{x})$ are the mean and variance of the prediction for an implant orientation $\mathbf{x}$ without using the i^{th} training point. $SCVR_i$ can therefore be computed for all training points removing the data of the corresponding points from the correlation matrix $\mathbf{R}$.

It is assumed that the maximum likelihood estimates for the hyperparameters is not subject to change when a point is removed form the training dataset. When $SCVR_i$ is roughly in the range $[-3,+3]$, the Gaussian model is considered as appropriate, which means that the emulator predicts the output of a new implant orientation in the range $\left[\hat{Y}(\mathbf{x})-3\sqrt{C(\mathbf{x},\mathbf{x})},\hat{Y}(\mathbf{x})+3\sqrt{C(\mathbf{x},\mathbf{x})}\right]$ with high level of confidence.

A sensitivity analysis can then be carried out to identify the input-output relationship. To this end, the effect of each input, i.e. ante-retoversion, varus-valgus and ante-posterior angles of the implant position, is isolated from the others. The response can be decomposed into main effects for each input and this main effect of the i^{th} input variable as follows:

$$\omega_i(x_i) = \frac{1}{V}\int Y(\mathbf{x}) \prod_{h\neq 1} dx_h. \tag{4.17}$$

The sensitivity trends S_i can also be calculated for each variable in terms of main effect ω_i as follows:

$$S_i = \frac{\int \omega_i^2(x_i)dx_i}{\sum_{j=1}^{p}\int \omega_j^2(x_j)dx_j} \tag{4.18}$$

4.3 Computational parameter variation studies

To assess the effect of the implant positioning, a contact analysis was carried out for each implant position. The tip of the stem was defined as a reference point and the implant position was modified within a selected range of angles from the neutral position (anterversion/retroversion angle = $[-15\,°; 8\,°]$, varus/valgus angle = $[-2\,°; 3.6\,°]$ and anterior/posterior angle = $[-1.8\,°; 1.2\,°]$). The present investigation uses a mesh morphing technique developed by Bah et al. [21] to automatically update the baseline mesh for each new implant position. A computational design of experiments methodology was employed to study the biomechanical response for 28 implant positions (using the Latin Hypercube Sampling).

Several outputs were investigated:

- micromotion at the bone-implant interface

- longitudinal displacements of the implant where the LVDTs were attached
- surface bone strains

The micromotion of each element was calculated in Ansys as a vector sum of the sliding distance and the gap distance. Longitudinal displacements of the stem at the distal end and shoulder of the stem were also measured for comparison with the experimental test. Surface bone strains were also analysed for comparison with DIC results.

The resulting data from the computational modelling was used to construct a Bayesian Gaussian process model that mapped the implant orientations to a set of biomechanical response metrics: implant motion and bone strain. The code used to build the Bayesian Gaussian process model was developed by Kolachalama et al. [83]. The emulators were subsequently validated using the leave-one-out tests described in Section 4.2. Postprocessing was then carried out to estimate the main effects and the sensivities of the output metrics with respect to the implant orientation variables.

The following outputs were computed in Ansys for 28 implant positions in order to assess their effects on the primary stability:

- strain over the cortex of the bone
- strain in bone volume
- micromotion at the interface
- displacement at the distal end of the stem
- displacement at the shoulder of the stem

Gaussian process models were constructed for all the five outputs listed above using the dataset obtained via 28 FE runs. The results obtained using the emulator constructed for the displacement at the distal end of the stem, shoulder of the stem and the maximum micromotion at the bone-implant interface are shown in Figures 4.3, 4.4 and 4.5, respectively. Each figure has been divided into four subplots. The subplot (a) shows the value predicted by the emulator against the actual value in a leave-one-out cross-validation test. The subplot (b) depicts the SCVR values for the corresponding emulator (see equation (4.16)). These two subplots hence provide measures of predictive capability of the emulator. Subplots (c) and (d) show the main effects and the sensivities of the output under consideration with respect to the implant orientation variables. In each figure, 'Ant/Ret' stands for anteversion/retroversion angle, 'Var/Val' stands for varus/valgus angle and 'Ant/Post' stands for anterior/posterior angle.

Figures 4.3, 4.4 and 4.5 show that predicted values by the emulator correlate well with the real values. Moreover, the SCVR lie within the interval [-3,3] which means

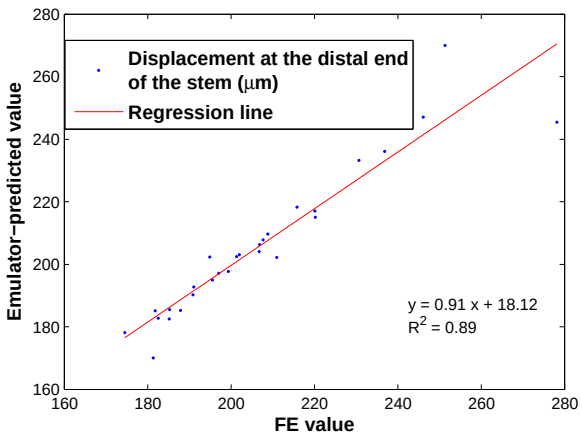

(a) Predicted value vs. actual value

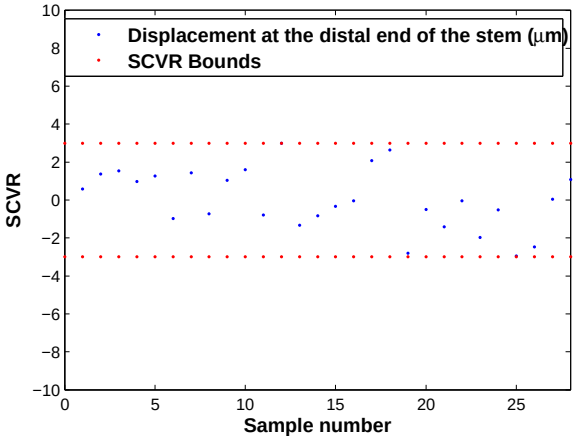

(b) SCVR when 28 training points are used

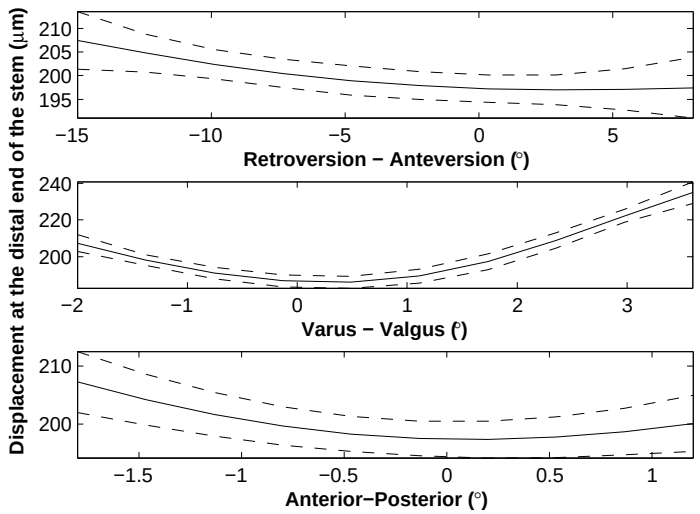

(c) Main effect

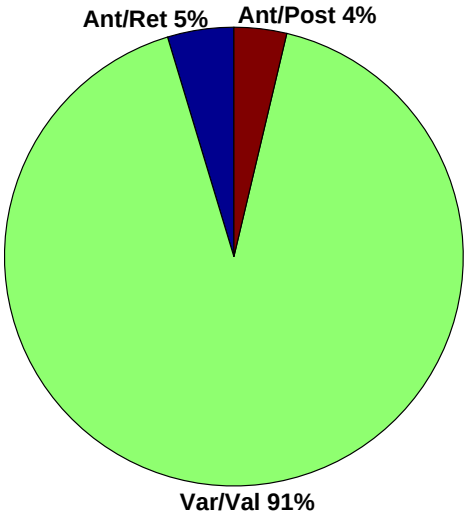

(d) Sensitivity results

Figure 4.3: Displacement at the distal end of the stem

that the approximation by the emulator was satisfactory. For the displacement at the distal end of the stem and maximum micromotion at the bone-implant interface, the sensitivity was highest for the varus/valgus angle; whereas the model was more sensitive to the anteversion/retroversion angle for the displacement at the shoulder of the stem. For the displacement at the distal tip of the stem, the sensitivity was highest for the varus/valgus angle (91%), followed by the anteversion/retroversion angle (5%) and the anterior/posterior angle (5%). For the maximum micromotion at the bone-implant interface, the sensitivity was highest for the varus/valgus angle (67%), followed by the the anterior/posterior angle (18%) and the anteversion/retroversion angle (15%). For the displacement at the shoulder of the stem, the sensitivity was highest for the anteversion/retroversion angle (74%), followed by the the varus/valgus angle (21%) and the anterior/posterior angle (4%). The emulators for each metric were run at 10,000 orientations within the bounds specified earlier to estimate the angles at which these

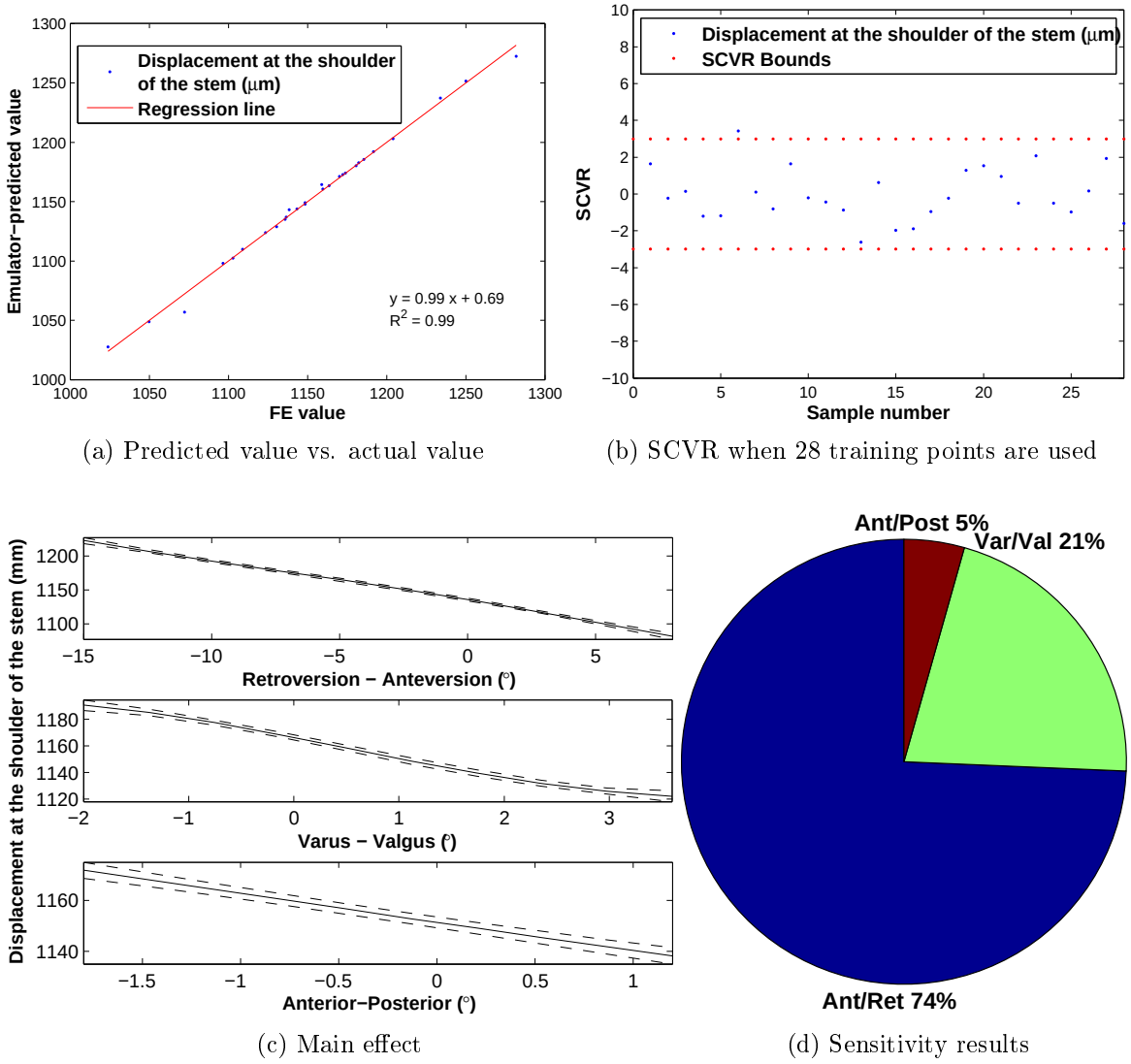

(a) Predicted value vs. actual value

(b) SCVR when 28 training points are used

(c) Main effect

(d) Sensitivity results

Figure 4.4: Displacement at the shoulder of the stem

outputs take maximum value. At the shoulder of the stem, the maximum displacement was found for an angle of $-14.7°$ for anteversion/retroversion angle, $-2.0°$ for the varus/valgus angle and $1.2°$ for the anterior/posterior angle. These values were chosen as critical angles for the experimental tests.

In summary, when the tip of the stem was kept as a reference point it was found that the implant micromotion and bone strain were most sensitive to variations in the varus/valgus angle. In particular, an increased varus angle resulted in higher strains and micromotions. For the experimental investigation, the implant orientation leading to a maximum displacement at the shoulder of the stem was considered as a 'poor' implant orientation; i.e. an implant orientation of $-14.7°$ for anteversion/retroversion angle, $-2.0°$ for the varus/valgus angle and $1.2°$ for the anterior/posterior angle.

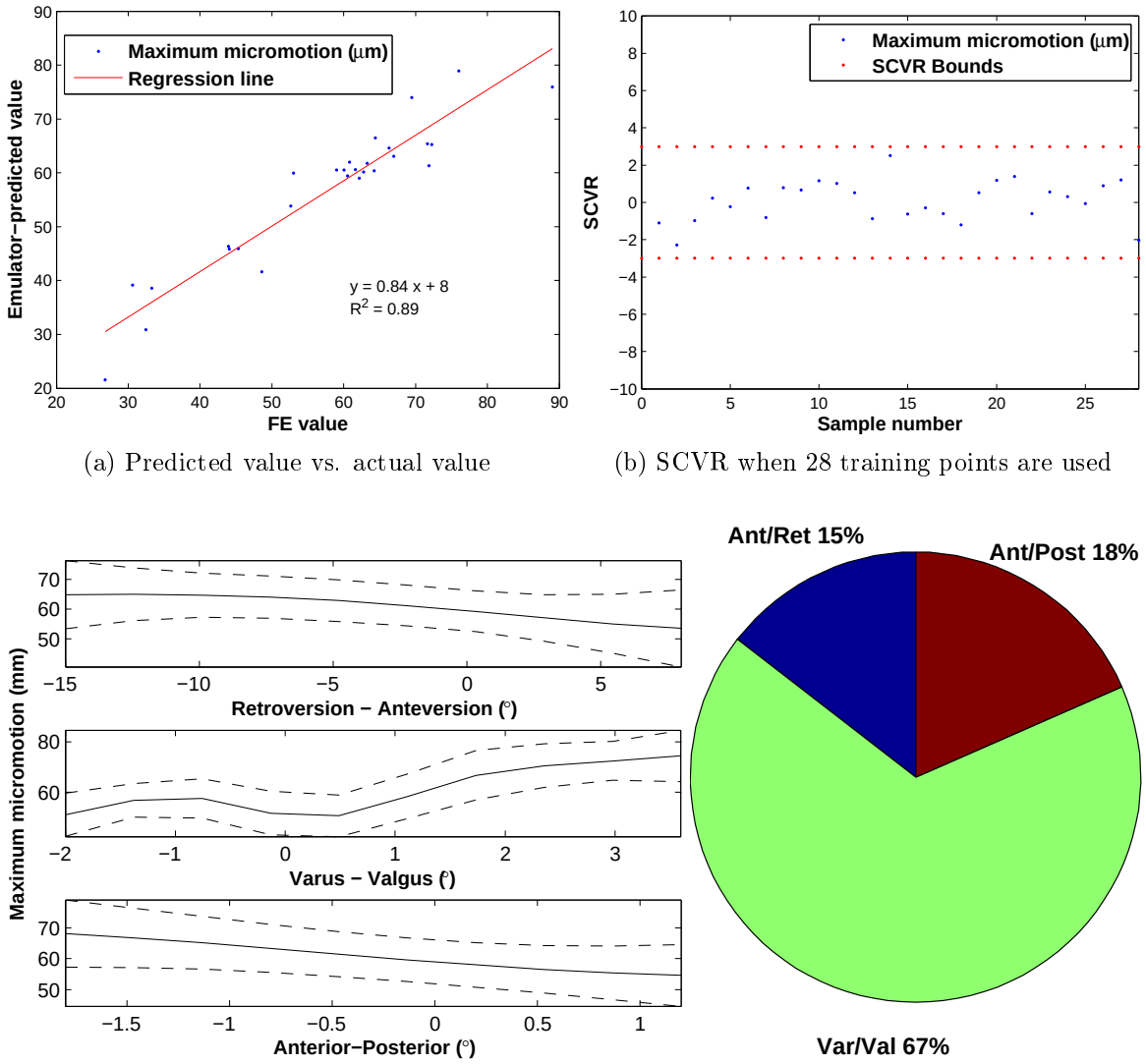

(a) Predicted value vs. actual value

(b) SCVR when 28 training points are used

(c) Main effect

(d) Sensitivity results

Figure 4.5: Maximum micromotion at the interface

4.4 Experimental parameter variation studies

The primary aim of the experimental test was to assess the effect of a stem position on the primary stability. A computational study was carried out prior to the experimental tests for reference. Then, six composite femurs were implanted with a cementless stem; three in a neutral position and three in a 'poor' position defined by the computational study. This study was carried out to assess the effect of the anterversion/retroversion, varus/valgus and anterior/posterior angles. *In vitro* tests were carried out to corroborate the implant motion and bone strain measurements.

Six sawbones were implanted with the Furlong stem with a 28 mm diameter femoral head by an experienced orthopaedic surgeon. Three sawbones, called femur 1 to 3, were implanted in a neutral stem position and three sawbones, called femur 4 to 6, were

implanted in a 'poor' position (ie. position leading to highest implant micromotion and bone strain) as defined by the computational study.

Each femur was sectioned at two-thirds of its length below the femoral head, i.e. about 250 mm distal to the lesser trochanter. The distal part of each sawbone was embedded in a metal cup using a resin based on methyl-methacrylate (Technovit 3040, Heraus Kulzer GmbH, Wehrheim, Germany). The femurs were positioned at 9° flexion and in 10° abduction (conforming to the British Standard for testing total hip replacement BS 7206: Part 4: 2002). Anterior-posterior movement of the distal end of the bone was allowed and the two other directions were constrained. Each implanted sawbone was sinusoidally loaded between -0.2 to -1.6 kN at a frequency of 0.5 Hz for 50,000 cycles on a servo-hydraulic test machine (Losenhausen Maschinenbau AG, Dusseldorf with a MTS Controler). The duration of each test was approximately 28 hours. In previous papers, Bergmann et al. [27] reported that during normal walking, the average peak forces acting on the hip joint were between two and three times body weight and this is the reason why a maximum load corresponded to two times body weight was selected for the study. As descibed in section 3.2, two LVDTs (Solartron, RS Components Ltd, Corby, UK) were used to measure the longitudinal movement of the stem to the bone: one of the LVDTs was fixed inside the medullary canal and was directly in contact with the tip of the stem. The second LVDT was fixed on the lateral part of the bone (called gluteal ridge) and was in contact with a target device attached to the shoulder of the stem.

The movement of the stem was monitored continuously using the two LVDTs. The stem micromotion and migration were calculated in Matlab using the data from the LVDTs. To refresh, the stem micromotion is known as the inducible motion of the stem and the stem migration as the permanent motion of the stem (see section 2.2.4.2).

Deformation and strain measurements over the sawbone surface were undertaken at the end of the cyclic test on one implanted bone of each set using a DIC system (Limess GmbH, Pforzheim, Germany). This system consists of two cameras and Vic3D software to process the recorded data. For the testing, 28 mm lenses were used and the calibration was performed using a 5 mm calibration grid. The outer surfaces of the sawbones were prepared by applying random dot patterns to measure the surface strain. To improve the contrast, white paint and then black paint was applied to get a speckle pattern on the surface. The DIC measurement process consisted of applying a ramp load gradually raised in 0.100 N increments from 0 to -1.600 kN and taking images of the sample at different stages.

The stem micromotions measured at two locations (tip of the stem and shoulder of the stem) during 50,000 cycles are shown in Figures 4.6 and 4.7. In each graph, the

stem micromotion of each implanted femur was plotted to compare how the implant behaved for each configuration over time. It should be noted that the fatigue test was run continuously for femurs 1, 3 and 5; whereas mechanical problems occurred with the testing machine for femurs 2, 4 and 6. Therefore, it should be kept in mind that for femur 2, 4 and 6, the measurements were carried out including resting periods during the test. For femur 2, the test stopped at 46,075 cycles; for femur 4, it stopped at 925, 2,779 and 46,231 cycles and for femur 6, it stopped at 75 and 31,111 cycles.

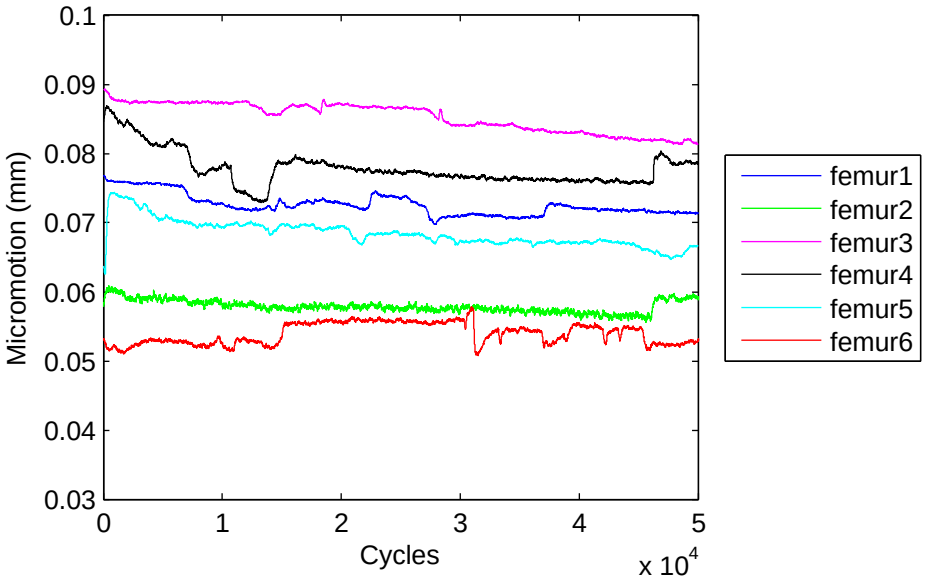

Figure 4.6: Axial motion (in mm) measured at the tip of the stem of the 6 implanted bones, during 50,000 cycles

It is difficult to compare the micromotion trends for the different implanted bones. However, there are notable changes that can be identified at particular stages and some of the changes are due to the stops in the test (underlined below); these are not thought to have a significant effect when the rest of the test is considered:

- changes identified at the tip of the stem (Figure 4.6):
  - at 7,500 cycles for femur 1 and femur 4
  - at 15,000 cycles for femur 3, femur 4 and femur 6
  - at 27,000 cycles for femur 1 and femur 3
  - at 31,000 cycles for femur 6
  - at 46,000 cycles for femur 2, femur 4 and femur 6
- changes identified at the shoulder of the stem (Figure 4.7):
  - 14000 cycles for femur2, femur3 and femur6
  - 17000 cycles for femur2 and femur6

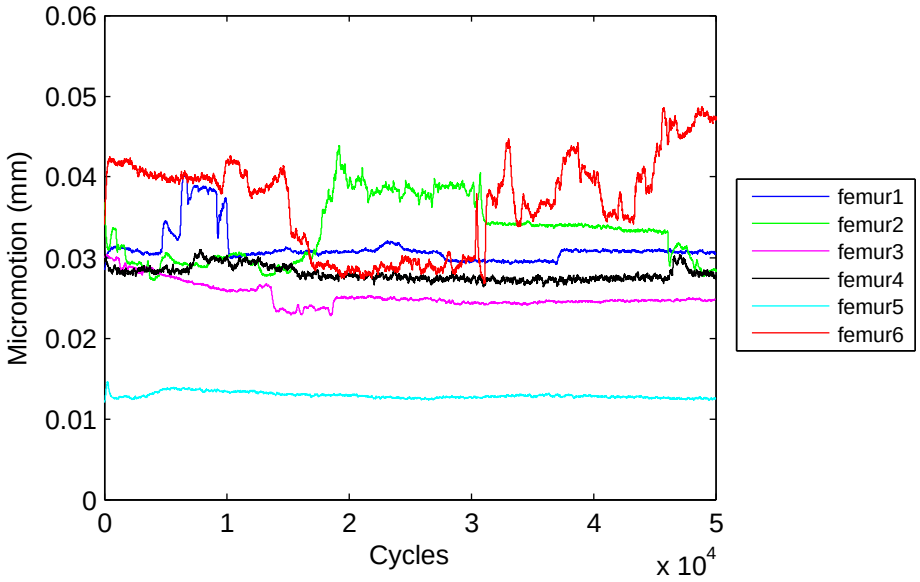

Figure 4.7: Axial motion (in mm) measured at the shoulder of the stem of the 6 implanted bones, during 50,000 cycles

- 31000 cycles for femur2 and femur6
- 46000 cycles for femur2, femur4

The mean micromotion and standard deviation measured at the two locations within 50,000 cycles are shown in Figures 4.8 and 4.9 for each implanted bone, which are numbered from 1 to 6.

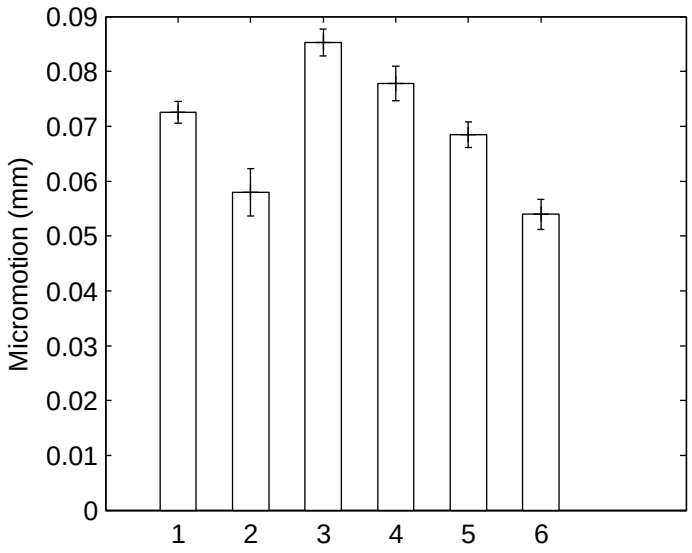

Figure 4.8: Axial motion (in mm) measured at the tip of the stem (mean micromotion ± standard deviation) for each implanted femur, numbered from 1 to 6

Figure 4.8 shows that the highest mean micromotion at the distal end of the stem was recorded for femur 3 and the smallest mean micromotion for femur 2 and femur 6.

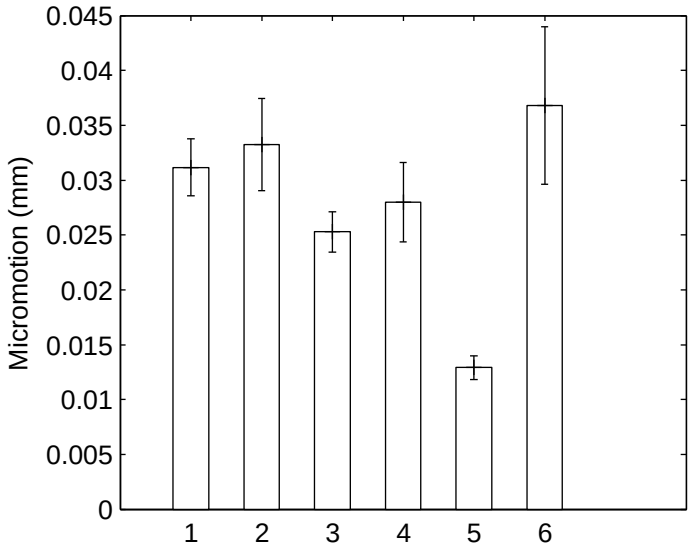

Figure 4.9: Axial motion (in mm) measured at the shoulder of the stem (mean micromotion ± standard deviation) for each implanted femur, numbered from 1 to 6

Figure 4.9 shows that the highest mean micromotion at the shoulder of the stem was recorded for femur 6 and the smallest mean micromotion for femur 5.

A more revealing method of discerning differences in performance was found when plotting the stem migration at the end of 10,000 cycles, 20,000 cycles, 30,000, 40,000 and 50,000 cycles. The migrations at the two locations are shown in Figures 4.10 and 4.11. The first bar of each set corresponds to femur 1, the 2nd bar to femur 2 till the 6th bar that corresponds to femur 6.

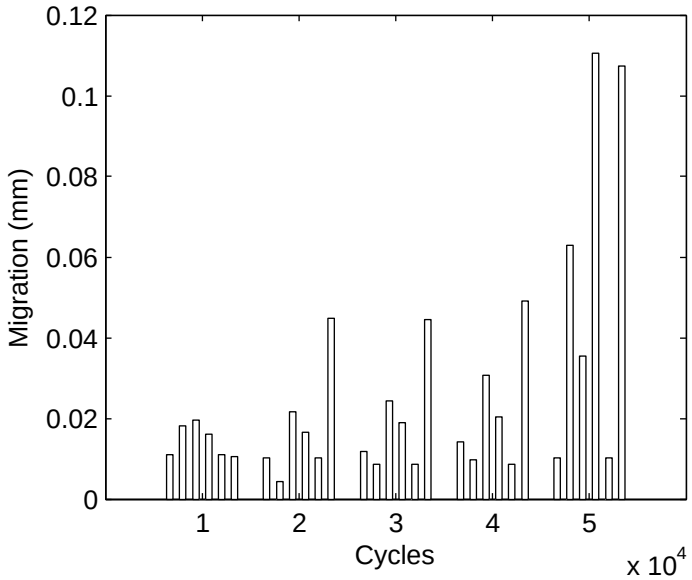

Figure 4.10: Migration measured at the tip of the stem of the six implanted femurs after 10,000; 20,000; 30,000; 40,000 and 50,000 cycles

After 50,000 cycles, at the tip of the stem, the highest migration was exhibited by

femurs 4 and 6 and the lowest migrations were found for femurs 1 and 5.

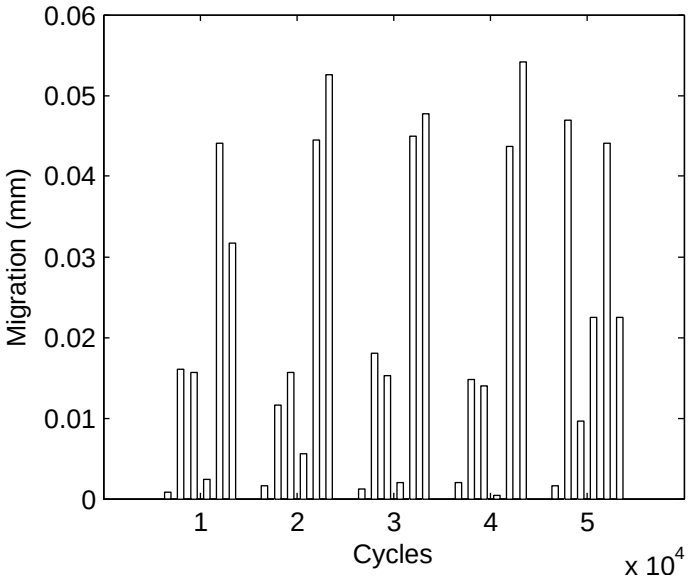

Figure 4.11: Migration measured at the shoulder of the stem of the six implanted femurs after 10,000; 20,000; 30,000; 40,000 and 50,000 cycles

After 50,000 cycles, at the shoulder of the stem, the highest migration was found for femurs 2 and 5 and the lowest migration was found for femur 1. However, it should be noted that throughout the test, largest migrations were observed in femurs 5 and 6.

4.5 Concluding remarks

In this study, a mesh morphing strategy was used to automatically generate new implanted femur meshes based on the neutrally positioned implant mesh. In total 28 implant positions were run in batch mode on a cluster of nine dual core nodes each with 8 Gb of RAM. The average run time for each implant position (including the mesh morphing and contact analysis) was 45 min and as the job was divided and submitted in parallel, the total run time for 28 implant positions was about 150 minutes. As a comparison, the full mesh morphing and contact analysis can take the same time as the study of one single implant position when implanting using CAD (computer aided design) software [21].

The Gaussian process was used to define the worst implant position based on the biomechanical responses. Considering the displacement at the stem shoulder as one of the outputs, it was identified that an anteversion/retroversion angle of $-14.7°$, varus/valgus angle of $-2.0°$ and anterior/posterior angle of $1.2°$ predicted the worst implant orientation. The computational study also showed that the stem micromotion and bone strain were most sensitive to the varus/valgus angle. This correlates with

clinical assessments that suggested that varus alignment of the femoral component leads to instability [49, 156, 134], which may be explained by the fact that the stem may not get support from the cortical bone [156]. In the experimental study, six implanted bones were tested: three in a neutral position and three in a poor position. Two types of motion were measured: the micromotion and migration along the axial axis of the stem. Again, these tests show that the axial motion of the stem measured for the six implanted bone was quite small under the loads applied. The maximum axial motion was found at the tip of the stem and did not exceed $90\mu m$, which may not represent complications in terms of loosening as the threshold inhibiting bone ingrowth is believed to be $150\mu m$ [119, 76]. Although no firm conclusions can be drawn from the micromotion studies, the findings of this study correlate well with the work presented by Arizono et al. [18]. In their study, they carried out experimental tests to assess the effect of the varus position of a cementless stem. They investigated implant primary stability when a stem was implanted in a neutral orientation and when a stem was in a varus orientation. They identified that there were no significant differences in implant micromotion along the axial direction of the implant, which was also found in this present study. No differences were measured in the medial direction but they observed a difference of 6 microns in the torsional direction, which might not have a huge impact on the long-term stability.

The experimental tests show that femurs 5 and 6, which were implanted in a 'poor' position, migrated the most with time, which corroborates the results of the computational work. It should be noted that in the present study, the fatigue test was run continuously for femurs 1, 3 and 6 without resting periods, which was not the case for the other femurs as some mechanical problems occurred with the testing machine, which could have affected the micromotion measurements. In another study, Verdonschot et al. [151] noted that migration of a cemented stem was greater including resting periods during the cyclic test. As it has been noted in Chapter 3, it should be kept in mind that the distal tip is more constrained towards uniaxial motion and representative of the monitoring procedures used in other LVDT based analyses of implant migration.

The experimental tests also show that the accuracy of the implantation depends strongly on the surgical equipment used. For example, in this project, there was difficulty in obtaining the same implant positioning for the tests and hence difficult to carry out a repeatability study. Figure 4.12 shows in the coronal view, the variations observed for three different implanted femurs when the implant is implanted in the neutral position and Figure 4.13 shows the variations in the transversal plane. It can be seen that the stem of the femur 1 and 2 are in slightly varus position.

One of the limitations of this study is the use of synthetic bones instead of human cadaver bone. However, synthetic bones are now increasingly used in implant testing

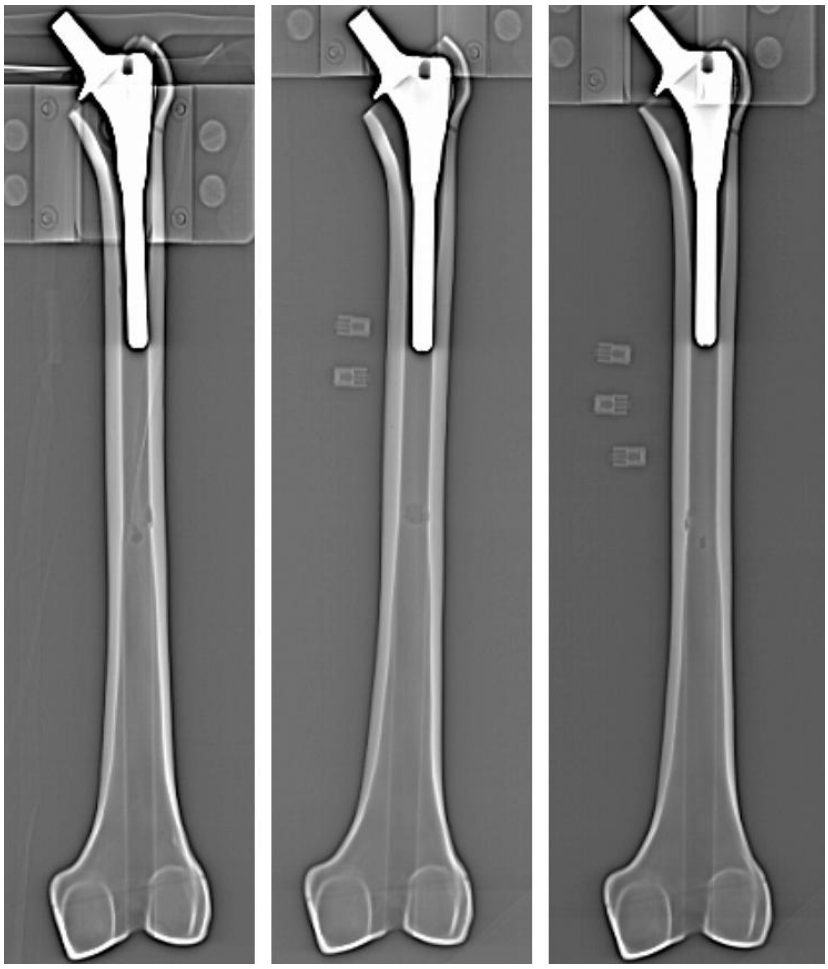

Figure 4.12: Three implanted sawbones in a neutral position - coronal plane

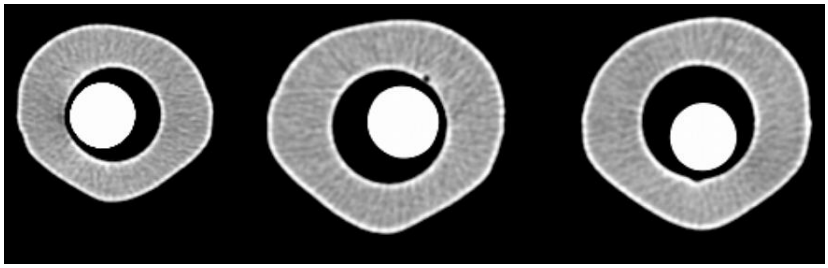

Figure 4.13: Three implanted sawbones in a neutral position - transversal plane

([34, 44, 77]) In addition, they are readily available when compared to cadaveric bones and avoid problems associated with sterility.

Another limitation is that the loading scenario was simplified; for instance, the load simulated the peak force applied at the hip joint while walking. The force consisted of a resultant force of two times body weight applied at the top of the femoral head of the implant, and the influence of muscle forces was not included. As the tests were carried out on a cementless stem, higher loads were not applied to avoid bone failure, especially at the distal end of the bone, as stress concentrations were previously observed at the bone/pot junction. In another study, Speirs et al. [135] carried out experimental tests

on cemented implants and noticed that micromotion increased with increasing load; which might also be the case for a cementless implant.

Another limitation of the study is that micromotion was measured at two locations: the tip of the stem and the shoulder of the stem; but not at the bone-implant interface. It is believed that these two measurements show the axial movement of the whole implant as it is a rigid body. Measurements in the other directions were not carried out mainly to avoid making holes on the bone surface to hold the LVDT or to access the implant surface. It has been noted that holes in bone introduce a mechanical weakening of the bone as mentioned by [118].

Chapter 5

Validation of the Digital Image Correlation Technique for Biomechanical Measurements

The previous chapter has highlighted the potential of the digital image correlation system as a method for the accurate assessment of surface strains in the implanted system. In biomechanics, strain gauges have been widely used for bone strain measurements [48, 140, 148]. However, its application has limitations as it provides measurement only at the site of attachment thereby requiring the use of many gauges in order to measure large surface areas.

Compared to strain gauges, the use of an optical system can provide strain values in the measured field of view. It is in this regard that the DIC is being used increasingly for biomechanical testing, but a systematic validation exercise has not, to the author's knowledge, been published. The aim of this chapter therefore is to prove the viability of the DIC system for bone strain measurement; via a rigorous cross comparison with an established strain monitoring method. In addition, the potential to utilise the capabilities of DIC for implant motion assessment is investigated.

5.1 Bone strain measurements

5.1.1 Methods

Two, fourth-generation composite femurs (item 3406, Sawbones Europe AB, Sweden) were prepared for the measurements. The strain in the first bone was measured using three rectangular rosette strain gauges (Vishay Measurements Group UK Ltd). The

strain on the second femur was measured using a DIC system (DIC, Limess Messtechnik & Software Gmbh). Thereafter, the femurs were subjected to a compression load of 3.6 kN on a servo-hydraulic test machine (Instron Ltd., High Wycombe, UK). In this phase of the work, whole femurs were used to allow higher loads to be employed. A custom metallic jig was created to hold the bone, with a mould in shape of the condyles to constrain the bone (Mavro Engineering, Southampton, UK), see Figures 5.1 and 5.2.

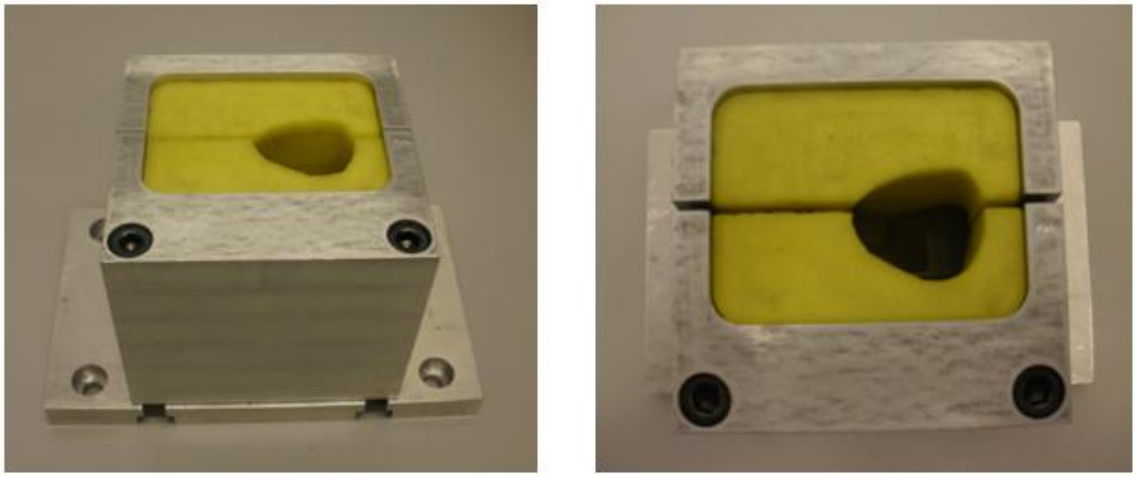

Figure 5.1: Metallic jig containing the condyles mould to hold the femur

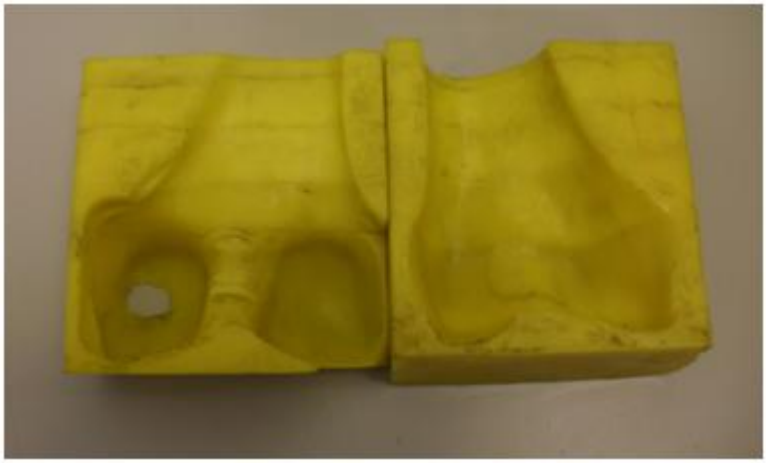

Figure 5.2: Mould of the condyles

The following sub-sections describe the methodology employed for the strain gauges and the DIC measurement techniques.

5.1.1.1 Measurement using strain gauges

A wire strain gauge can effectively measure strain in only one direction. To determine the three independent components of plane strain, strain rosettes can be used to de-

termine the principal strains. For example, gauges of a three-gauge rosette can have their axes at either 45° or 60° to each other.

In biomechanics, strain gauges have often been used to measure bone strain, and in the majority of these studies, the measurements were carried out using three-gauge rosettes, also called triaxial strain gauges [48, 140, 148]. In this experimental test, the rosettes had their axes aligned at 45° to each other, these were bonded to the anterior surface of the first femur as shown in Figure 5.3. The rosettes were numbered from 1 to 3: rosette 1 corresponded to the rosette on the femoral head, rosette 2 corresponded to the rosette on the neck of the femur and rosette 3 was fixed 6 cm below the greater trochanter. These locations were selected according to the field of view of the DIC measurements, and because higher strains were likely in these areas.

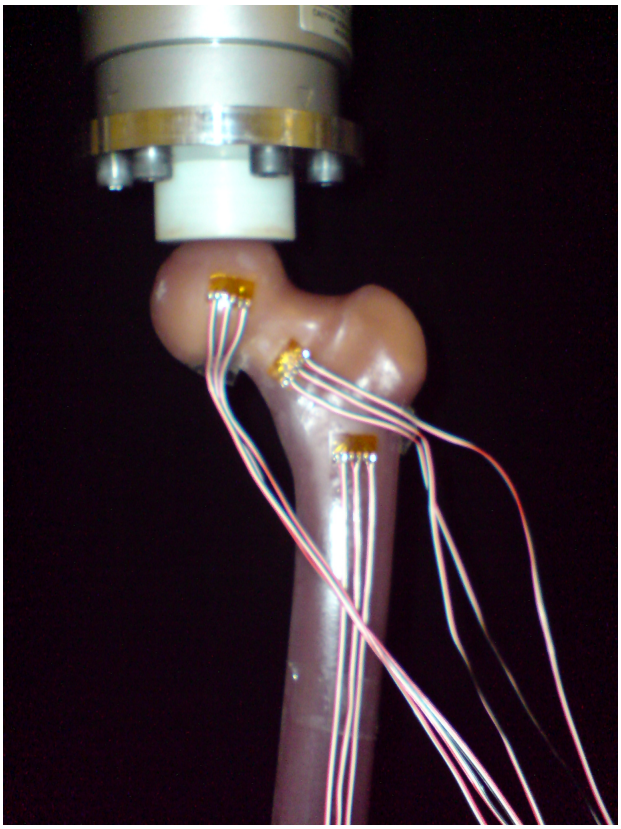

Figure 5.3: Three rectangular rosettes bonded on the intact femur

The strain gauge rosettes were fixed at the anterior proximal part of the synthetic bone, following these steps:

1. the outer surface of the bone was first smoothed using sandpaper and conditioner
2. after drying the surface, a neutralizer was applied, which helps the surface bond with the glue (used in step 4)
3. strain rosettes were manipulated with caution, and a catalyser was applied at the back of the rosette

4. strain rosettes were then glued to the bone surface with cyanoacrylate
5. after bonding the strain rosettes, leadwires were soldered
6. the gauge surfaces and solder joints were then cleaned with a resin solvent

Figure 5.4 shows the tests set-up consisting of the testing machine, sawbone and data processor linked to a laptop. The strain gauges were first calibrated and the data acquired during testing was processed using the micro-measurements system 7000 (Vishay Measurements Group UK Ltd).

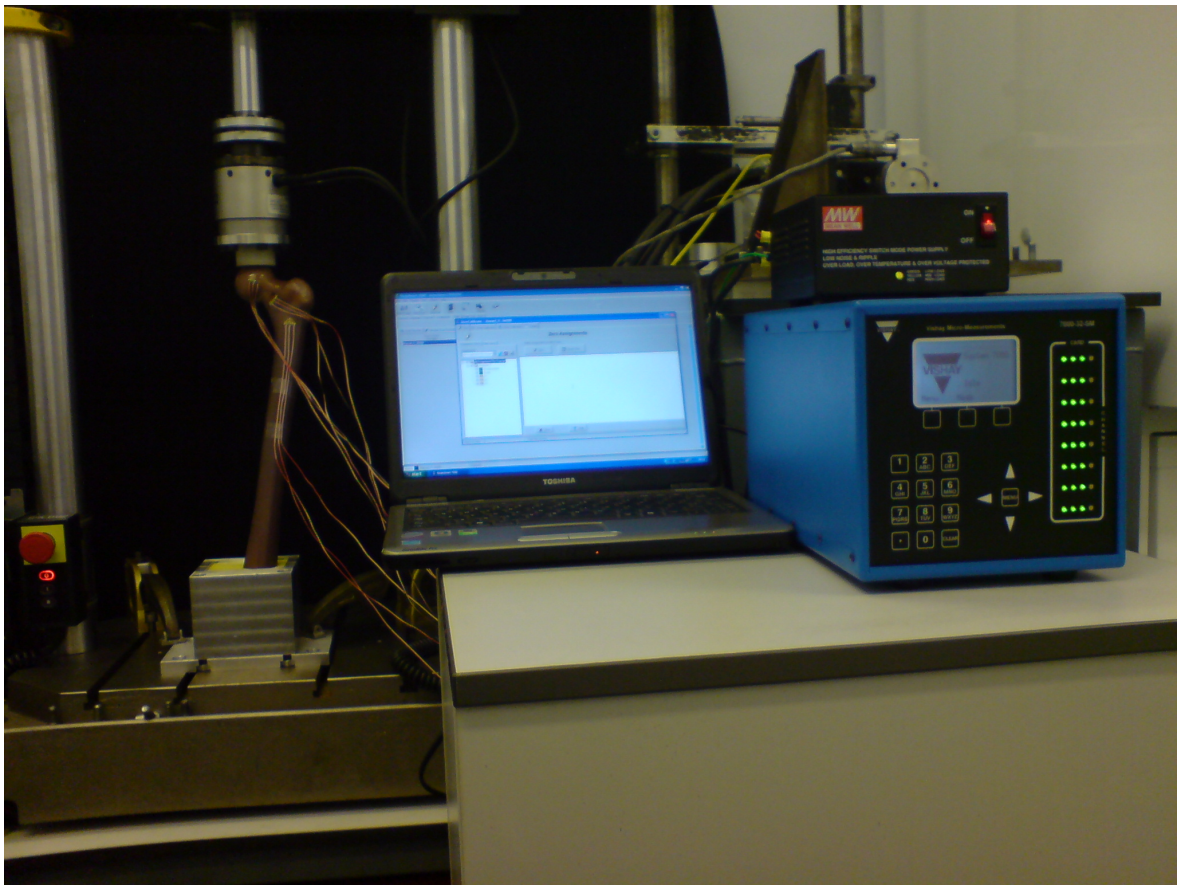

Figure 5.4: Test set-up using the strain gauges

5.1.1.2 Measurement using the DIC system

Test set up is an important aspect of DIC measurement: the two cameras had to be mounted on stable tripods and positioned symmetrically about the specimen to avoid distortion effects. Based on the manufacturer's guidelines, the angle between the cameras was not considered critical to the measurements. However, an angle between 15° and 45° was recommended for best results. After selecting the lenses, the next step consisted of adjusting the focus and the brightness of the image, i.e. the aperture

and exposure time. In this study, two CCD cameras (resolution: 1628 * 1236 pixels, dynamic range: 8 bits) with 28 mm lenses were used.

To perform the calibration, different sizes of calibration grids were used to determine the optical properties of the system set-up, including relative cameras orientation and lens distortion. The calibration grid consisted of a range of points arranged as a matrix (9 by 12), in which 3 points of the grid were different and could be identified by the software, see Figure 5.5.

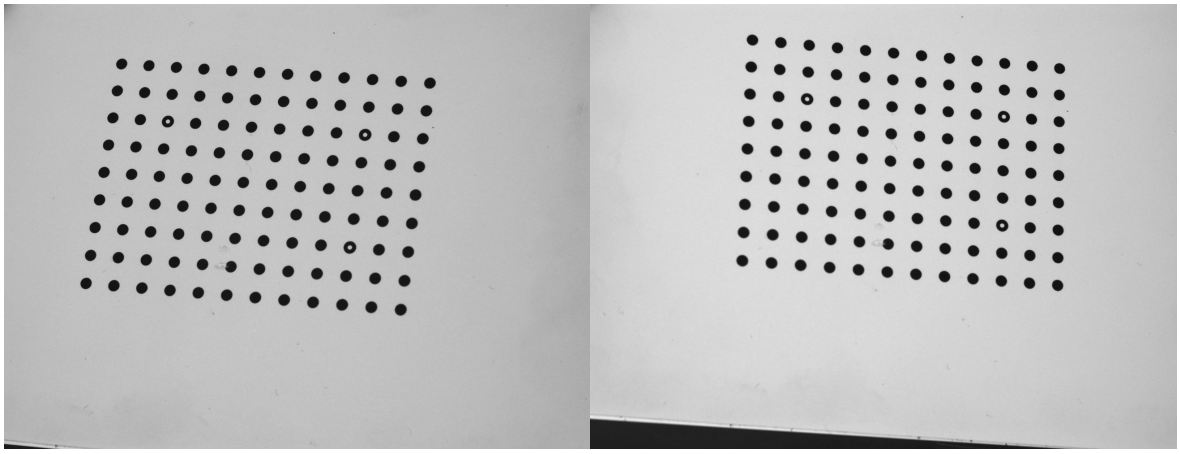

(a) Image from the first camera (b) Image from the second camera

Figure 5.5: Camera calibration for the DIC system

Calibration images were then captured by moving the grid in the 3 different axes. To get an accurate result, it was recommended to get at least 15 calibration images. In this study, the images were taken using the software Vic-Snap (Version 2008, build 281, Correlated Solutions, Inc.) and the calibration was carried out using the Vic-3D software, which provides the standard deviation of each calibration image and the standard deviation of residuals. Here, the standard deviation corresponds to the confidence interval.

Before testing, random patterns were applied on the bone surface as there are no natural patterns on the bone. When the sample is subjected to an external force, the DIC captures the deformations of these patterns; in other words, it tracks their movement.

The system resolution depends on the pixel size. The more pixels on the images, the higher the resolution, therefore the system will be more sensitive to the deformation of the sample surface. To get a better contrast, a standard light source can be used to light the sample if the light of the experimental environment is not enough. For this test, the sample was lit using fluorescent lamps, which produce less heat than other lights such as tungsten lights. Heat generated by the lamp can affect the results; for

example, the heat can produce smoke, which can be recorded by the cameras. To enhance the images contrast, a black background was also used.

A compressive load was applied to the femur gradually from 0 to -3.6 kN in steps of 100 N. Images were acquired for each step of the analysis; with a total of 37 loading cases.

Figure 5.6 shows the test set-up using the DIC system, light and computer to process the data.

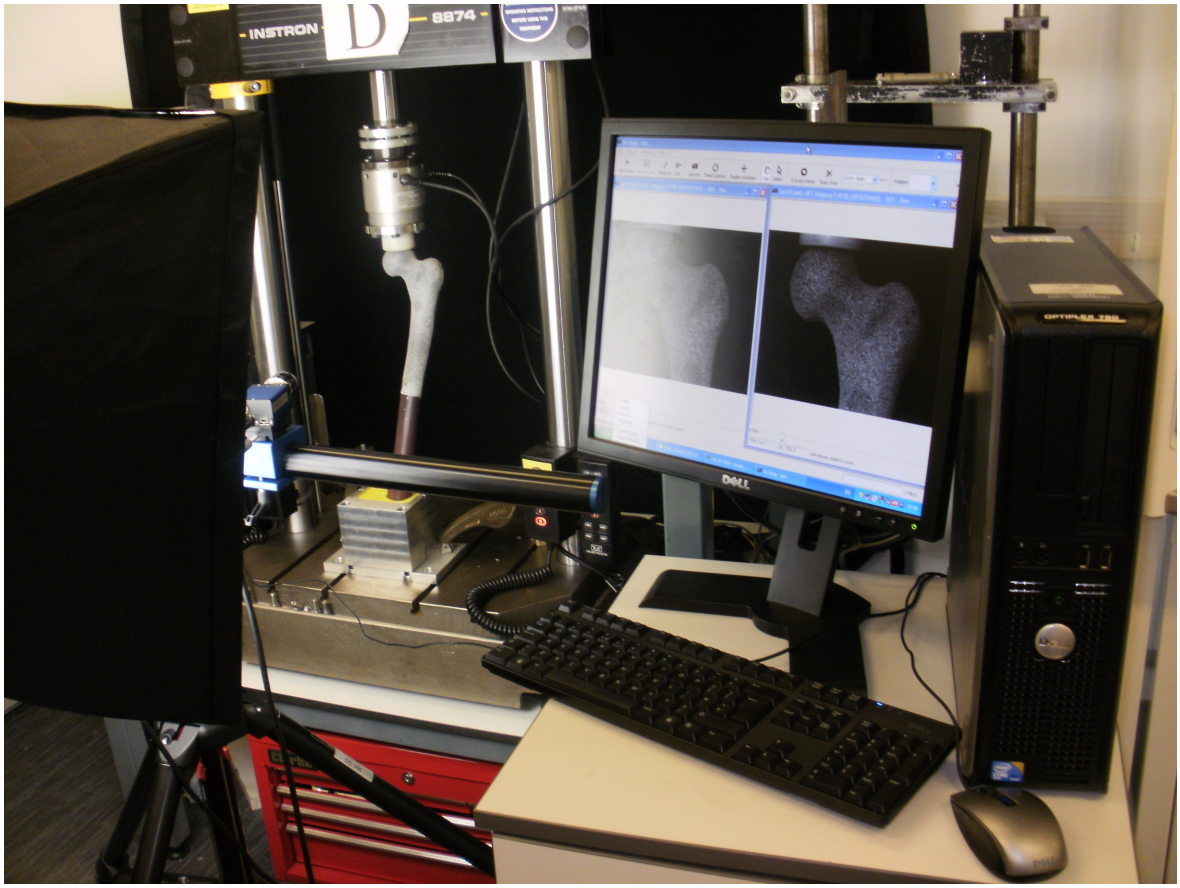

Figure 5.6: Test set-up using the DIC system

The strain results obtained were exported in two separate formats; as image (or video), or as raw data. The image data provided strain data superimposed on the bone images whereas the raw data could be used for further processing.

To replicate the measurement area of each rosette, four points were selected on the bone surface, defining the rectangular area. The X, Y and Z coordinate of each point on each image were exported as a *.csv file. Figure 5.7 shows a screen-shot using the Vic-3D software of the four points selected for the 3 rosettes used.

Thereafter, to match the measurement carried out by the strain rosettes, a coordinate system was defined replicating the rosette orientation by selecting the origin and the x-

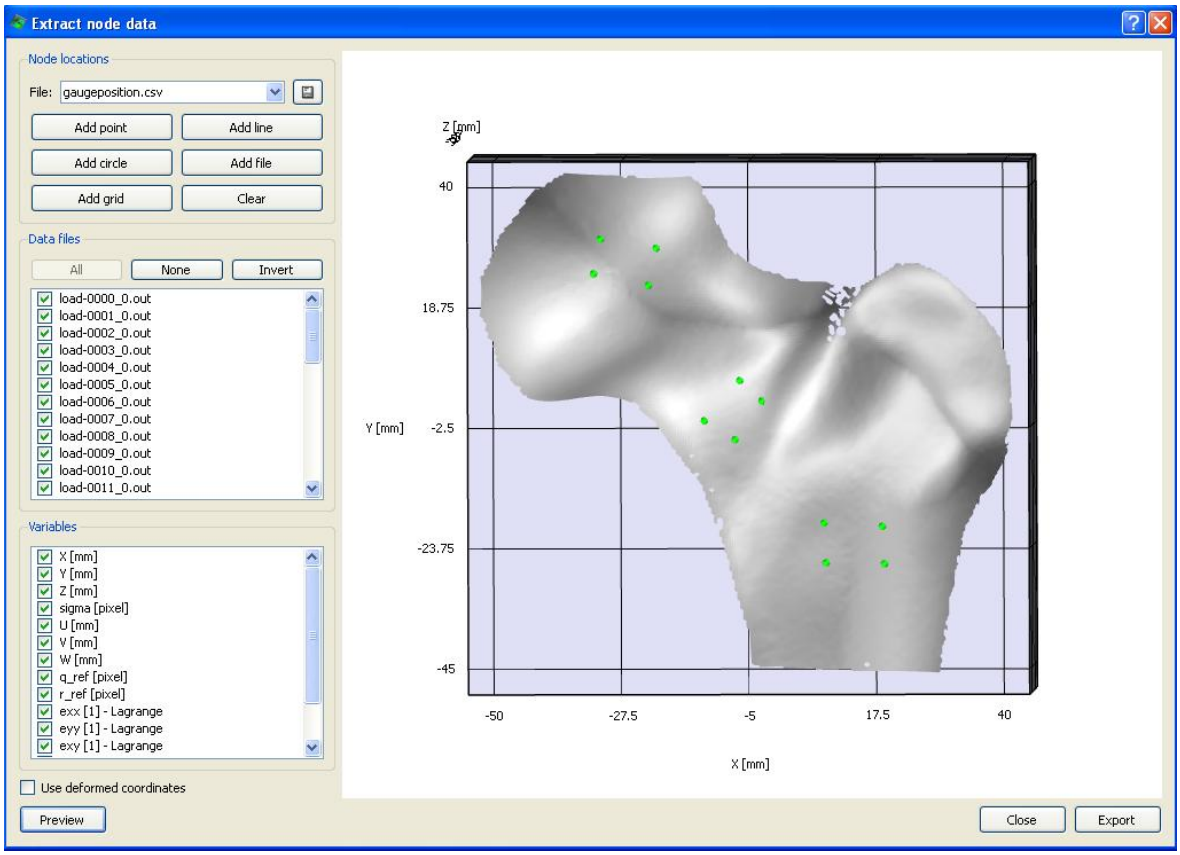

Figure 5.7: Extract node data in Vic-3D

axis. The orientations of each of the rosettes differed, therefore an individual coordinate system was defined for each of the rosettes. The strains were then computed for each rosette configuration, and data of all the points in the field of view were exported as a *.csv file; one file for each load step resulting in 37 files in total.

In the absence of built in functions for the required post processing, it was necessary to write a custom code in Matlab (presented in Appendix C) to automatically select the points inside the rectangle (defining the rosette area) and calculating the mean value and standard deviation of the strain along the x-axis, y-axis and the maximum and minimum strains in each area.

5.1.2 Comparison of results

The axis along the length of the first gauge was considered the x-axis, with the y-axis, corresponding to the third gauge, set at 90° to the first gauge.

Figures 5.8 and 5.9 show respectively the strain along the x and y axis against the load applied at rosette 1. The continuous line corresponds to the results from the strain gauges and the plot of cross values with standard deviations corresponds to the results obtained using the DIC.

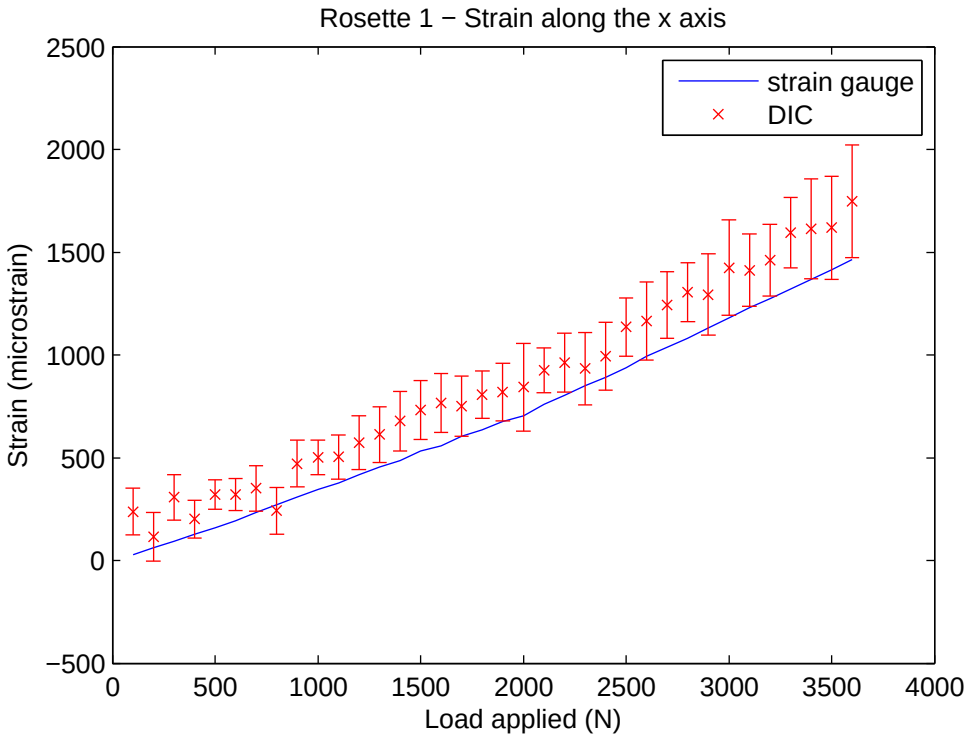

Figure 5.8: Rosette 1 - Strain along the x-axis for both techniques

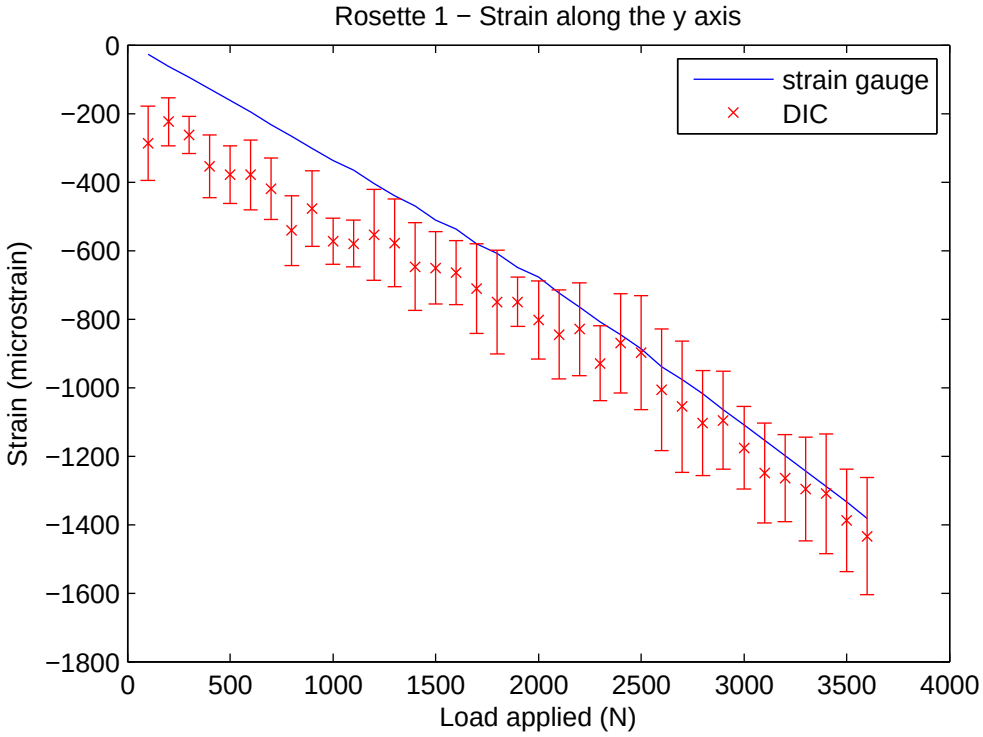

Figure 5.9: Rosette 1 - Strain along the y-axis for both techniques

Figures 5.10 and 5.11 show respectively the maximum and minimum principal strain against the load applied at rosette 1.

Similar results were obtained from other two rosettes, these are presented in Appendix

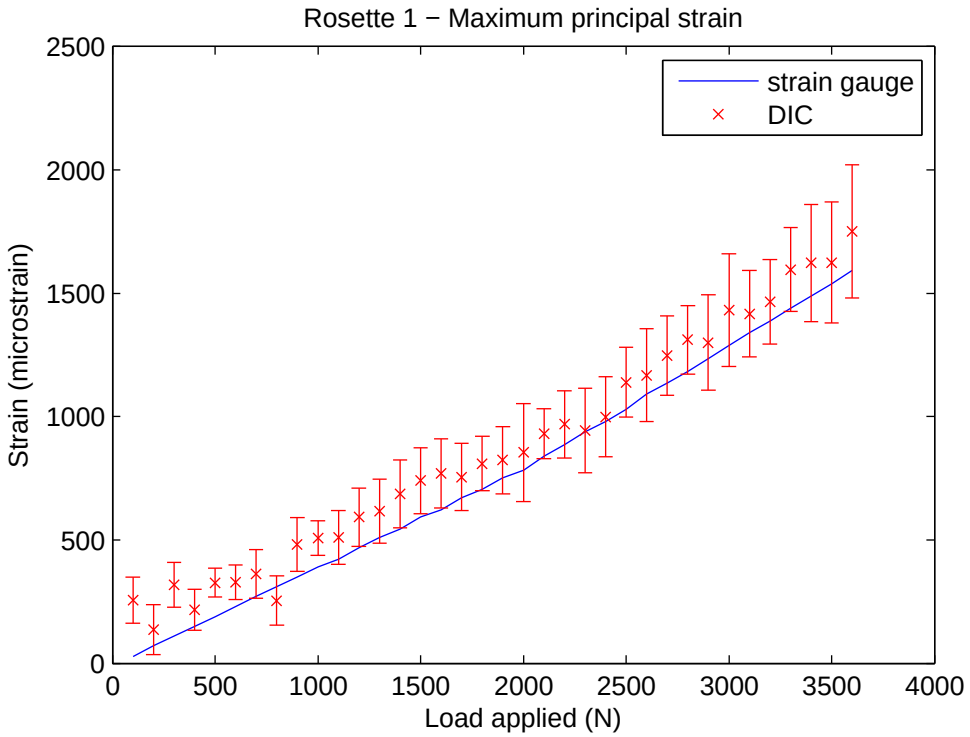

Figure 5.10: Rosette 1 - Maximum principal strain for both techniques

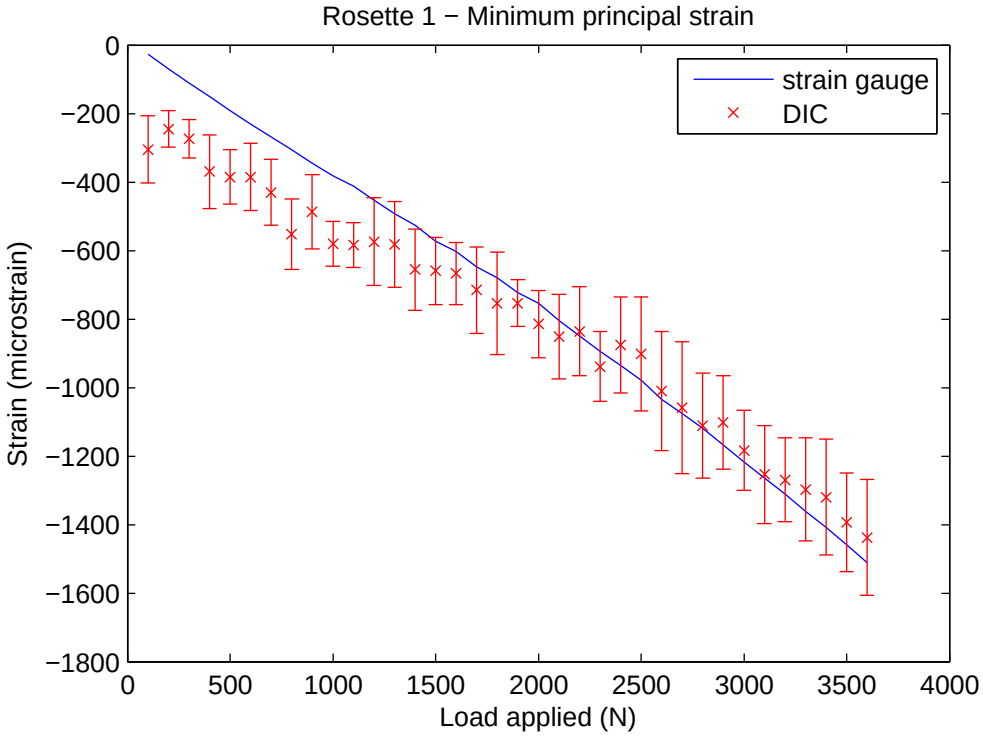

Figure 5.11: Rosette 1 - Minimum principal strain for both techniques

D. To compare the results, strains measured by the DIC system were plotted against the strains measured by the strain gauges. As an example, Figure 5.12 shows the strain measured along the x-axis by the DIC system against those measured by the

strain gauges and Figure 5.13 shows the strain measured along the y-axis by the DIC system against those measured by the strain gauges at rosette 1. The coefficient of determination R^2 was 0.99 for the two graphs.

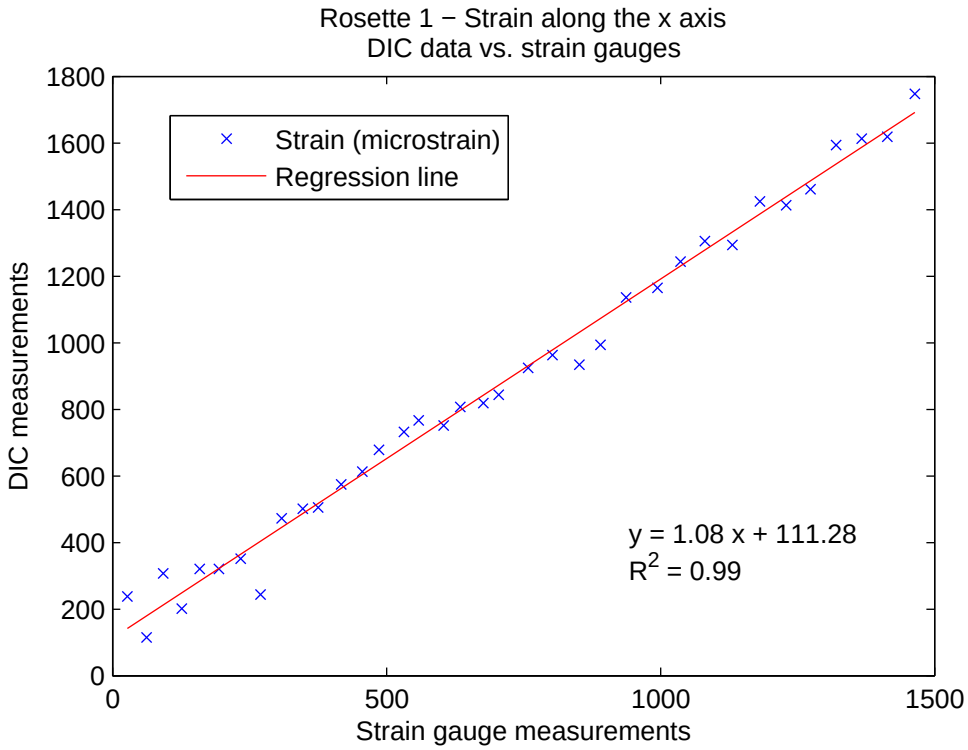

Figure 5.12: Rosette 1 - Strain along the x-axis measured by the DIC system vs data measured by the strain gauges

Figure 5.14 shows the maximum principal strain measured by the DIC system against those measured by the strain gauges and Figure 5.15 shows the minimum principal strain measured by the DIC system against those measured by the strain gauges. The coefficient of determination R^2 was about 0.99 for the two graphs.

5.1.3 Assessing DIC results: method 2

In the DIC technical specifications, the manufacturer claims an accuracy of 0.02% for strain measurements. The aim of the following test was to assess the accuracy of the strain and displacement using a calibrator. To this end, a plate of 24 mm * 54 mm *2 mm was translated in one direction (in this case the Y direction). The plate was prepared for the testing, i.e. it was first painted in white and then a black speckle pattern was applied on the surface, see Figure 5.16.

The plate was first translated from 0 to 30 mm in 5 mm increments (Table 5.1) to verify whether the system could measure small displacement following which the plate was translated from 0 to 0.05 mm in 0.005 mm increments (Table 5.2) to verify whether

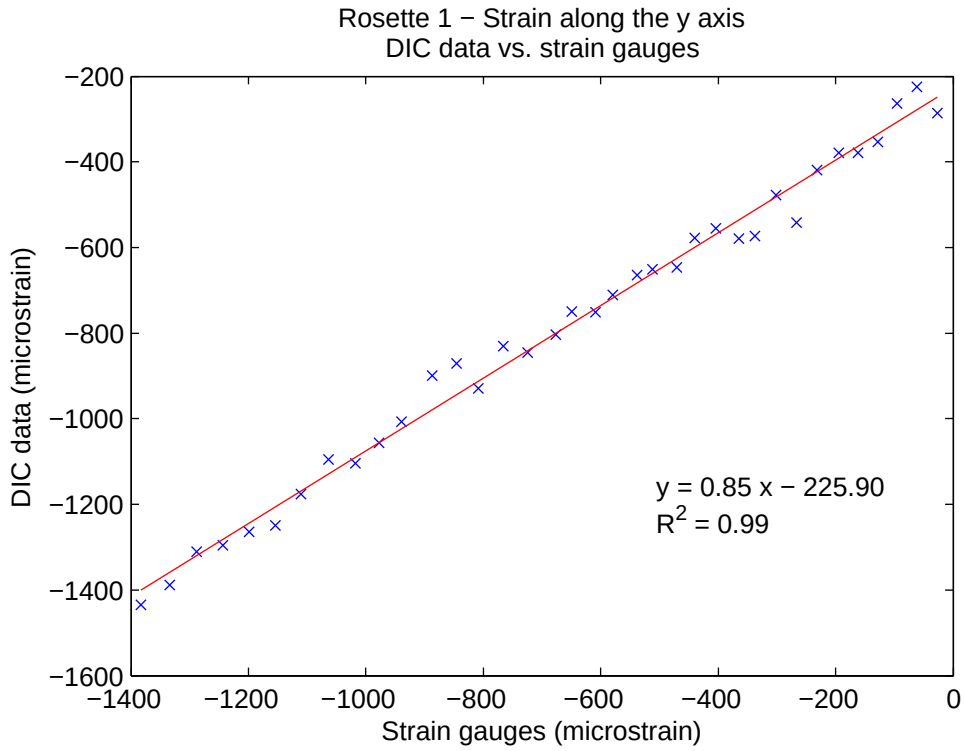

Figure 5.13: Rosette 1 - Strain along the y-axis measured by the DIC system vs data measured by the strain gauges

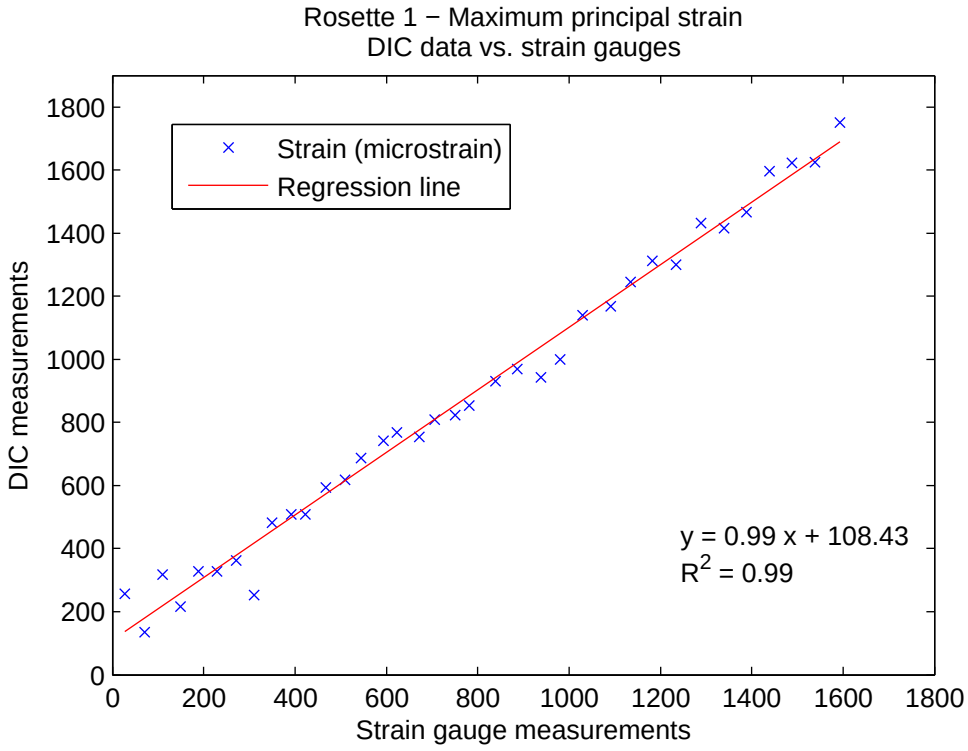

Figure 5.14: Rosette 1 - Maximum principal strain measured by the DIC system vs data measured by the strain gauges

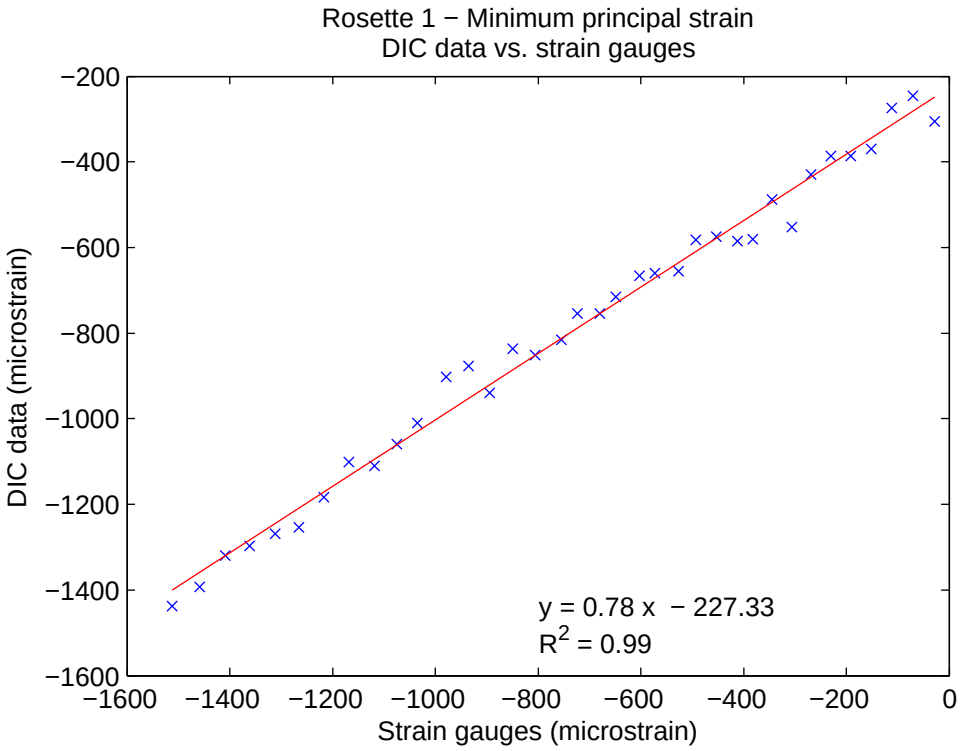

Figure 5.15: Rosette 1 - Minimum principal strain measured by the DIC system vs data measured by the strain gauges

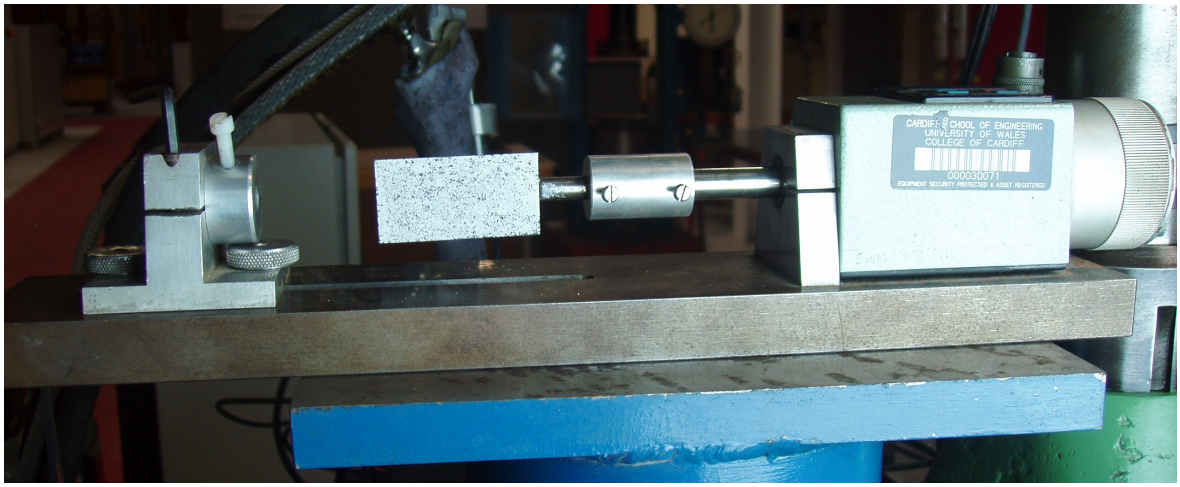

Figure 5.16: Plate assembled to a micrometer for displacement and strain measurements using the DIC

very small displacements of the order of 0.005 mm could be measured. The plate was not loaded, therefore the strain on the surface should be zero.

The displacement of each point was calculated using a custom code in Matlab. The total displacement of the plate was calculated as the vectorial sum of the displacement along each axis.

From these measurements, it was noted that the DIC could measure up to 5 mm of

Table 5.1: Translation of the plate from 0 to 30 mm in 5 mm increments

Displacement measured by the micrometer (mm)	Mean displacement calculated (mm)	Standard Deviation (mm)
5	4.9799	0.0030
10	10.0083	0.0036
15	15.0192	0.0039
20	20.0010	0.0043
25	24.9501	0.0037
30	29.9535	0.0051

Table 5.2: Translation of the plate from 0 to 30 mm in 0.005 mm increments

Displacement measured by the micrometer (mm)	Mean displacement calculated (mm)	Standard Deviation (mm)
0.005	0.0108	0.0032
0.010	0.0145	0.0047
0.015	0.0200	0.0069
0.020	0.0183	0.0048
0.025	0.0254	0.0024
0.030	0.0354	0.0021
0.035	0.0418	0.0030
0.040	0.0479	0.0035
0.045	0.0474	0.0019
0.050	0.0546	0.0024

displacement with good accuracy. The smallest displacement that could be measured was 0.010 mm with an accuracy of 0.005 mm. As stated previously, in theory, the strains recorded during this test should have been zero. To check this, the strains in all directions and the principal strains were calculated in Vic3D. Figure 5.17 shows the percentage of points for selected strain ranges.

From the strain measurements, the accuracy of the system was found to be 0.05%. As an example, Figure 5.18 shows the strain exx superimposed on the original image.

5.2 Implant motion measurements

Having established the accuracy of the DIC to monitor translations, the technique was applied to the implanted femur with a view of assessing micromotion and migration.

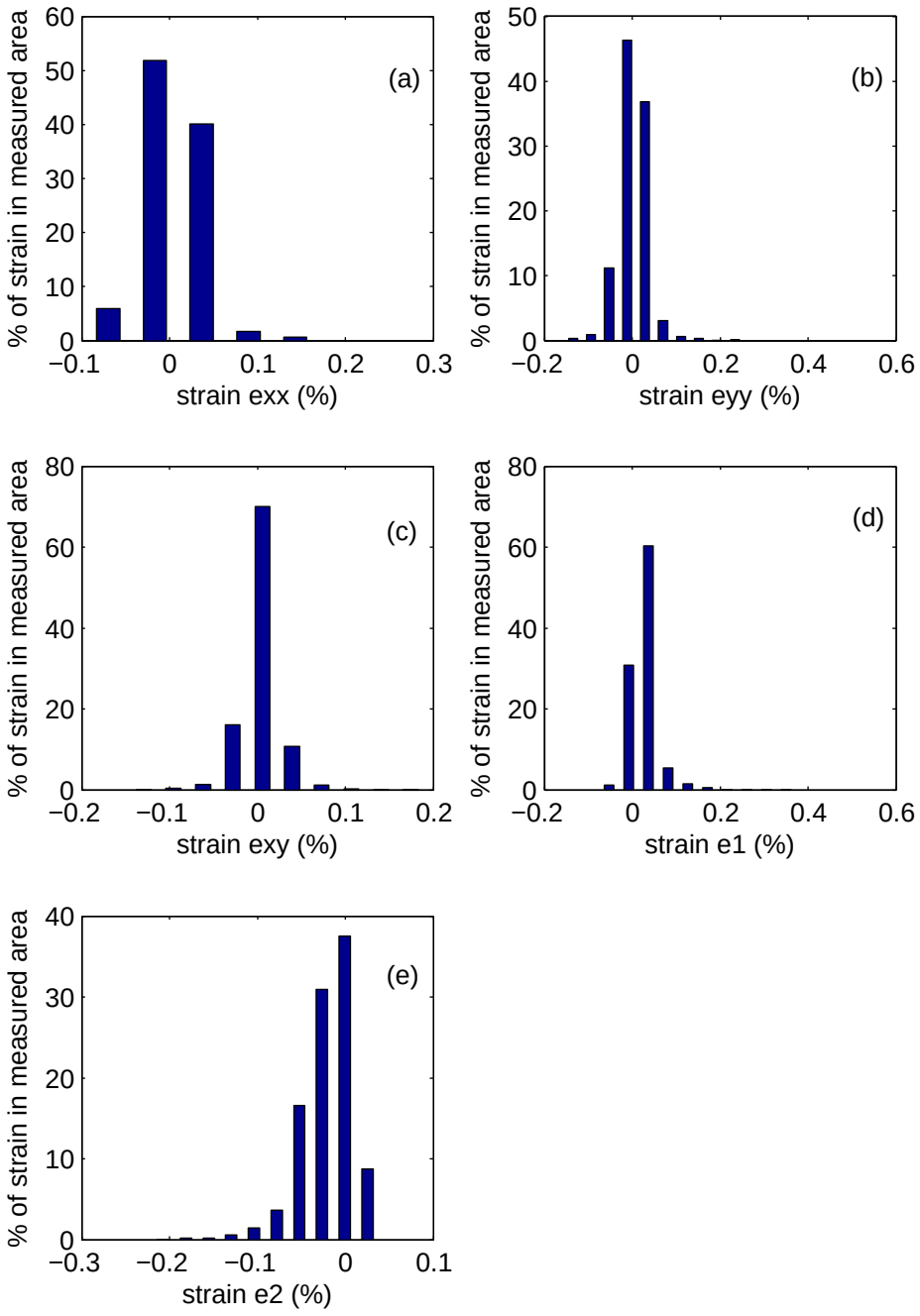

Figure 5.17: Strain measurements during plate translation measurements: (a) exx, (b) eyy, (c) exy, (d) e1 and (e) e2

5.2.1 Methods

Five synthetic bones (item 3406, Sawbones Europe AB, Sweden) were implanted using the cementless Furlong stem (JRI Ltd, Sheffield, UK) by an experienced surgeon in the following orientations: (i) neutral position with 15° of anteversion, (ii) varus position (with the proximal stem medially) with 15° of anteversion, (iii) valgus position (with

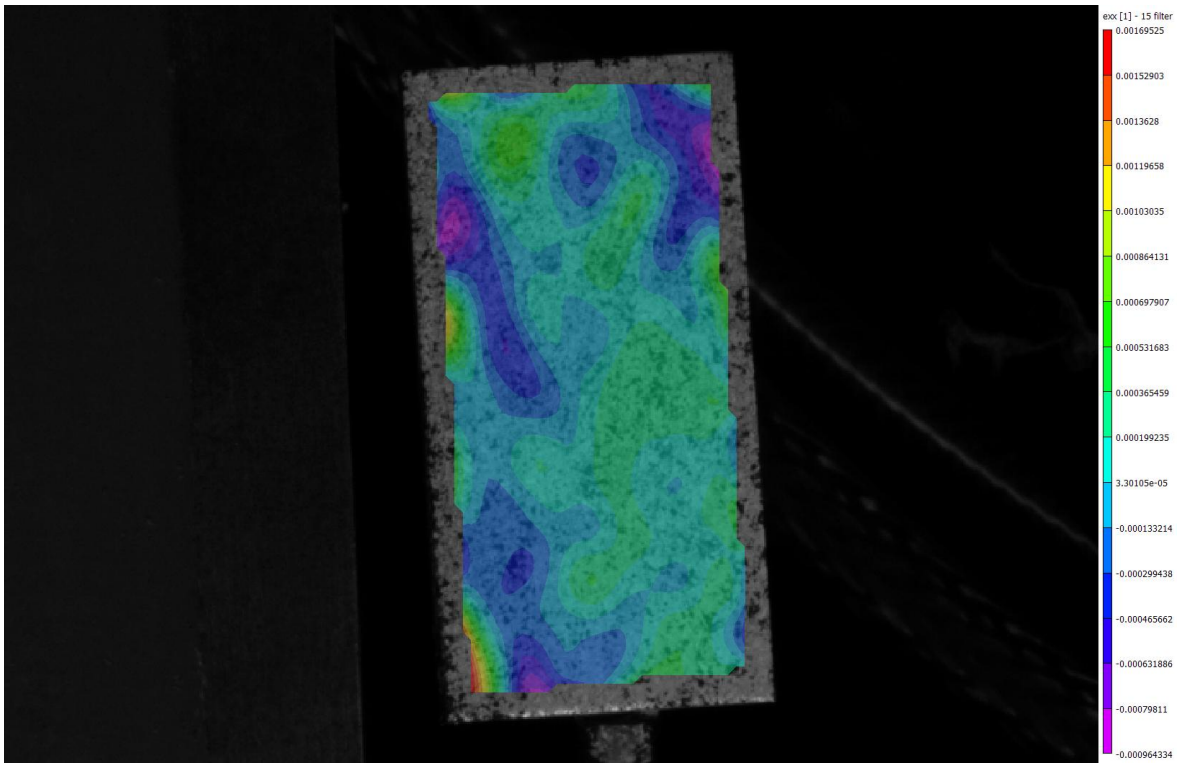

Figure 5.18: Strain exx superimposed on the original image

the proximal stem laterally) with 15° of anteversion and (iv) varus position with 0° of anteversion, see Figure 5.19.

Note, two implants were implanted in the valgus position as the first implantation resulted in fracture of the bone. However, this bone was retained for testing as the fracture was not severe; the surgeon rounded the fracture with a grinding tool to reduce any stress concentration.

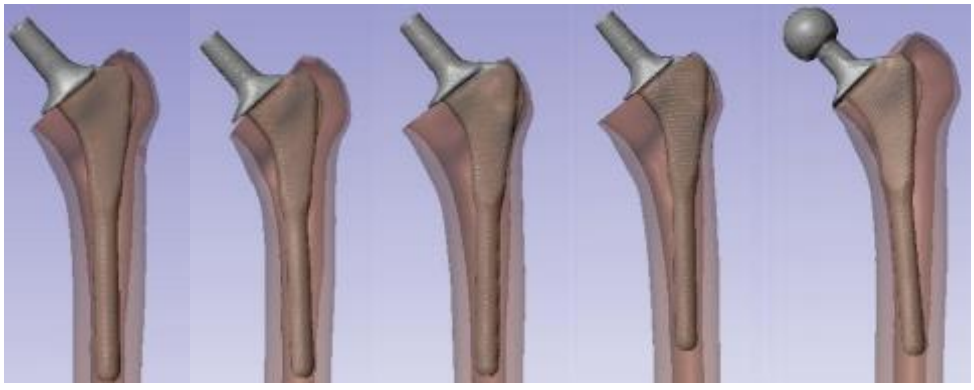

(a) (b) (c) (d) (e)

Figure 5.19: Implant positioned in: (a): neutral aligned femoral stem with 15° of anterversion, (b): varus aligned femoral stem with 15° of anterversion, (c) and (d): valgus aligned femoral stem with 15° of anterversion,(e): varus aligned femoral stem with 0° of anterversion

CT images were taken for each implanted bone at the Southampton General Hospital using a Siemens Sensation scanner (64-slice) with a fine resolution of 0.3 mm x 0.3 mm x 0.7 mm and the models were created using ScanIP (Simpleware Ltd, Exeter, UK) according to the procedure shown in Section 3.3.1.

Each implanted bone was subjected to a sinusoidal load varying between -0.1 kN and -2.4 kN for 1000 cycles. The DIC was used after the first 2 cycles and also at the end of 500 and 1000 cycles.

A random speckle pattern was applied to the bone and implant to track deformations on both surfaces. To this end, various techniques were used to get the best speckle patterns. First, a custom spray gun based on the use of an airbrush was developed to apply fine speckles; but as the air flow affects the size and density of the patterns; this technique was not considered. In this test, the most effective way of applying the speckles was spraying on the sample's surface from a distance of a meter using a commercial spray paint. Figure 5.20 shows the field of view of the two cameras of the DIC system.

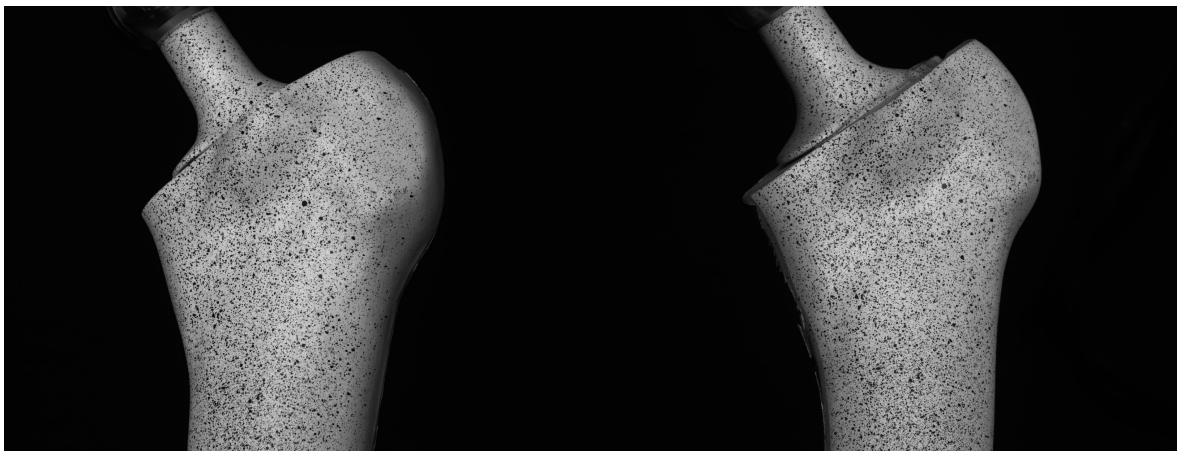

(a) Image from the first Camera (b) Image from the second camera

Figure 5.20: Field of view of the two cameras of the DIC system showing the speckle patterns on the bone and implant surfaces

To measure the implant motion against the bone, four points were selected on the implant and four points on the bone using the Vic-3D software, see Figure 5.21.

The micromotion of each point of the implant was then calculated relative to the associated point on the bone, therefore, the micromotion was measured four times to minimize the error of measurement. The coordinate X, Y, Z and the displacements U, V, Z respectively along the x, y and z axes were exported as a *.csv file, one file for each load step.

The micromotion in three-dimensions was computed using a custom code in Matlab

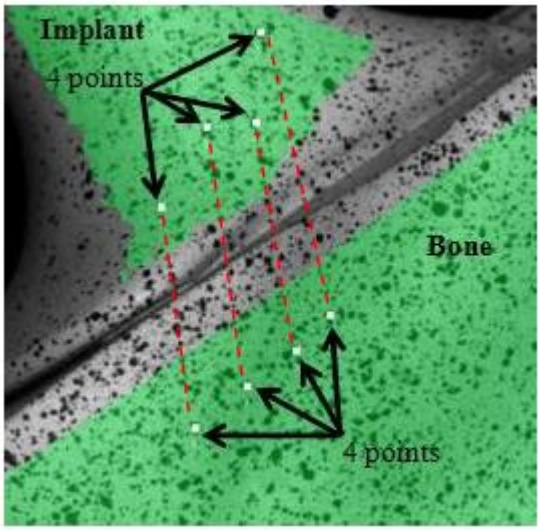

Figure 5.21: Points locations selected on the implant and bone

(presented in Appendix C) and it was assumed to be equal to the magnitude of displacement of one point on the implant against one point on the bone between the loaded and unloaded conditions (U_{LI}, V_{LI}, W_{LI} corresponds to the displacement U,V,W of one point of the implant when a load is applied, U_{UI}, V_{UI}, W_{UI} corresponds to the displacement U,V,W of the same point when the sample is unloaded, and U_{LB}, V_{LB}, W_{LB} corresponds to the displacement U,V,W of the associated point on the bone when a load is applied and U_{UB}, V_{UB}, W_{UB} corresponds to the displacement U,V,W of the same point when the sample is unloaded):

$$micromotion = \sqrt{micromotionX^2 + micromotionY^2 + micromotionZ^2} \tag{5.1}$$

where $micromotionX = \sqrt{((U_{LI} - U_{LB}) - (U_{UI} - U_{UB}))^2}$ corresponds to the micromotion along the x-axis, $micromotionY = \sqrt{((V_{LI} - V_{LB}) - (V_{UI} - V_{UB}))^2}$ corresponds to the micromotion along the y-axis, and
$micromotionZ = \sqrt{((W_{LI} - W_{LB}) - (W_{UI} - W_{UB}))^2}$ corresponds to the micromotion along the z-axis.

5.2.2 Results

Figure 5.22 shows the micromotion obtained at specific cycles. Micromotion along the x, y and z axes are presented in Appendix E.

The migration, i.e the non recoverable motion within a cycle, was also computed within the first, second, 500^{th} and 1000^{th} cycles, see Figure 7.14. Migration along the x, y and z axes are presented in Appendix E.

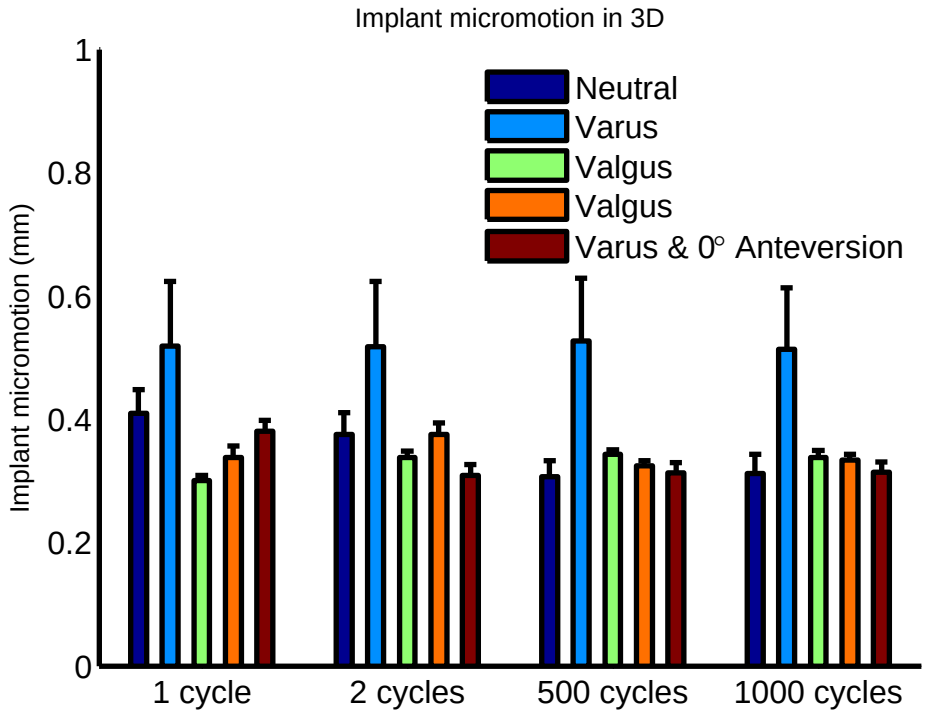

Figure 5.22: Implant micromotion during 1, 2, 500 and 1000 cycles for each implanted bone

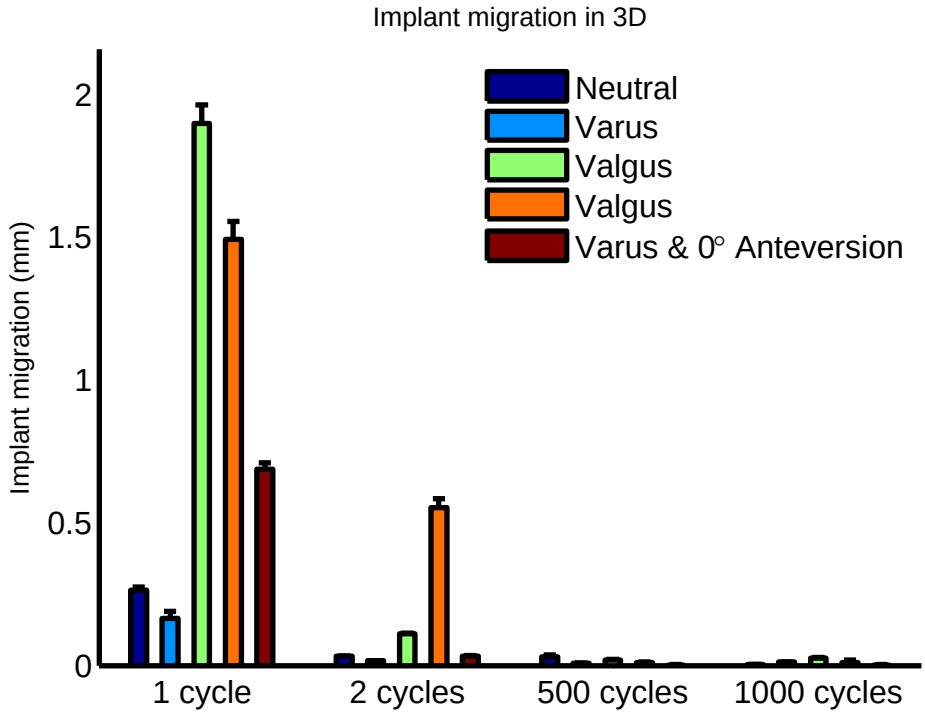

Figure 5.23: Implant migration during the 1st, 2nd, 500th and 1000th cycles for each implanted bone

5.3 Concluding remarks

The first part of this study demonstrated the potential of the DIC system as a viable means of assessment of bone surface strains during biomechanical testing. Strain gaug-

ing has been successfully employed [48, 140, 148] in research for decades and provides a robust means for assessing bone strains and the DIC system is a novel strain measurement technique that is being increasingly employed in bioengineering [101, 141, 146]. Although the strains measured by the DIC system are near the resolution limits of the DIC, good agreement is observed with strain gauging which suggests that the DIC system gives accurate results.

It should be noted that both DIC and the use of strain gauges have specific requirements in terms of sample preparation: random speckle patterns have to be applied to enable the DIC measurements; however, if the specimen already has a natural pattern or contrast, there would be no need to apply an artificial pattern. If a specimen requires preparation, the preparation for DIC is quicker and simpler when compared to that required for strain gauges as it only involves painting the surface. In contrast, strain gauging requires more intricate preparation (as described in section 5.1.1.1).

Strains are measured solely at the location of the gauges and if the region of interest is within a wide field of view, it requires a greater number of strain gauges [129, 148] to cover the whole area. One gauge requires three wires and a rectangular rosette requires nine wires, which shows how fastidious the preparation can become if the sample requires several gauges. Compared to the strain gauging technique, the DIC system is a non-contact technique and provides a map of displacements and strains and it can also provide results in three dimensions. It should also be mentioned that the Vic-3D software uses native images, which means that the image quality is optimum, as they are not compressed by the software. However, it is highly recommended to light the specimen well to enhance the quality of the image acquisition while using the DIC technique.

The first part of this study shows a very good correlation between the strain measured by the DIC technique and strain gauges. The coefficient of determinations for each measurement were $R^2 = 0.99$. However, it should be noted that the accuracy of the measurements seems to get higher for higher applied load along the y-axis, i.e. the longitudinal axis of the femur. For instance, at 3,600 N, the maximum relative error for the strain measurement along the y-axis was 4%.

The second part of the study demonstrated the potential of the DIC system for implant motion in three-dimensions. A custom made code was created to compute the micromotion. The use of this system for this kind of measurement is very interesting because there is no contact with the sample (the bone or implant), therefore the measurement technique does not interfere with the sample and the results are not affected. In addition, it does not require the time consuming or elaborate set up involved with LVDT analyses [94]. Five bones were implanted with various orientations: (i) neutral

position with 15° of anteversion, (ii) varus position with 15° of anteversion, (iii) valgus position with 15° of anteversion, (iv) varus position with 0° of anteversion, see Figure 5.19. Two bones were implanted with the implant in valgus orientation as the first implantation resulted in a minor fracture of the bone on the proximal lateral side of the bone. As regards the implant orientations, it should be noted that the maximum valgus orientation of the implant may not be possible to achieve in a surgery of a patient as the muscles and surrounding tissues will prevent this. To demonstrate the concept however, these analyses used the maximum angle permissible.

Throughout the test, the highest micromotion was found for the implanted bone with the implant in varus and 15° of anteversion, which corroborates the findings of the computational model, where anteversion was highlighted to be a sensitive parameter at the proximal end of the implant (Chapter 4).

During the first cycle, the highest migration was found for the implanted bone with the implant in valgus orientation (note this had a minor fracture) followed by the second bone implanted in valgus orientation and the implant in varus and 0° of anteversion. During the second cycle, the implanted bone in valgus orientation (without fracture) presented the highest migration, followed by the implant in varus orientation. As predicted by the model created in Chapter 4, the performance of the implant is most sensitive to the varus/valgus angle.

The migration for each bone measured using the DIC system lies within the range [0.002mm; 0.026mm] and the migration measured at the shoulder of the stem in Chapter 4 lies within the range [0.002mm; 0.047mm], which gave confidence on the use of the DIC system for implant micromotion measurements.

In most studies on implant micromotion measurements, LVDTs were used and in contrast to the DIC technique, LVDT measures in only one direction; therefore three LVDTs are needed to measure the micromotion in three-dimensions. Moreover, to measure the implant micromotion against the bone, the LVDTs need to be fixed to the bone and making holes for the fixation may weaken the bone. However, one of the limitations of using an optical system for measuring the implant micromotion is that the measurement is not carried out at the interface; however, it can be calculated against the bone at any visible point.

The DIC system has great potential for measuring implant micromotion but the associated software offers limited functionality for post processing the results obtained. For example, in the present study, comparison of the results with the outputs of the strain gauges needed custom code written in Matlab.

These tests were carried out on synthetic bone and the strain measurements using the

DIC technique provided satisfactory results. Measurement of strain on a cadaveric bone may be difficult due to surface moisture. In fact, cadaveric bones are usually in a wet condition. However, Sztefek et al. [141] investigated the strain of a mice bone using the DIC technique and compared their results with strain gauges. This study shows that with an appropriate surface preparation, the DIC technique can provide accurate strain measurements for cadaveric bone.

Chapter 6

Studies on the effect of loading and implant orientations on implant performance

Traditionally, computational studies of the total hip replacement employ an implant placed in the neutral position [11, 154] and subjected to a single load case; this load case is usually stair climbing as it is believed to be the most critical load case scenario [152]. While some studies, such as that by Abdul-Kadir and Hansen [11] have investigated the effect of loading during walking, recent advances in computational modelling now allow the combined effects of such factors to be assessed. Using such approaches, multiple scenarios may be investigated in a single analysis; this has the potential to lead to a better understanding of what factors affect implant primary stability. This chapter presents a novel methodology to assess implant performance when the implant orientation and the loading to which it is subjected are both subject to uncertainty. The aim was to construct a surrogate model to mimic the behaviour of the finite element model while reducing the computational expense considerably. A design of experiments approach was first employed to generate a set of different implant orientation and loading case scenarios. To do so, Latin hypercube sampling was used to generate a sample with different combinations of implant positions and applied loads, and a contact analysis was run for each combination. The micromotion at the bone-implant interface and bone strain were both computed as they are recognised as good criteria for assessing implant performance. The data generated was then used to construct a Bayesian Gaussian process emulator to predict biomechanical response. Successful proof of concept would enable many possible scenarios to be modelled in a rapid, computationally efficient manner.

6.1 Methodology

6.1.1 Sample selection

The 3D meshed model of the implanted sawbone employed in Chapter 3 was used in this study to generate the surrogate model. In contrast to the studies presented in the earlier chapters, both the loading and implant orientations are simultaneously varied. A total of six input variables were involved in the parametric study and they are described below.

- angle α : anteversion/retroversion angle of the femoral implant
- angle β : varus/valgus angle of the femoral implant
- angle γ : anterior/posterior angle of the femoral implant
- force Fx : horizontal force in the lateral/medial direction applied at the top of the femoral head
- force Fy : horizontal force in the anterior/posterior direction applied at the top of the femoral head
- force Fz : vertical force from proximal to distal end (i.e. longitudinal force) applied at the top of the femoral head

Using the same methodology described earlier in Chapter 4, the distal end of the stem was defined as a reference point and the implant orientations were varied within selected range of angles from the neutral position: anterversion/retroversion angle = $[-15\,°; 8\,°]$, varus/valgus angle = $[-2\,°; 3.6\,°]$ and anterior/posterior angle = $[-1.8\,°; 1.2\,°]$.

The three forces were derived from the website *www.orthoload.com* edited by Professor Bergmann from the Charité University in Berlin. Two activities of the patient designated EBL in the Bergmann study were selected: free walking velocity and normal stair climbing velocity (up and down). Table 6.1 shows the minimum and maximum forces, Fx, Fy and Fz for both activities in percentage of body weight with a body weight of 650 Newtons. The two gait patterns were combined to find the maximum and minimum forces of both activities; these values were used as the upper and lower bounds of the loading variables Fx, Fy and Fz.

As in chapter 3, the forces, Fx, Fy and Fz were tilted to conform to the British standards. A design of experiments was used to study implant micromotion and bone strain for 120 random combinations defined using Latin hypercube sampling. The mesh morphing technique was employed to automatically update implant position, and for each implant position, a different load case was applied at the top of the femoral component.

Table 6.1: Minimum and maximum forces through walking and stair climbing gait patterns measured for patient EBL, *www.orthoload.com*

	Fx % body weight		Fy % body weight		Fz % body weight	
	Min	Max	Min	Max	Min	Max
Walking	19	147	-24	31	14	315
Stair climbing	15	173	-23	76	13	374
Forces used in this study	**15**	**173**	**-24**	**76**	**13**	**374**

A contact analysis was run for each case using the same method employed in chapter 3; to summarize, the contact analysis used the Penalty method with surface-to-surface elements and contact detection at the Gauss points. A coefficient of friction of 0.3 was applied between the implant and the synthetic bone. A normal contact stiffness of 6,000 N/mm was used and the force convergence tolerance was set to 0.5%.

6.1.2 Construction of the surrogate model

The data generated by running FE simulations at the 120 implant orientation and loading cases obtained via LHS was used to construct Bayesian Gaussian process models. The emulators were subsequently validated using the methodology described earlier in Chapter 4. It is worth noting here that in contrast to the study presented in Chapter 4 which had three input variables, the study in this Chapter involves six input variables. The objective of this study is to investigate if Bayesian Gaussian process modelling can be used to construct a computationally cheap emulator of the FE simulation in such situations.

6.1.3 Assessment of accuracy of the model

To assess the predictive capability of the emulators constructed using the 120 training points, the leave-one-out cross-validation tests described earlier in Chapter 4 were carried out. This involved first comparing the posterior mean of the emulator prediction with the actual value followed by computation of the SCVR values to verify the accuracy of the emulator error bars.

The emulator accurately predicted the average micromotion at the bone-implant interface and average strain of the bone; the coefficients of determination were R^2=0.99 for both responses; whereas the model predicted with less accuracy the maximum micromotion and the coefficients of determination was R^2=0.91. Figures 6.1 and 6.2

show the emulator predicted value against the finite element value for the average and maximum micromotion.

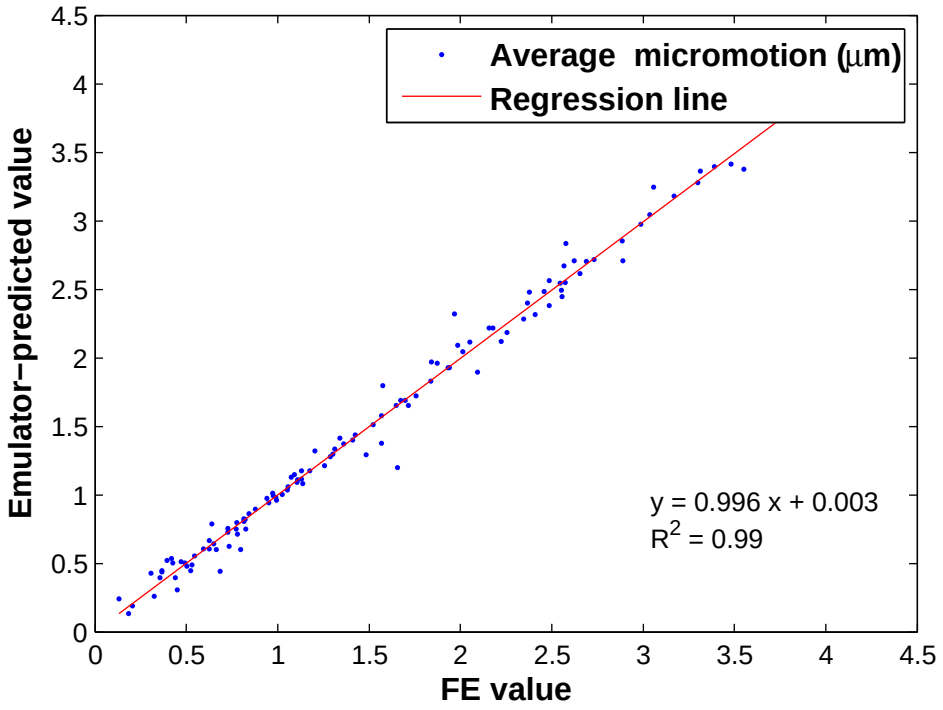

Figure 6.1: Emulator-predicted values against finite element values of average micromotion at the bone-implant interface

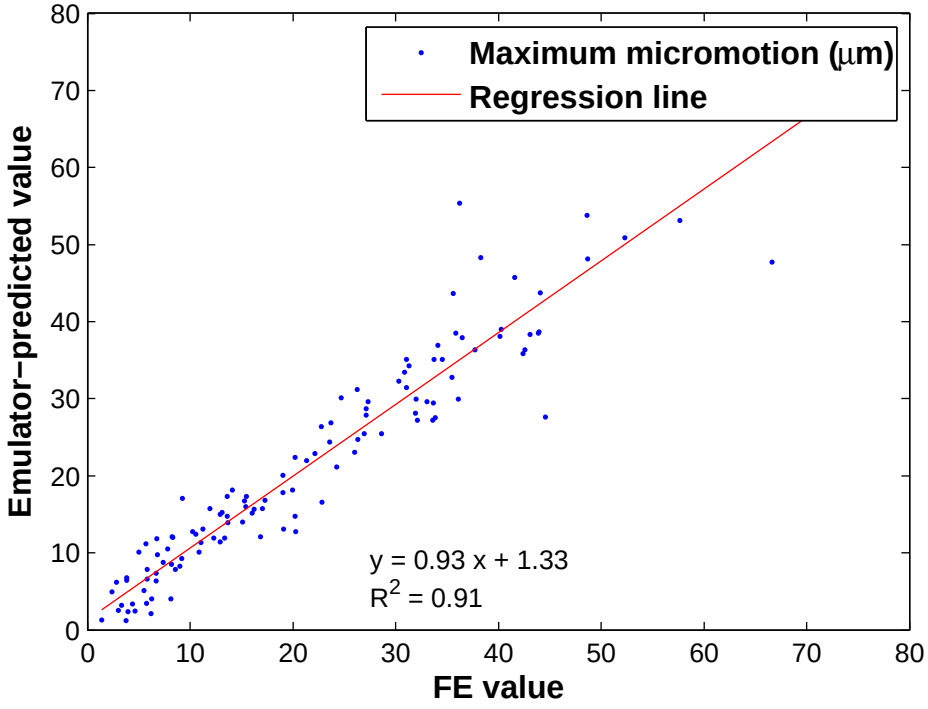

Figure 6.2: Emulator-predicted values against finite element values of maximum micromotion at the bone-implant interface

The SCVR defined earlier in equation (4.16) was used to assess the accuracy of the error bars predicted by the Gaussian process model. If the model is appropriate for model approximation, the SCVR lies within the range [-3,3]. Figures 6.3 and 6.4 show respectively the SCVR for the average and maximum micromotion at the bone-implant interface.

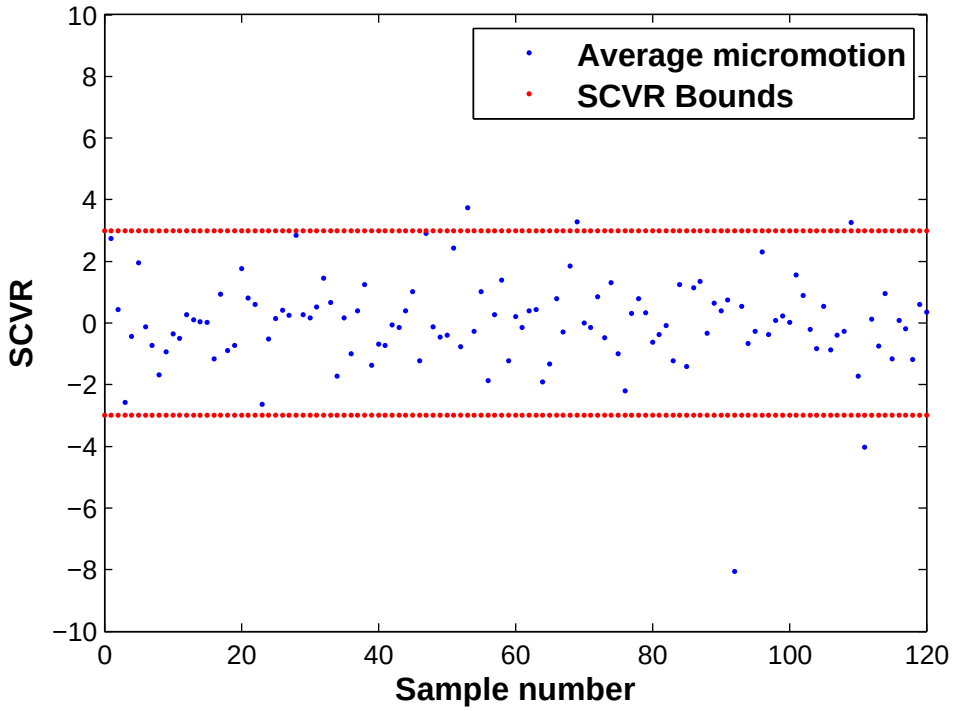

Figure 6.3: Standardised cross validated residuals (SCVR), based on leave-one-out tests for the average micromotion

After validating the Bayesian Gaussian process model, the outputs from the emulator can be used to check the sensitivity of the model to the implant orientations and loads and also predict responses to random inputs.

6.1.4 Prediction of implant primary stability with the implant in a neutral position during stair climbing

The forces used to predict the micromotion at the bone-implant interface and bone strain are shown in Figure 6.5. This Figure shows the forces Fx, Fy, Fz and Fres, which corresponds to the resultant force. The FE simulations for the loading history were run for each load step independent of each other.

Implant stability was assessed for an implant inserted in a neutral position during stair climbing. The loading was discretized into thirty steps and finite element simulations were carried out at all these points. The FE predictions at these points were then

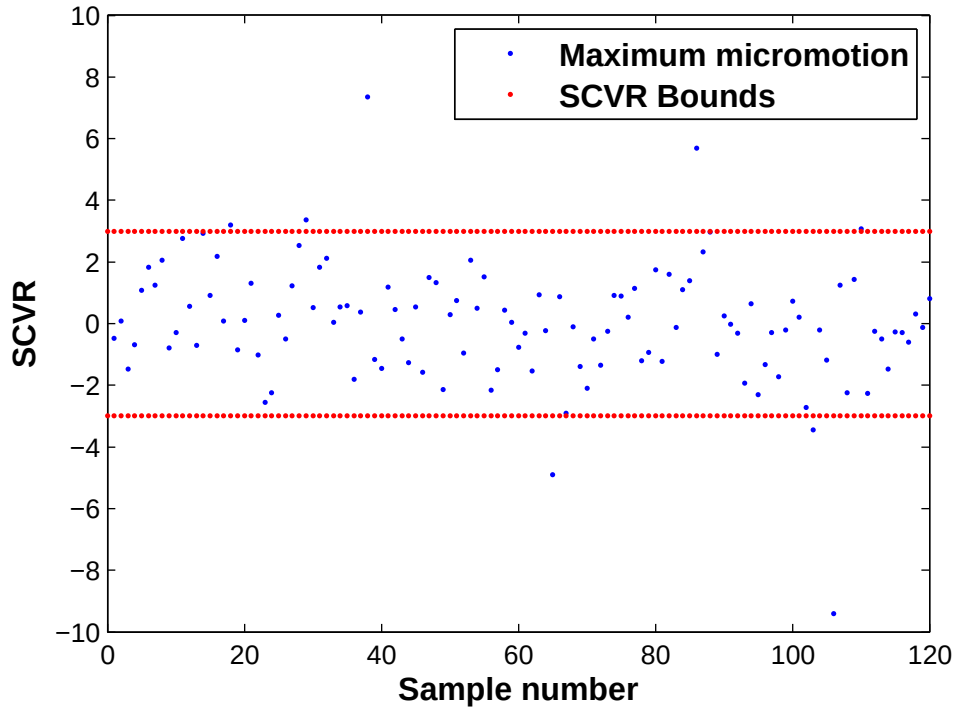

Figure 6.4: Standardised cross validated residuals (SCVR), based on leave-one-out tests for the maximum micromotion

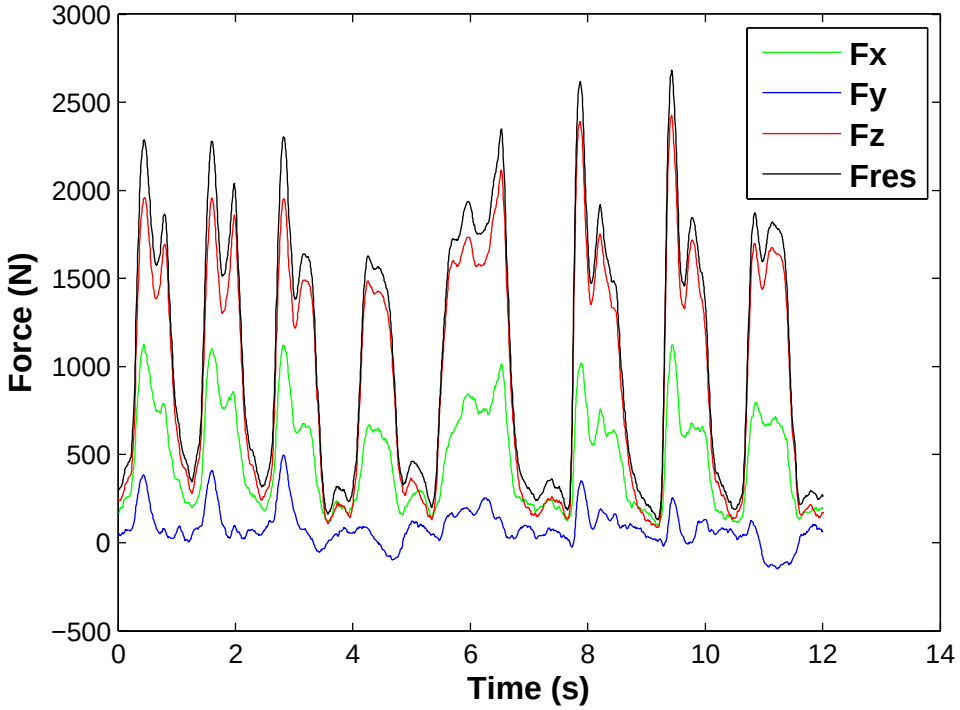

Figure 6.5: Stair climbing forces applied at the top of the femoral head [Stair climbing forces applied at the top of the femoral head from *www.orthoload.com*]

compared to those computed using the emulator.

6.2 Results

Figures 6.6 and 6.7 show respectively a comparison of average and maximum micromotion as a function of the loading step predicted using FE analysis and the emulator. It can be observed from the figures that the average and maximum micromotion at the bone-implant interface did not exceed 2.5μm and 40 μm, respectively.

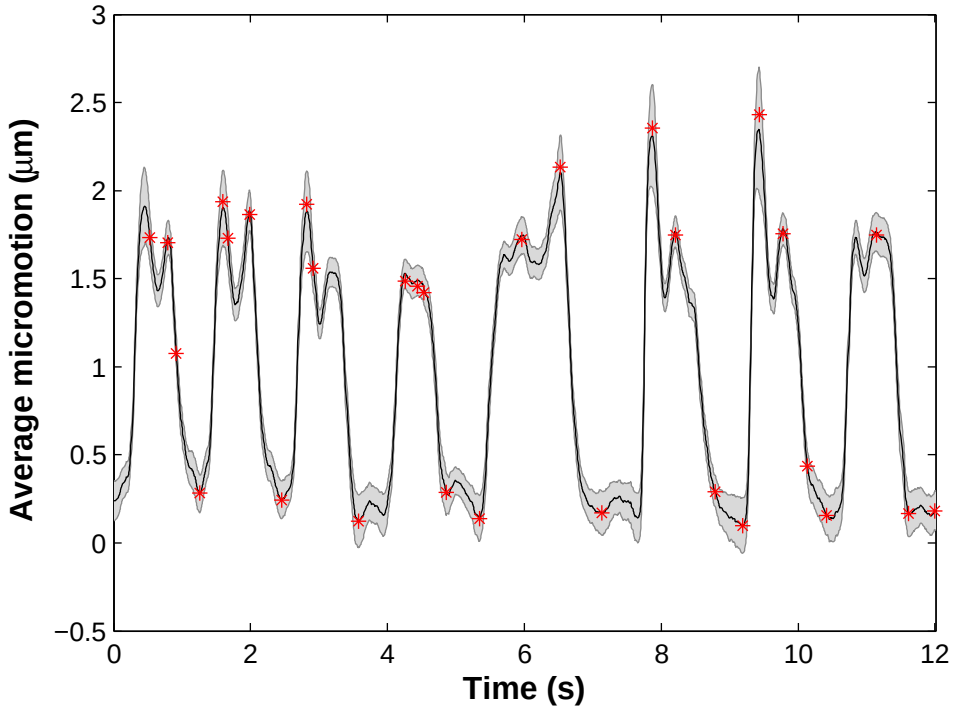

Figure 6.6: Average micromotion predicted by the emulator and finite element analysis through time. The shaded bar indicates the emulator prediction ± 3 standard deviations and the cross indicates the FE results

It can also be noted from Figures 6.6 and 6.7 that the emulator provides a better approximation of average micromotion compared to the maximum micromotion metric. This is not unexpected since the leave-one-out cross-validation test conducted in 6.1.3 suggested that the emulator for average micromotion has better predictive accuracy than the emulator for the maximum micromotion.

Figures 6.8 and 6.9 show respectively the prediction of the displacement at the distal end and shoulder of the stem as a function of the loading step predicted using FE and the emulator. It can be observed from the figures that the emulator predicts accurately these two metrics.

The effect of each parameter was isolated from the others to evaluate the input-output relationships. Figure 6.10 shows the main effects of each variable for the maximum micromotion at the bone-implant interface.

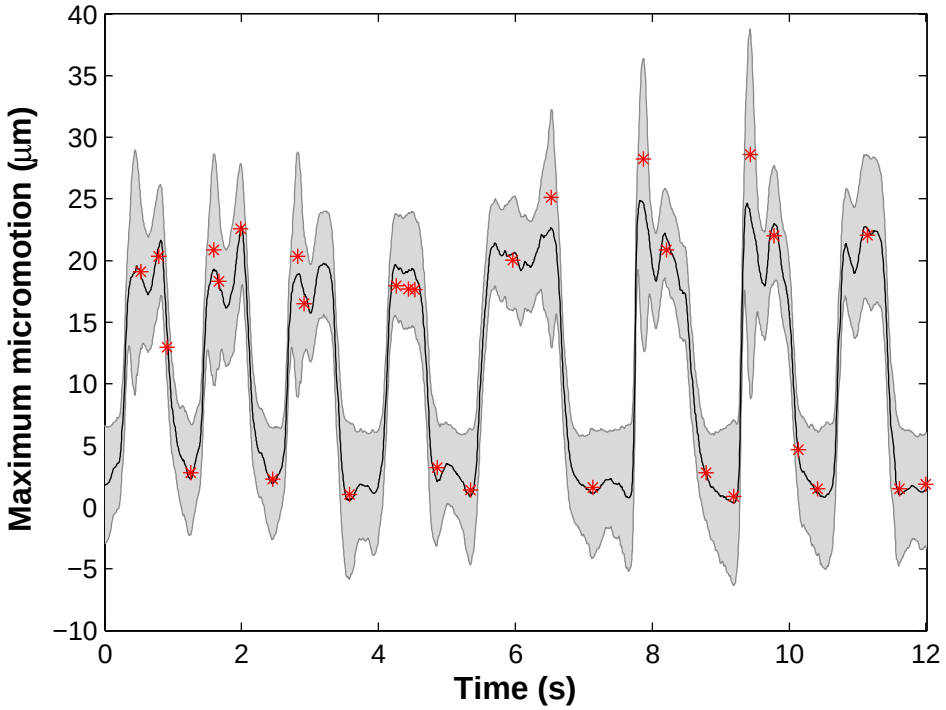

Figure 6.7: Maximum micromotion predicted by the emulator and finite element analysis through time. The shaded bar indicates the emulator prediction ± 3 standard deviations and the cross indicates the FE results

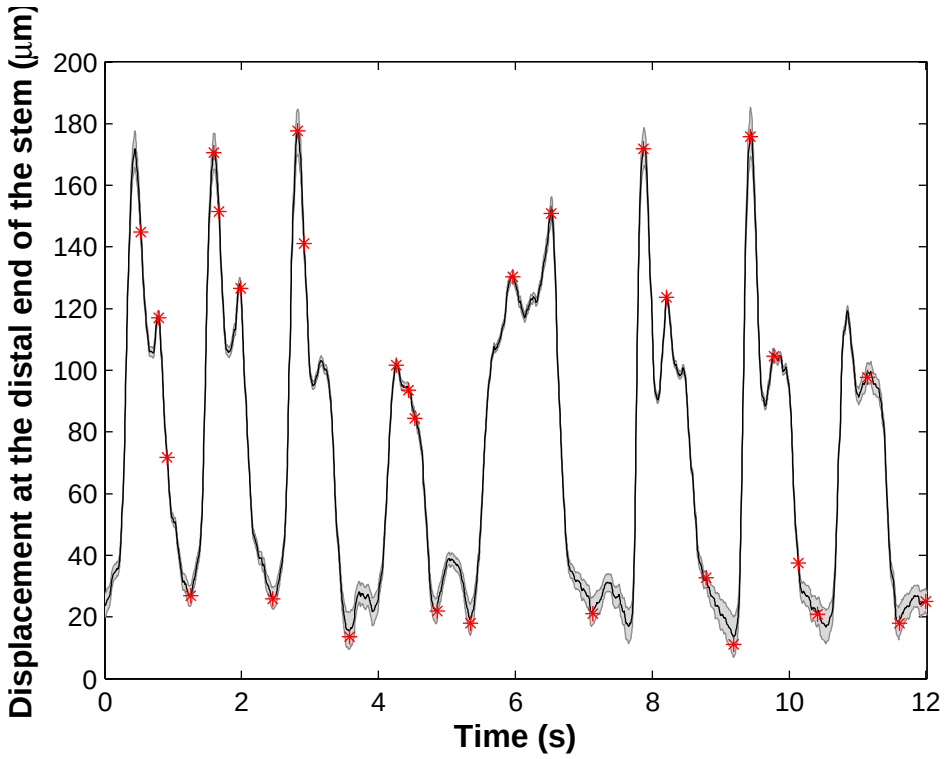

Figure 6.8: Displacement at the distal end of the stem predicted by the emulator and finite element analysis through time. The shaded bar indicates the emulator prediction ± 3 standard deviations and the cross indicates the FE results

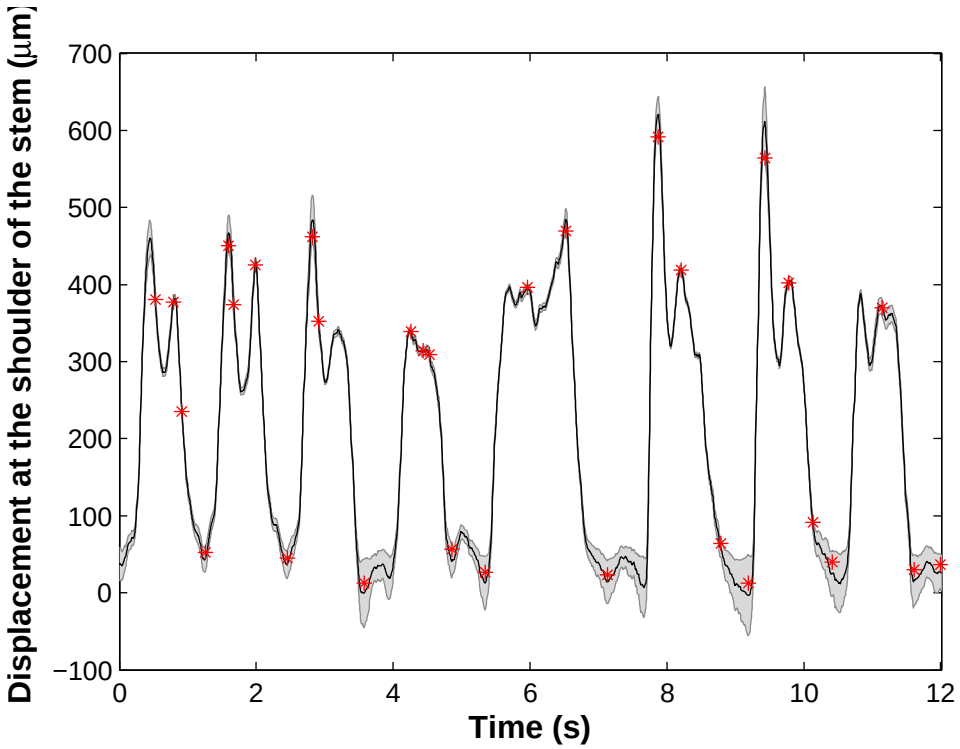

Figure 6.9: Displacement at the shoulder of the stem predicted by the emulator and finite element analysis through time. The shaded bar indicates the emulator prediction ± 3 standard deviations and the cross indicates the FE results

The outputs from the emulator can also be used to check the sensitivity of the model to the implant orientations and loads. As an example, the maximum micromotion at the bone interface was mostly sensitive to the axial loading (86%), followed by the varus/valgus angle of the implant (9%),the force Fx (from lateral to medial) (3%), the ante-retroversion angle (2%), the ante-posterior angle and the force Fy (from ventral to dorsal).

6.3 Concluding remarks

The developed surrogate model enabled the prediction of the effect of implant orientations on the primary stability of a cementless total hip replacement through a gait cycle in a cheap computational manner. The emulator predicted the biomechanical responses for any implant position within any activity.

This proof of concept study is extremely promising; a good correlation was found, specifically, to predict the displacement at the distal end and shoulder of the stem. However, it should be noted that adding more data in the training data set will lead to higher accuracy in the output prediction.

A limitation of the study is that the influence of muscles is not included. Thus, it

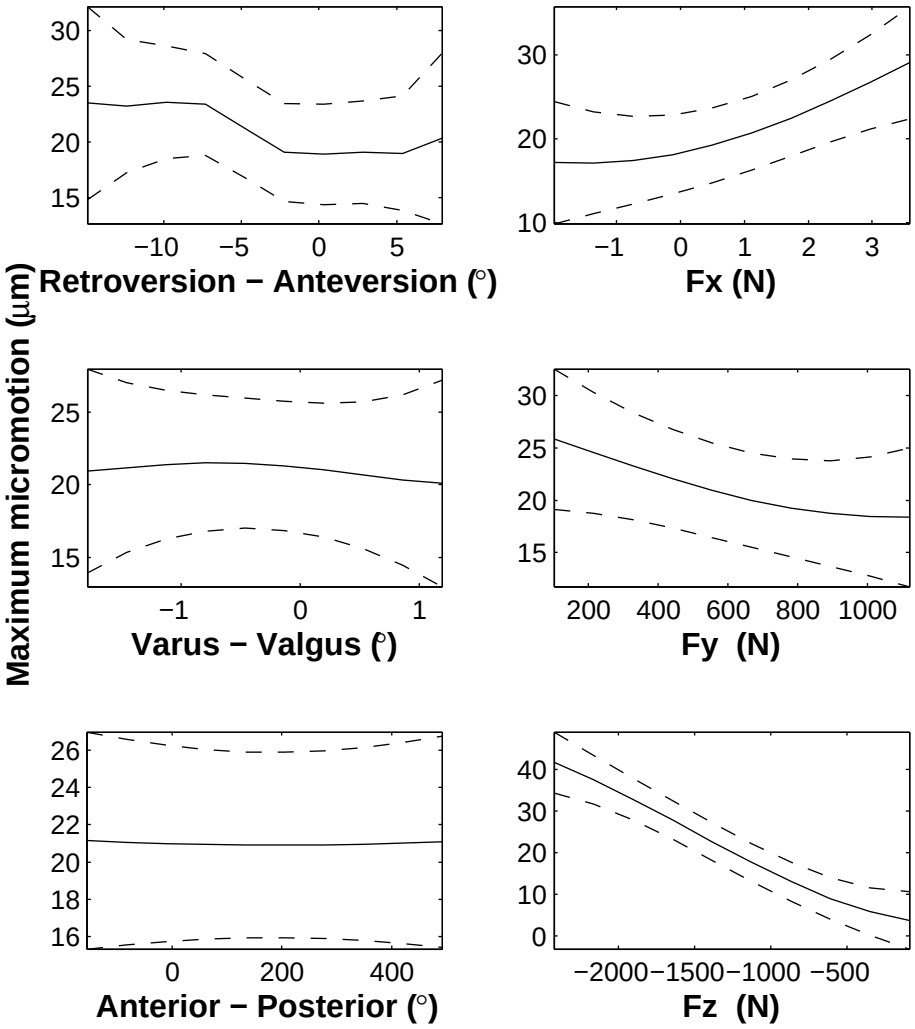

Figure 6.10: Main effect plots of maximum micromotion at the bone-implant interface

should be kept in mind that the stability of total hip replacement may be overestimated compared to a real case scenario [11]. As this study involved non-linear analysis, the prediction between two outputs of the training points could be questionable; however, the finite element comparison shows a good correlation. However, the model predicts the implant performance at an instant time and given force, which can help to understand how the implant will behave for various case scenarios.

The loading scenario was derived from the website *www.orthoload.com*, and for the hip joint, moment forces were not provided. The patient selected for the study was arbitrary, and as medical images of the patient's femur were not provided, a synthetic bone was used for the analysis. However, the patient's weight, i.e. 650 Newtons, may be low for the bone size used. This may explain why the average micromotion at the bone-implant interface did not exceed $2.5\mu m$.

In this study, each parameter was isolated from the others and their effects on biomechanical responses were assessed. The model shows that perhaps as expected the force

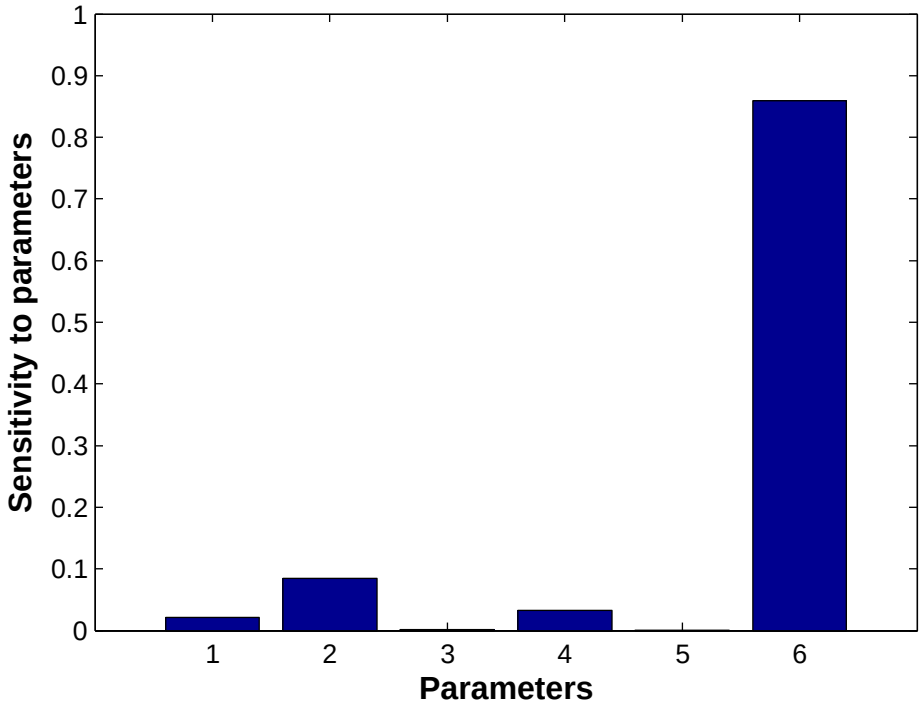

Figure 6.11: Sensitivity of the model to the parameters: (1) ante-retroversion angles, (2) varus-valgus angles, (3) antero-posterior angles, (4) Force Fx, (5) Force Fy and (6) Force Fz

applied along the axial direction has the greatest impact on the implant micromotion and therefore on the implant integrity. The secondary parameters affecting the implant micromotion are the varus/valgus orientation of the implant.

This study presented a methodology that can potentially be employed in preclinical assessments of implant performance at the early post-operative stage. Using such a method, implant stability can be predicted for a specific orientation and activity of a patient. Therefore, if the surgeon can control the implant orientation, and the patient can control the activity level, the outcome of hip replacement can be improved.

Chapter 7

Main Conclusions and Future work

7.1 Conclusions

The primary stability of a cementless total hip replacement depends on different parameters such as bone quality, the implant used, the initial implant orientation and the level of activity of the patient. The aim of the present work was to assess the primary stability of a cementless total hip replacement employing computational and experimental methods. The project consisted of four main studies:

- The aim of the first study was to define and assign parameters for the finite element analysis and corroborate them by conducting experimental tests. This was a deterministic study on a single implant orientation (neutrally positioned) while a static load was applied at the top of the femoral head.
- The aim of the second study was to assess the effects of implant orientations using a mesh morphing strategy and Bayesian Gaussian process model. Experimental tests were also conducted on femurs implanted in neutral and 'poor' orientations predicted by the computational study.
- The aim of the third study was to assess the use of the digital image correlation technique for bone strain measurements by comparing the results obtained with the output of the strain gauges. The potential of this technique for implant micromotion measurements was also investigated.
- The aim of the fourth study was to assess implant performance when implant orientation and loading are both subjected to uncertainty using a mesh morphing strategy and Bayesian Gaussian process model.

In the project, a 12 mm diameter Furlong prosthesis was implanted in a large bone composite femur. Two main sizes of synthetic bones were available in the market:

medium and large. The choice of the large bone was based on the greater range of implant positions that could be investigated. As the experimental tests were repeated, the use of composite bone was advantageous as it reduced variability between bones. In addition, they were also immediately available at lower cost.

To assess implant performance, two biomechanical responses: the stem micromotion/migration, and strain in the bone were studied. It is known that a certain amount of implant micromotion is needed for bone growth into/onto the implant surface. However, the threshold that inhibits bone ingrowth is still unclear, and in most studies it is believed that a micromotion greater than 150 μm inhibits bone ingrowth [119, 76]. Moreover, it has been suggested that the yield strain of bone is $0.78 \pm 0.04\%$ in tension and $0.84 \pm 0.06\%$ in compression [84]. These two factors were therefore defined as the main criteria for evaluating implant performance.

This project presents three main novelties: (1) the use of the mesh morphing technique and (2) Bayesian Gaussian process modelling in the biomedical computational field and (3) the use of the digital image correlation technique in biomedical experimental field. The mesh morphing technique was employed to update the implant position of the meshed implanted bone using a baseline mesh. This offered the possibility of generating a set of implanted bone meshed with a new implant position in the finite element software itself, hence avoiding the use of CAD and meshing software. The Bayesian Gaussian process model was used to assess the effect of implant orientations and loading scenario on the structural integrity of the implant. It was also used to predict the case which was most likely to lead to implant loosening. The combination of these techniques is unique to the biomedical field, and enable complex analyses to be undertaken rapidly and in a very computationally efficient manner.

The experimental work presented methodologies for the assessing primary stability of an implant. The first method used LVDTs to measure the stem micromotion and migration and the DIC system for bone strain measurement. At the outset of the project, no relevant studies had been published on bone strain measurements using the DIC system. Therefore, it was crucial to assess and validate its use, which was carried out in Chapter 5. Good corroboration between strain gauge and DIC measurements demonstrates its potential in this field, and the use of DIC for monitoring micromotion and migration (hitherto not reported on the academic literature) could represent a cost effective rapid alternative method to LVDTs. It was notable that better corroborations were observed between the computational and experimental models using migration as a metric. In particular, LVDT based measurements of micromotion were inconsistent and subject to great variability. DIC measurements, however, were more consistent and did corroborate with the sensitivity analysis in Chapter 4.

7.2 Future development

The aim of the PhD project was to computationally and experimentally assess the performance of a cementless total hip replacement. The project presented methodologies to evaluate implant performance when the orientation and load scenarios are both subjected to uncertainties. While designing the methodologies, limitations of current research have been identified and brought forth in each of the chapters.

One of the limitations of the computational work is that mechanical and biological metrics such as muscle forces and tissue differentiation were not simulated. These would be expected to influence the implant micromotion and bone strain measurements. The work of researchers such as Heller et al. [68] has enabled muscle forces to be ascertained for use in finite element models. Although the stochastic nature of the present research required that these were precluded from the models, advances in computational power should allow muscle forces to be incorporated in future investigations [136].

Previous work in the Bioengineering group has involved the development of tissue differentiation algorithms for the assessment of bone growth around short stemmed implant [124]. The same principles could be applied here for the case of long stemmed implants.

The computational study was carried out on a single bone; therefore it would be interesting to investigate the effect of implant positioning for various patients. This could be carried out by combining the existing work with the techniques and methods employed in a previous work in the Bioengineering group, which presented a methodology to build a statistical model of the geometry including material properties of the femur [37].

While the promising qualitative correlations observed experimentally are encouraging, the experimental techniques developed in this study were limited in number due to time and expense considerations; future studies would benefit from more extensive mechanical testing to increase confidence in the computational findings. Ideally, a more robust experimental model would be desirable. It has been found that the abductors have the greatest effect on the model in gait, and that iliotibial femoral band and adductors have relatively less effect [139]. Simulating them in an experimental model would therefore be beneficial in any future work. In the present research, this was sacrificed to limit the number of variables; however, in the longer term, analyses could incorporate this parameter, together with multi-femur investigations on cadaveric bone.

Appendix A - Conference publications

- H. Ozturk, P.B. Nair and M. Browne, (2011) Computational assessment of the coefficient of friction on cementless hip replacement stability. *At, the 36th Congress of the Society of Biomechanics*, August 31-September 2, 2011, Besançon, France.

- H. Ozturk, M.T. Bah, P.B. Nair, M. Browne, (2010) Does the implant pivot position affect the outputs of probabilistic analyses of the cementless total hip replacement? *At, the 6th World Congress on Biomechanics*, August 1-6, 2010, Singapore.

- H. Ozturk, P.B. Nair, M. Browne, (2010) Experimental validation and computational corroboration of bone surface strain measurement determined via digital image correlation. *At, the 18th European Orthopaedic Research Society*, June 30-July 2, 2010, Davos, Switzerland.

- H. Ozturk, P.B. Nair, M.T. Bah, S.L. Evans, A.M.H. Jones, M. Browne, (2010) Computational and experimental assessment of primary stability of a cementless total hip replacement: The effect of the stem positioning. *In Proceedings of the 9th International Symposium on the Computer Methods in Biomechanics and Biomedical Engineering*, February 24-27, 2010, Valencia, Spain.

- H. Ozturk, A.M.H. Jones, S.L. Evans, P.B. Nair, M. Browne, (2009) Experimental and finite element corroboration on the mechanical behaviour of a cementless hip replacement. *In Proceedings of the 22nd Annual Congress of the International Society for Technology in Arthroplasty*, October 22-24, 2009, Big Island, Hawaii.

Appendix B - Simpleware software

Simpleware software solutions are based on a core image processing platform, ScanIP, with optional bolt-on modules for FE/CFD mesh generation and CAD integration.

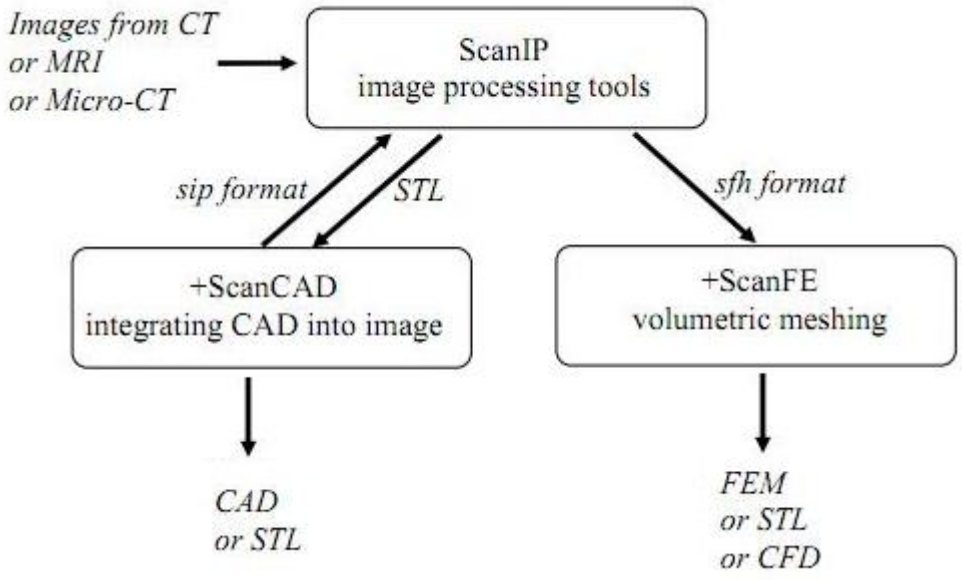

- Using ScanIP
  - 3D images from CT scan or MRI or Micro-CT can be imported by ScanIP
  - after using ScanIP, a STL file or a sfh format can be exported
- Using ScanFE
  - a sfh format can be imported from ScanIP
  - after using ScanFE, it is possible to export files in formats that can be used in different softwares for processing, such as finite element (Ansys), rapid prototyping (STL) or in computational fluid dynamics (FLUENT)
- Using ScanCAD
  - a CAD or STL model can be used
  - after using ScanCAD, the file can be exported to ScanIP

Appendix C - Matlab code for postprocessing the DIC measurements

The following code enables the calculation of the mean value and standard deviation of the strain along the x-axis, y -axis and the maximum and minimum strains in a specific area using data from Vic-3D software. To replicate the measurement of each rosette, four points were first selected defining the rectangular area. The X, Y, and Z coordinate of each point on each image were exported as a *.csv file.

```
% Hatice Ozturk, hatice.ozturk@soton.ac.uk
% 25/10/2010

clc
clear all

rosette=xlsread(sprintf('gaugeposition.csv')); % load x,y,z of the points
% corresponding to the edge of the gauge

for i=2:37 %no calculation in the first file
node{i-1}=[rosette(i,1) rosette(i,2); rosette(i,4) rosette(i,5);...
    rosette(i,7) rosette(i,8); rosette(i,10) rosette(i,11)];
end



for m=1:36 %no calculation in the first file

images=xlsread(sprintf('load%d.csv',m));
[row col]=size(images);

a=1;

% select the point within the gauge
for i=1:row
    in(i,1)= inpolygon(images(i,1),images(i,2),...
        node{1,m}(:,1),node{1,m}(:,2));

    if in(i,1) == 1
        pointsinarea{m,a}=images(i,:);
        a=a+1;
    end

end

end
```

```
37
38 [f g]=size(pointsinarea);
39
40 %calculation of the mean values from col 16 to 23
41 for i=1:g
42     for b=1:36
43         for c=1:8
44             if size(pointsinarea{b,i}) == [1 26]
45         values{b,c}(i)=pointsinarea{b,i}(c+15)*1000000;
46             end
47         end
48     end
49 end
50 meanvalues=cellfun(@mean, values);
51 stdvalues=cellfun(@std, values);
52
```

The following code enables micromotion and migration calculations based on data generated by Vic-3D software. Implanted femurs were tested and for each femur, a file consisting of [3,32] elements were created in Vic-3D. Assuming t0 as the beginning of a cycle and tf as the end of a cycle, measurements using the digital image correlation technique were carried out at t0, (tf-t0)/2 and at tf (which correponds to the number of rows of the imported file). Four points were selected on the implant and four points were selected on the bone and four outputs were extracted for each point (a total of (4+4)*4 outputs were used, which corresponds to the number of columns of the imported file)

```
1  % Hatice Ozturk, hatice.ozturk@soton.ac.uk
2  % 25/10/2010
3
4  clc
5  clear all
6  for m=1:5  % tests were carried out on 5 implanted femurs
7  for n=1:4   % 4 cycles were investigated
8  matrix=load(sprintf('femur%dcycle%d.csv',m,n));   % load the files
9  k=0;
10 for i=1:8:29   % a total of 8 points were selected: 4 on the
11 % bone and 4 on the implant.
12 for j=1:4  % 4 measurements were provided for each point:
13 % displacement U, V, W and the resultant
14 implantminusbone(:,j+4*k)=abs(matrix(:,i+(j-1))-...
15 matrix(:,i+4+(j-1))); % substraction of U, V, W, D of
16 % a point of the implant by the corresponding U, V, W, D of the bone
17 end
18 k=k+1;
19 end
20
```

```
%% MICROMOTION (calculation made when the peak load is applied)
b=1;
for a=1:4:13
micromotionX(1,b)=implantminusbone(2,a)-...
implantminusbone(3,a);
micromotionY(1,b)=implantminusbone(2,a+1)-...
implantminusbone(3,a+1);
micromotionZ(1,b)=implantminusbone(2,a+2)-...
implantminusbone(3,a+2);
micromotionUVW(1,b)=sqrt(micromotionX(1,b)).^2+...
(micromotionY(1,b)).^2+(micromotionZ(1,b).^2);
b=b+1;
end
mean_micrX(n,m)=mean(micromotionX);
% column of matrix mean_micrUVW corresponds to the femur tested,
% row of matrix mean_micrUVW corresponds to the cycle
std_micrX(n,m)=std(micromotionX);
mean_micrY(n,m)=mean(micromotionY);
std_micrY(n,m)=std(micromotionY);
mean_micrZ(n,m)=mean(micromotionZ);
std_micrZ(n,m)=std(micromotionZ);
mean_micrUVW(n,m)=mean(micromotionUVW);
std_micrUVW(n,m)=std(micromotionUVW);

%%MIGRATION (calculation made at the end of the cycle)
b=1;
for a=1:4:13
migrationX(1,b)=sqrt(implantminusbone(3,a).^2);
migrationY(1,b)=sqrt(implantminusbone(3,a+1).^2);
migrationZ(1,b)=sqrt(implantminusbone(3,a+2).^2);
migrationUVW(1,b)=sqrt(implantminusbone(3,a).^2+...
implantminusbone(3,a+1).^2+implantminusbone(3,a+2).^2);
b=b+1;
end
mean_migrX(n,m)=mean(migrationX);
std_migrX(n,m)=std(migrationX);
mean_migrY(n,m)=mean(migrationY);
std_migrY(n,m)=std(migrationY);
mean_migrZ(n,m)=mean(migrationZ);
std_migrZ(n,m)=std(migrationZ);
mean_migrUVW(n,m)=mean(migrationUVW);
std_migrUVW(n,m)=std(migrationUVW);
end
end
```

Appendix D - Results from the DIC technique and strain gauges (Chapter 4)

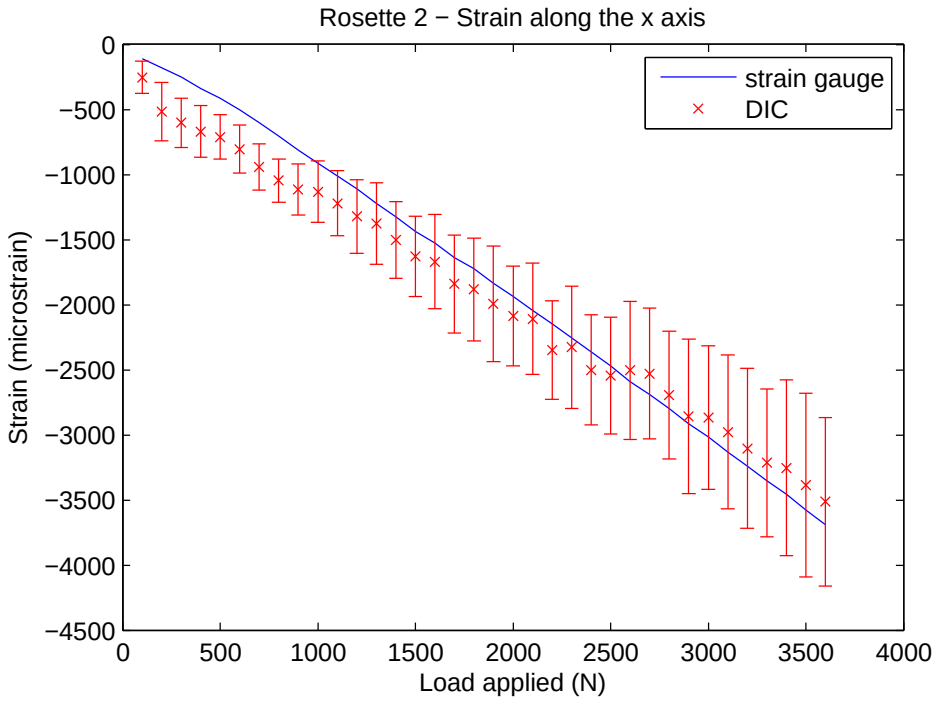

Figure 7.1: Rosette 2 - Strain along the x-axis for both techniques

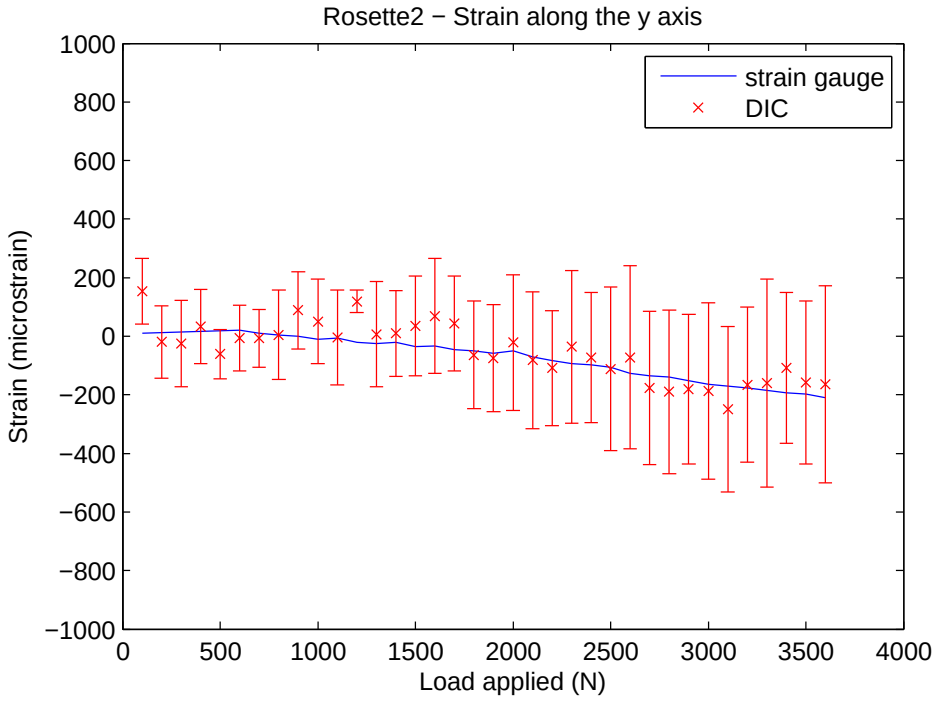

Figure 7.2: Rosette 2 - Strain along the y-axis for both techniques

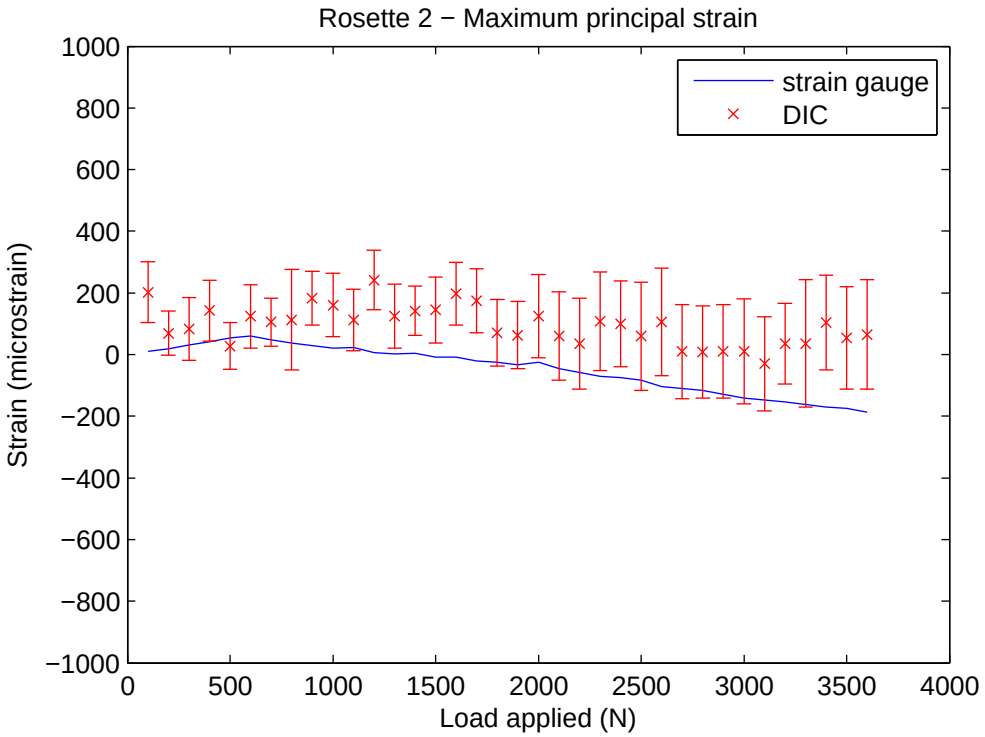

Figure 7.3: Rosette 2 - Maximum principal strain for both techniques

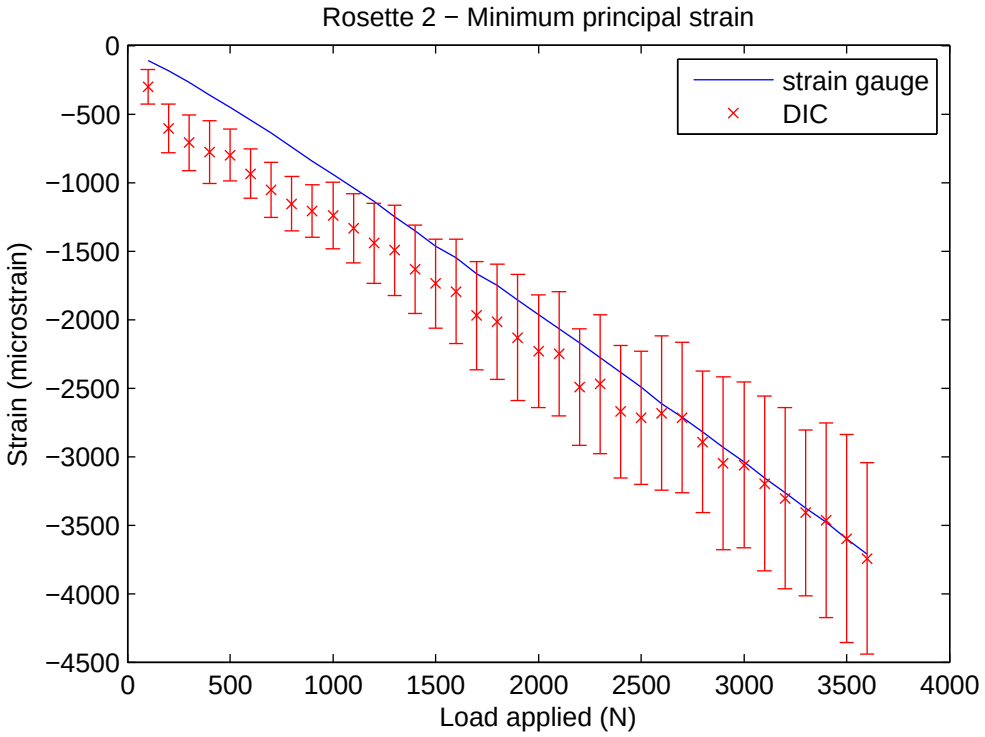

Figure 7.4: Rosette 2 - Minimum principal strain for both techniques

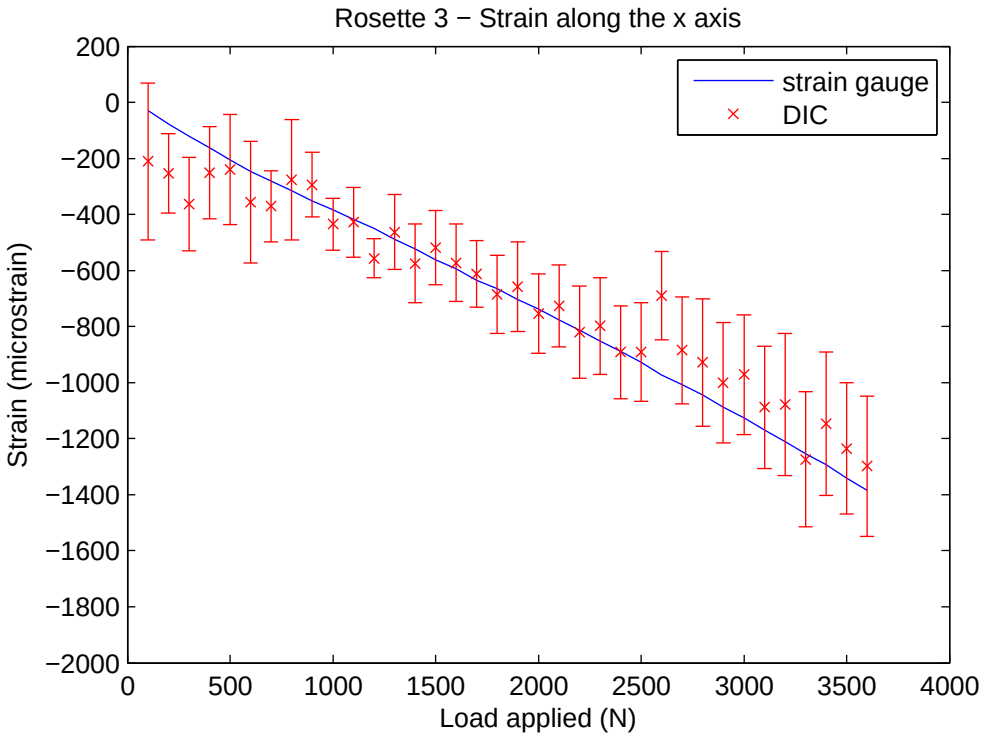

Figure 7.5: Rosette 3 - Strain along the x-axis for both techniques

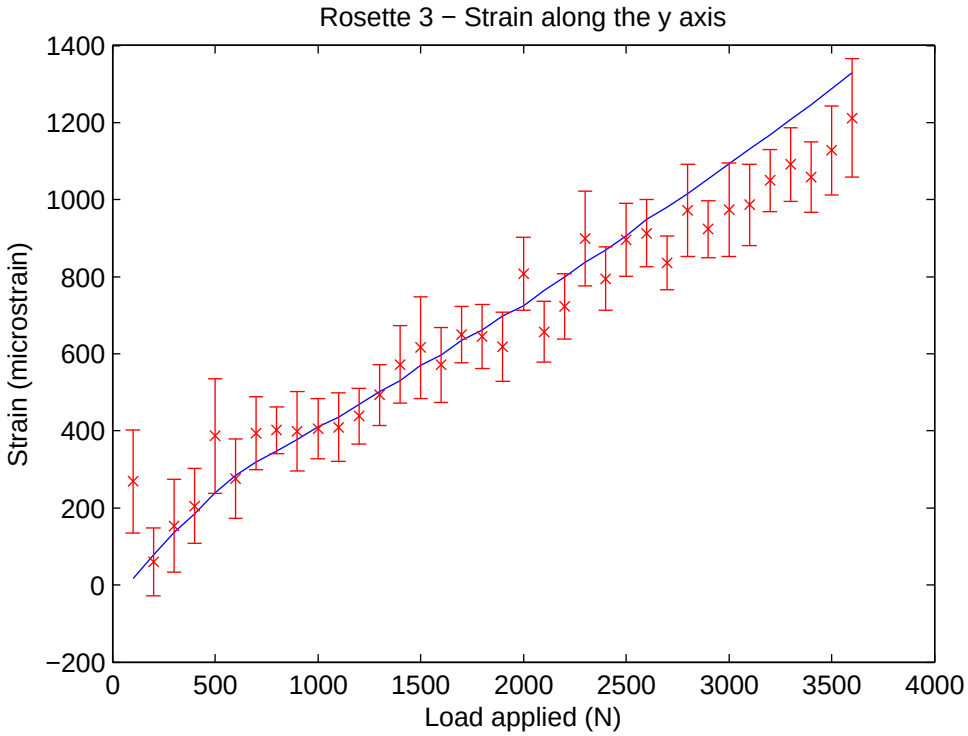

Figure 7.6: Rosette 3 - Strain along the y-axis for both techniques

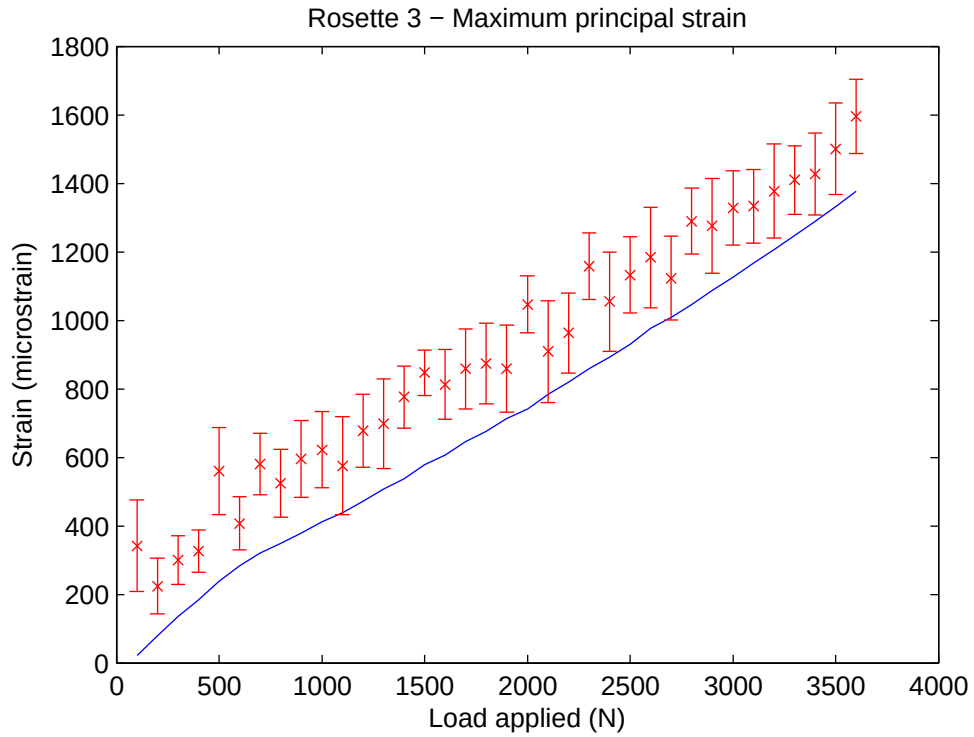

Figure 7.7: Rosette 3 - Maximum principal strain for both techniques

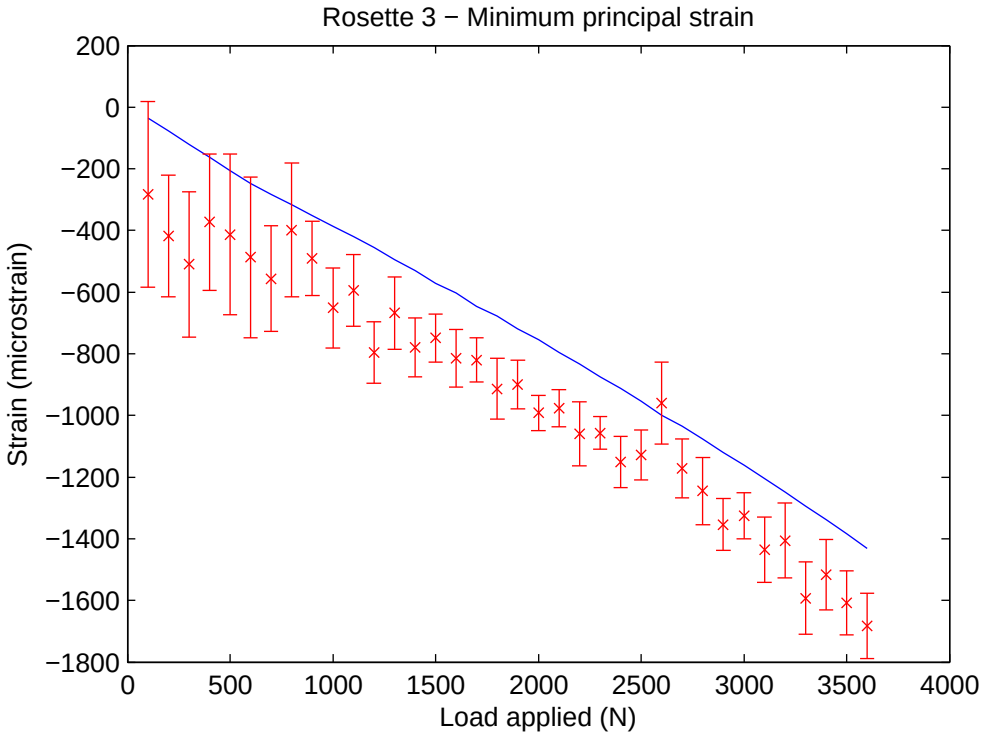

Figure 7.8: Rosette 3 - Minimum principal strain for both techniques

Appendix E - Micromotion and migration calculations along the x, y and z axes (Chapter 4)

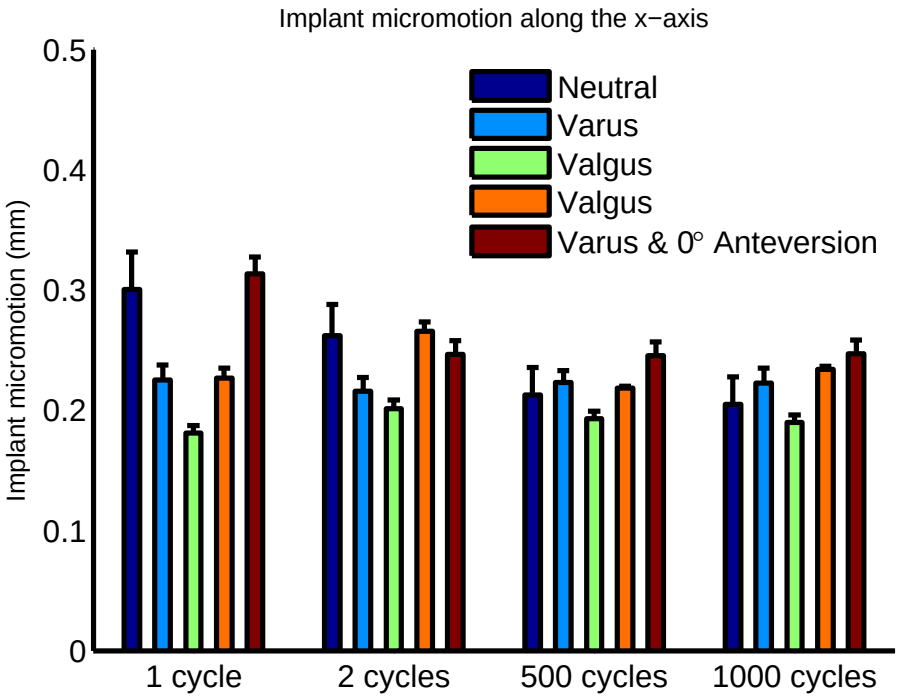

Figure 7.9: Implant migration along the x-axis during the 1st, 2nd, 500th and 1000th cycles for each implanted bone

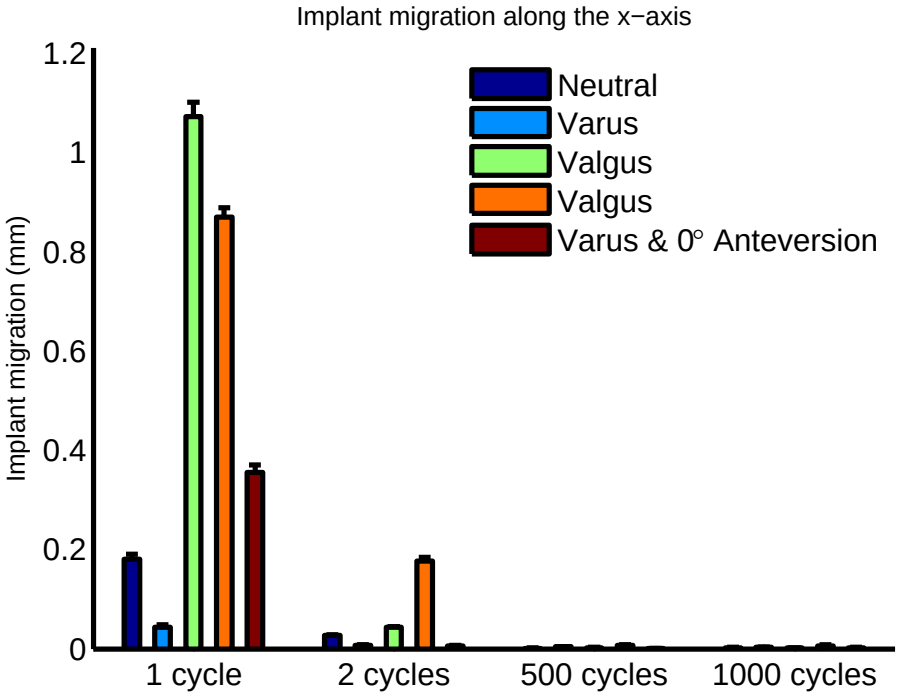

Figure 7.10: Implant migration along the x-axis during the 1st, 2nd, 500th and 1000th cycles for each implanted bone

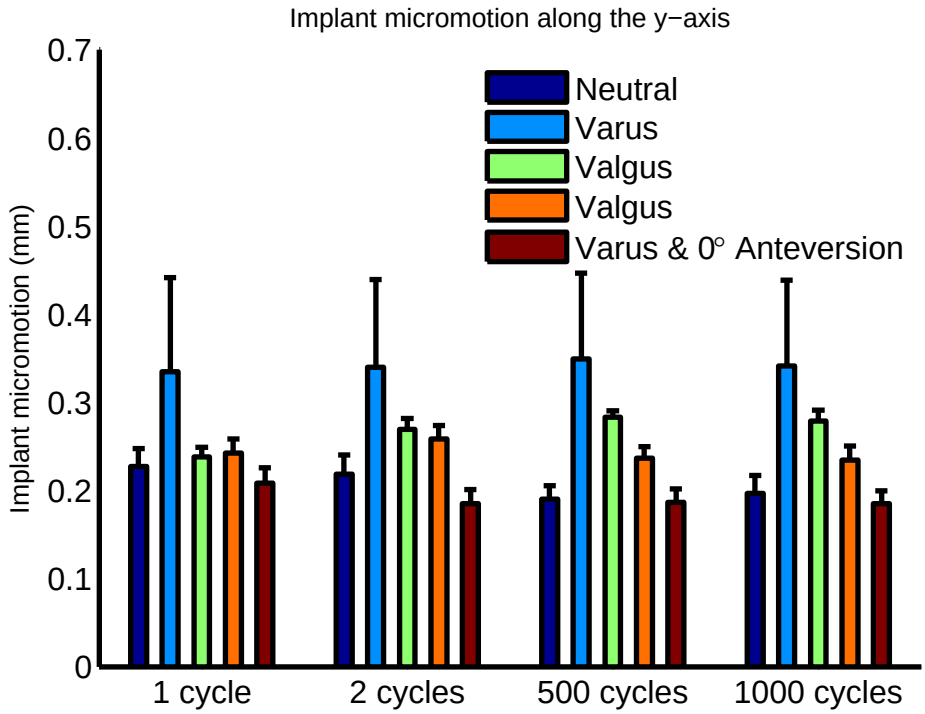

Figure 7.11: Implant migration along the y-axis during the 1st, 2nd, 500th and 1000th cycles for each implanted bone

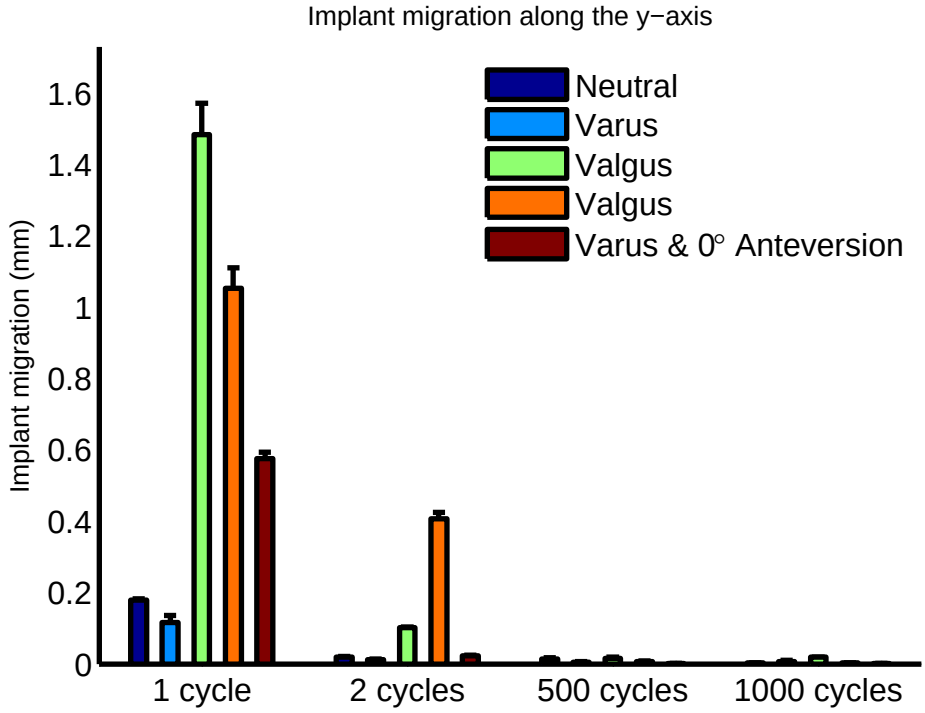

Figure 7.12: Implant migration along the y-axis during the 1st, 2nd, 500th and 1000th cycles for each implanted bone

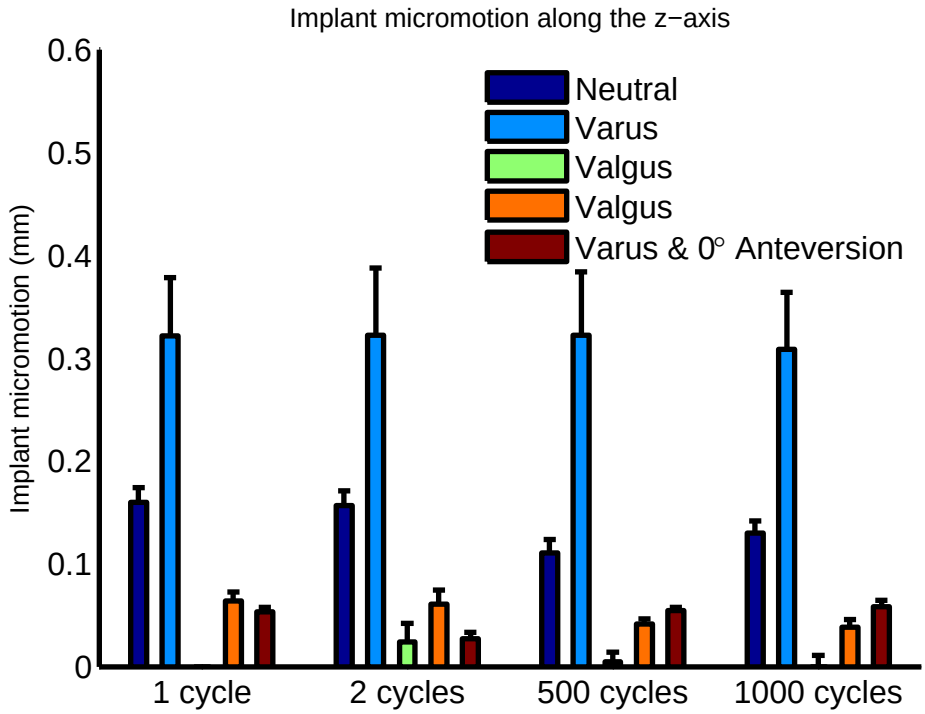

Figure 7.13: Implant migration along the z-axis during the 1st, 2nd, 500th and 1000th cycles for each implanted bone

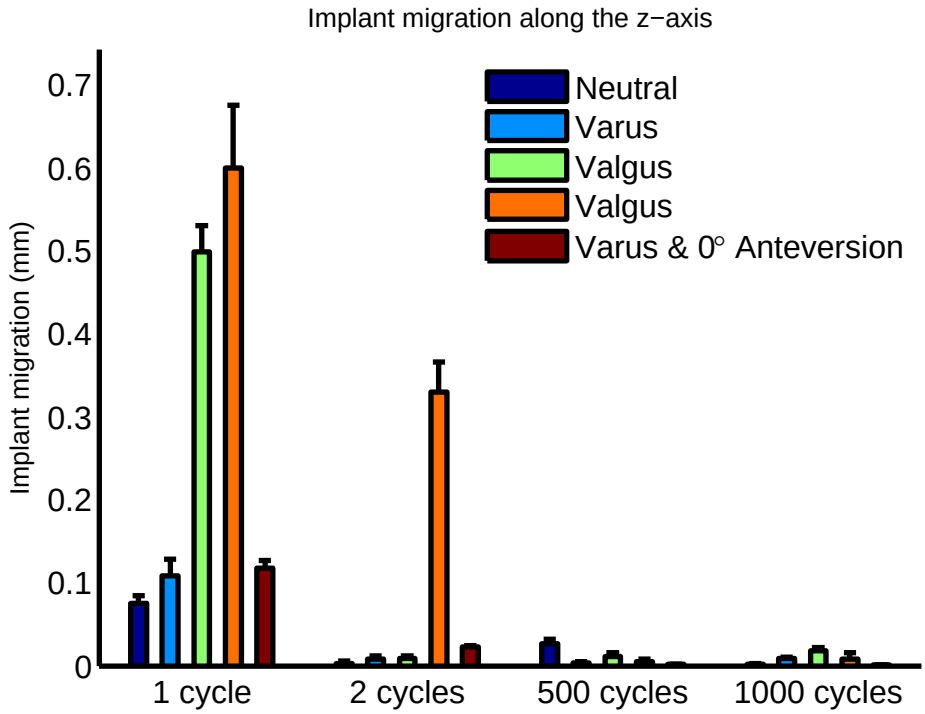

Figure 7.14: Implant migration along the z-axis during the 1st, 2nd, 500th and 1000th cycles for each implanted bone

References

[1] *National Joint Registry for England and Wales - 4th Annual Report.* www.njrcentre.org.uk, 2007.

[2] *The Swedish National Hip Arthroplasty Register - Annual Report 2008.* 2008.

[3] *Canadian Joint Replacement Registry (CJRR) - Hip and Knee Replacements in Canada - 2008-2009 Annual Report.* http://www.cihi.ca, 2009.

[4] *National Joint Registry for England and Wales - 6th Annual Report.* www.njrcentre.org.uk, 2009.

[5] *National Joint Registry for England and Wales - 7th Annual Report.* www.njrcentre.org.uk, 2009.

[6] *Prostheses used in hip and knee replacement procedures - 2008, National Joint Registry for England and Wales - 6th Annual Report.* 2009.

[7] *World Population Prospects: The 2008 Revision, Population Division of the Department of Economic and Social Affairs of the United Nations Secretariat.* 2009.

[8] *Australian Orthopaedic Association (AOA) Annual Report - National joint replacement registry.* http://www.aoa.org.au, 2010.

[9] *Britannica Online Encyclopedia, Search for osteoarthritis.* http://www.britannica.com.

[10] *JRI Website, The Furlong Hydroxy-apatite Ceramic (Supravit) Coated Femoral Stem.* http://www.jri-ltd.co.uk.

[11] M.R. Abdul-Kadir and U. N. Hansen. The effect of physiological load configuration on interface micromotion in cementless femoral stems. *Jurnal Mekanikal*, 23:50–61, 2007.

[12] M.R. Abdul-Kadir, U.N. Hansen, R. Klabunde, D. Lucas, and A. Amis. Finite element modelling of primary hip stem stability: The effect of interference fit. *Journal of Biomechanics*, 41(3):587–594, 2008.

[13] N. Y. Afoke, P. D. Byers, and W. C. Hutton. The incongruous hip joint. a casting study. *Journal of Bone and Joint Surgery Br*, 62-B(4):511–514, 1980.

[14] S. Agarwal. OsteolysisŮbasic science, incidence and diagnosis. *Current Orthopaedics*, 18(3):220–231, 2004.

[15] M.A. Ali Khan, P.H. Brakenbury, and I.S. Reynolds. Dislocation following total hip replacement. *Journal of Bone and Joint Surgery - British Volume*, 63-B(2): 214–218, 1981.

[16] H.C. Amstutz and D. Grigoris. Evolution and future of surface replacement of the hip. *Journal of Orthopaedic Science*, 3(3):169–186, 1998.

[17] L. Andersson, A. Wesslau, H. Boden, and N. Dalen. Immediate or late weight bearing after uncemented total hip arthroplasty: A study of functional recovery. *Journal of Arthroplasty*, 16(8):1063–1065, 2001.

[18] T. Arizono, G. Emoto, and L. A. Whiteside. Initial stability of a cementless femoral component in varus malposition. *45th Annual Meeting, Orthopaedic Research Socety*, 1999.

[19] B.M. Ayyub and G.J. Klir. *Uncertainty modeling and analysis in engineering and the sciences*. CRC Press, 2006.

[20] M.T. Bah and M. Browne. Probabilistic analysis of a cemented hip implant. *International congress on computational bioengineering*, 2003.

[21] M.T. Bah, P.B. Nair, and M. Browne. Mesh morphing for finite element analysis of implant positioning in cementless total hip replacements. *Medical Engineering & Physics*, 69-B(3):374–380, 2009,in press.

[22] M. Baleani, L. Cristofolini, and A. Toni. Initial stability of a new hybrid fixation hip stem: experimental measurement of implant-bone micromotion under torsional load in comparison with cemented and cementless stems. *Journal of biomedical materials research*, 15(50):605–615, 2000.

[23] D. Baraff. Fast contact force computation for nonpenetrating rigid bodies. *Computer Graphics Proceedings, Annual Conference Series*, pages 23–34, 1994.

[24] D.L. Bartel, D.T. Davy, and Keaveny T.M. *Orthopaedic Biomechanics - Mechanics and Design in Musculoskeletal Systems*. Pearson Prentice Hall, 2006.

[25] T. J. Beck, C. B. Ruff, R. A. Shaffer, K. Betsinger, D. W. Trone, and S. K. Brodine. Stress fracture in military recruits: gender differences in muscle and bone susceptibility factors. *Bone*, 27(3):437–444, 2000.

[26] B. A. Behrens, C. J. Wirth, H. Windhagen, I. Nolte, A. Meyer-Lindenberg, and A. Bouguecha. Numerical investigations of stress shielding in total hip prostheses. *Journal Proceedings of the Institution of Mechanical Engineers, Part H: Journal of Engineering in Medicine*, 222(5):593–600, 2008.

[27] G. Bergmann, G. Deuretzbacher, M. Heller, F. Graichen, A. Rohlmann, J. Strauss, and G. N. Duda. Hip contact forces and gait patterns from routine activities. *Journal of Biomechanics*, 34(7):859 – 871, 2001.

[28] M. Bernakiewicz and M. Viceconti. The role of parameter identification in finite element contact analyses with reference to orthopaedic biomechanics applications. *Journal of biomechanics*, 35(1):61–67, 2002.

[29] A. Berzins, D. R. Sumner, T. P. Andriacchi, and J. O. Galante. Stem curvature and load angle influence the initial relative bone-implant motion of cementless femoral stems. *Journal of Orthopaedic Research*, 11(5):758–769, 1993.

[30] M. Bessho, I. Ohnishi, J. Matsuyama, T. Matsumoto, K. Imai, and K. Nakamura. Prediction of strength and strain of the proximal femur by a ct-based finite element method. *Journal of Biomechanics*, 40(8):1745–1753, 2007.

[31] C. Bitsakos, J. Kerner, I. Fisher, and Amis A.A. The effect of muscle loading on the simulation of bone remodelling in the proximal femur. *Journal of Biomechanics*, 38(1), 2005. 133-139.

[32] K. J. Bozic, P. Katz, M. Cisternas, L. Ono, M. D. Ries, and J. Showstack. Hospital resource utilization for primary and revision total hip arthroplasty. *Journal of Bone and Joint Surgery - American Volume*, 87(3):570–576, 2005.

[33] R.A. Brand, C.M. Stanford, and Swan C.C. How do tissues respond and adapt to stresses around a prosthesis? a primer on finite element stress analysis for orthopaedic surgeons. *The Iowa Orthopaedic Journal*, 23:13–22, 2003.

[34] J. R. Britton, L. A. Walsh, and P. J. Prendergast. Mechanical simulation of muscle loading on the proximal femur: analysis of cemented femoral component migration with and without muscle loading. *Clinical Biomechanics*, 18(7):637–646, 2003.

[35] J. R. Britton, C. G. Lyons, and P. J. Prendergast. Measurement of the relative motion between an implant and bone under cyclic loading. *Strain*, 40(4):193Ű202, 2004.

[36] B. D. Browner, Levine A. N., J. B. Jupiter, P. G. Trafton, and C. Krettek. *Skeletal trauma: basic science, management, and reconstruction*, volume 1. Philadelphia, Pa., fourth edition, 2009.

[37] B. Bryan. *Statistical Modelling of the Human Femur*. PhD thesis, University of Southampton - Bioengineering Research Group - School of Engineering Sciences, 2010.

[38] T.M. Buzug. *Computed Tomography: From Photon Statistics to Modern Cone-beam CT*. Springer, 1 edition, 2008.

[39] H.C. Cameron. Essential design considerations for microporous implants: preliminary communication. *Journal of the Royal Society of Medicine*, 74:887–891, 1981.

[40] K. Choi and S.A. Goldstein. A comparison of the fatigue behavior of human trabecular and cortical bone tissue. *Journal of Biomechanics*, 25(12):1371–1381, 1992.

[41] L. Claes, S. Fiedler, M. Ohnmacht, and G. N. Duda. Initial stability of fully and partially cemented femoral stems. *Clinical Biomechanics*, 15(10):750–755, 2000.

[42] A. Completo, F. Fonseca, and J.A. Simões. Experimental validation of intact and implanted distal femur finite element models. *Journal of Biomechanics*, 40 (11):2467–2476, 2007.

[43] L. Cristofolini, M. Viceconti, A. Cappello, and A. Toni. Mechanical validation of whole bone composite femur models. *Journal of Biomechanics*, 29(4):525–535, 1996.

[44] L. Cristofolini, A. S. Teutonico, L. Monti, A. Cappello, and A. Toni. Comparative in vitro study on the long term performance of cemented hip stems: validation of a protocol to discriminate between "good" and "bad" designs. *Journal of Biomechanics*, 36(11):1603–1615, 2003.

[45] L. Cristofolini, P. Erani, P. Savigni, T. Grupp, O. Thies, and M. Viceconti. Increased long-term failure risk associated with excessively thin cement mantle in cemented hip arthroplasty: A comparative in vitro study. *Clinical Biomechanics*, 22(4):410–421, 2007.

[46] L. Cristofolini, A. Saponara Teutonico, P. Savigni, P. Erani, and M. Viceconti. Preclinical assessment of the long-term endurance of cemented hip stems. part 1: Effect of daily activities - a comparison of two load histories. *Proceedings*

of the Institution of Mechanical Engineers, Part H: Journal of Engineering in Medicine, 221(6):569–584, 2007.

[47] J. Daniel, P.B. Pynsent, and D.J. McMinn. Metal-on-metal resurfacing of the hip in patients under the age of 55 years with osteoarthritis. *Journal of Bone and Joint Surgery Br*, 86-B:177–184, 2004.

[48] R. Decking, W. Puhl, U. Simon, and L. E. Claes. Changes in strain distribution of loaded proximal femora caused by different types of cementless femoral stems. *Clinical Biomechanics*, 21(5):495–501, 2006.

[49] A. Devitt, T. O'Sullivan, and W. Quinlan. 16- to 25-year follow-up study of cemented arthroplasty of the hip in patients aged 50 years or younger. *Journal of Arthroplasty*, 12(5):479–489, 1997.

[50] M. Ding. Age variations in the properties of human tibial trabecular bone and cartilage. *Acta Orthopaedica Scandinavica Supplementum*, 292:1–45, 2000.

[51] A. J. Donaldson, H. E. Thomson, N. J. Harper, and N. W. Kenny. Bone cement implantation syndrome. *British Journal of Anaesthesia*, 102(1):12–22, 2009.

[52] C. Dopico-González, A.M. New, and M. Browne. Probabilistic analysis of an uncemented total hip replacement. *Medical Engineering & Physics*, 31(4):470–476, 2009. Finite Element Modelling of Medical Devices.

[53] C. Dopico-González, A.M. New, and M. Browne. Probabilistic finite element analysis of the uncemented hip replacement-effect of femur characteristics and implant design geometry. *Journal of Biomechanics*, 43(3):512–520, 2010.

[54] G.N. Duda, M. Heller, J. Albinger, O. Schulz, E Schneider, and Claes L. Influence of muscle forces on femoral strain distribution. *Journal of Biomechanics*, 31(9): 841–846, 1998.

[55] J. Dumbleton and M.T. Manley. Hydroxyapatite-coated prostheses in total hip and knee arthroplasty. *Journal of Bone and Joint Surgery Am*, 86:2526–2540, 2004.

[56] B. Engfeldt. Recent observations on bone structure. *Journal of Bone and Joint Surgery Am*, 40(3):698–706, 1958.

[57] S.L. Evans, C. A. Holt, H. Ozturk, K. Saidi, and N. G Shrive. Measuring soft tissue properties using digital image correlation and finite element modelling. *International Conference on Experimental Mechanics*, 2007.

[58] M.A. Freeman and P. Plante-Bordeneuve. Early migration and late aseptic failure of proximal femoral prostheses. *Journal of Bone and Joint Surgery - British Volume*, 76-B(3):432–438, 1994.

[59] B. R. Furman and S. Saha. The mechanical properties of bone cement as controlled by processing technique: a critical review of the literature. *Biomedical Engineering Conference, 1997., Proceedings of the 1997 Sixteenth Southern*, pages 301 –304, 1997.

[60] J. Galante, W. Rostoker, R. Lueck, and R.D. Ray. Sintered fiber metal composites as a basis for attachment of implants to bone. *Journal of Bone and Joint Surgery - American Volume*, 53(1):101–114, 1971.

[61] C. J. Good. *Passive osteokinematics motion palpation of the peripheral joints.* Elsevier Health Sciences, 2000.

[62] H.A. Gray, A.B. Zavatsky, F. Taddei, L. Cristofolini, and H.S. Gill. Experimental validation of a finite element model of a composite tibia. *Proceedings of the Institution of Mechanical Engineers, Part H: Journal of Engineering in Medicine*, 221(3):315–324, 2007.

[63] A.G. Gristina and J.W. Costerton. Bacterial adherence to biomaterials and tissue. The significance of its role in clinical sepsis. *Journal of Bone and Joint Surgery - American Volume*, 67(2):264–273, 1985.

[64] M. Grotle, K. Hagen, B. Natvig, F. Dahl, and T. Kvien. Obesity and osteoarthritis in knee, hip and/or hand: An epidemiological study in the general population with 10 years follow-up. *BMC Musculoskeletal Disorders*, 9(1):132, 2008.

[65] D.J. Hart and T.D. Spector. The relationship of obesity, fat distribution and osteoarthritis in women in the general population: the chingford study. *J Rheumatol.*, 20(2):331–335, 1993.

[66] D.N.D. Hartford and G.B. Baecher. *Risk and uncertainty in dam safety.* Thomas Telford, 2004.

[67] P. Harvie, M. Haroon, N. Henderson, and M. El-Guindi. Fracture of the hydroxyapatite-ceramic-coated jri-furlong femoral component. *Journal of Bone and Joint Surgery*, 89B:742–745, 2007.

[68] M. O. Heller, G. Bergmann, G. Deuretzbacher, L. Dürselen, M. Pohl, L. Claes, N. P. Haas, and G. N. Duda. Musculo-skeletal loading conditions at the hip during walking and stair climbing. *Journal of Biomechanics*, 34(7):883 – 893, 2001.

[69] G.J. Hooper, A.G. Rothwell, M. Stringer, and C. Frampton. Revision following cemented and uncemented primary total hip replacement: a seven-year analysis from the new zealand joint registry. *Journal of Bone and Joint Surgery Br*, 91 (4):451–458, 2009.

[70] S. Hoppenfeld, P. DeBoer, and H.A. Thomas. *Surgical Exposures in Orthopaedics: The Anatomic Approach*. Lippincott Williams & Wilkins, 3 edition, 2003.

[71] R. Huiskes and S.J. Hollister. From structure to process, from organ to cell: Recent developments of fe-analysis in orthopaedic biomechanics. *Journal of Biomechanical Engineering*, 115(4B):520–527, 1993.

[72] D. W. Hummel, O. I. Lanz, and S. R. Werre. Complications of the cementless total hip replacement. a retrospective study of 163 cases. *Veterinary and comparative orthopaedics and traumatology*, 23(6):424–432, 2010.

[73] T. Huusko, M. Korpela, P. Karppi, V. Avikainen, H. Kautiainen, and R. Sulkava. Threefold increased risk of hip fractures with rheumatoid arthritis in central finland. *Annals of the Rheumatic Diseases*, 60:521–522, 2001.

[74] R. L. Iman, J. M. Davenport, , and D. K. Zeigler. Latin hypercube sampling (program user's guide). *Technical Report SAND79-1473, Sandia National Laboratories, Albuquerque, NM*, 1980.

[75] G. Jaroszynski, I. Woodgate, K. Saleh, and A. Gross. Total hip replacement for the dislocated hip. *Journal of Bone and Joint Surgery Am*, 83(2):272, 2001.

[76] M. Jasty, C. Bragdon, D. Burke, D. O' Connor, J. Lowenstein, and W.H. (1) Harris. In vivo skeletal responses to porous-surfaced implants subjected to small induced motions. *Journal of bone and joint surgery. American volume*, 79(5): 707–714, 1997.

[77] J.P. Kassi, M. O. Heller, U. Stoeckle, C. Perka, and G. N. Duda. Stair climbing is more critical than walking in pre-clinical assessment of primary stability in cementless tha in vitro. *Journal of Biomechanics*, 38(5):1143–1154, 2005.

[78] O. Kayabasi and B. Ekici. Probabilistic design of a newly designed cemented hip prosthesis using finite element method. *Materials and Design*, 29(5):963–971, 2008.

[79] S. S. Kelley, P. F. Lachiewicz, M. S. Gilbert, M. E. Bolander, and J. J. Jankiewicz. Hip arthroplasty in hemophilic arthropathy. *Journal of Bone and Joint Surgery*, 77(6):828–834, 1995.

[80] S. Kessler and W. Kafer. Overweight and obesity: Two predictors for worse early outcome in total hip replacement? *Obesity*, 15(11):2840–2845, 2007.

[81] H. Kienapfel, C. Sprey, A. Wilke, and P. Griss. Implant fixation by bone ingrowth. *Journal of Arthroplasty*, 14(3):355–368, 1999.

[82] J. Kiss, D. W. Murray, A. R. Turner-Smith, and C. J. Bulstrode. Roentgen stereophotogrammetric analysis for assessing migration of total hip replacement femoral components. *Proc Inst Mech Eng H.*, 209(3):169–75, 1995.

[83] V. Kolachalama, N. Bressloff, and P. Nair. Mining data from hemodynamic simulations via bayesian emulation. *BioMedical Engineering OnLine*, 6(1):47, 2007.

[84] D.L. Kopperdahl and T.M. Keaveny. Yield strain behavior of trabecular bone. *Journal of Biomechanics*, 31(7):601–608, 1998.

[85] P. J. Laz and M. Browne. A review of probabilistic analysis in orthopaedic biomechanics. *Proceedings of the Institution of Mechanical Engineers, Part H: Journal of Engineering in Medicine*, 224(8):927–943, 2010.

[86] P.L. Laz, S. Pal, J.H. Halloran, M.A. Baldwin, Langenderfer J.E., and P.J. Rullkoetter. Probabilistic finite element analysis in orthopaedic biomechanics. *CIMNE*, 2007.

[87] I. M . Lee and D. M. Buchner. The importance of walking to public health. *Medicine & Science in Sports & Exercise*, 40(7 Suppl):512–518, 2008.

[88] T. Q. Lee, D. A. Lewis, S. L. Barnett, W. C. Kim, and S. H. Anzel. Structural integrity of implanted wmt infinity hip and osteonics omnifit hip in fresh cadaveric femurs. *Journal of Biomedical Materials Research*, 39(4):516–523, 1998.

[89] B. Li and R. M. Aspden. Composition and mechanical properties of cancellous bone from the femoral head of patients with osteoporosis or osteoarthritis. *Journal of Bone and Mineral Research*, 12:641–651, 1997.

[90] J.R. Lieberman, D.J. Berry, M.A. Mont, R.K. Aaron, J.J. Callaghan, A. Rayadhyaksha, and J.R. Urbaniak. Osteonecrosis of the hip: management in the twenty-first century. *Journal of Bone and Joint Surgery*, 84:834–853, 2002.

[91] T. Löfqvist, L. Sanzén, C. Petersson, and I. A. Nilsson. Total hip replacement in patients with hemophilia: 13 hips in 11 patients followed for 1-16 years. *Acta Orthopaedica*, 67(4):321–324, 1996.

[92] J. C. Lotz, T. N. Gerhart, and W. C. Hayes. Mechanical properties of metaphyseal bone in the proximal femur. *Journal of Biomechanics*, 24(5):317–325,327–329, 1991.

[93] K. Lundon. *Orthopaedic rehabilitation science: principles for clinical management of bone*. Butterworth-Heinemann, 2000.

[94] S. A. Maher and P. J. Prendergast. Discriminating the loosening behaviour of cemented hip prostheses using measurements of migration and inducible displacement. *Journal of Biomechanics*, 35(2):257 – 265, 2002.

[95] S. A. Maher, P. J. Prendergast, and C. G. Lyons. Measurement of the migration of a cemented hip prosthesis in an in vitro test. *Clinical Biomechanics*, 16(4): 307–314, 2001.

[96] N. N. Mahomed, J. A. Barrett, J. N. Katz, C. B. Phillips, E. Losina, R. A. Lew, E. Guadagnoli, W. H. Harris, R. Poss, and J. A. Baron. Rates and outcomes of primary and revision total hip replacement in the united states medicare population. *Journal of Bone and Joint Surgery - American Volume*, 85(1):27–32, 2003.

[97] K.A. Mann, M.A. Miller, R.J. Cleary, D. Janssen, and N. Verdonschot. Experimental micromechanics of the cementÚbone interface. *Journal of Orthopaedic Research*, 26(6):872–879, 2008.

[98] J.R. McLaughlin and K.R. Lee. The outcome of total hip replacement in obese and non-obese patients at 10- to 18-years. *Journal of Bone and Joint Surgery - British Volume*, 88-B(10):1286–1292, 2006.

[99] S.A. McNally, J.A Sheppard, C.V. Mann, and J.P. Walczak. The results at nine to twelve years of the use of a hydroxyapatite-coated femoral stem. *Journal of Bone and Joint Surgery*, 82B:378–382, 2000.

[100] L. Mehrez. *The application of probabilistic methods for the assessment of hip implant performance*. PhD thesis, University of Southampton - Bioengineering Research Group - School of Engineering Sciences, 2007.

[101] K. M. Moerman, Holt C. A., S. L. Evans, and C. K. Simms. Digital image correlation and finite element modelling as a method to determine mechanical properties of human soft tissue in vivo. *Journal of Biomechanics*, 42(8):1150 – 1153, 2009.

[102] L. Monti, L. Cristofolini, and m. Viceconti. Methods for quantitative analysis of the primary stability in uncemented hip prostheses. *Artificial Organs*, 23(9): 851–859, 1999.

[103] Matthew Moran, P. Walmsley, A. Gray, and I.J. Brenkel. Does body mass index affect the early outcome of primary total hip arthroplasty? *Journal of Arthroplasty*, 20(7):866–869, 2005.

[104] W.R. Myers. Response surface methodology. *Encyclopedia of Biopharmaceutical Statistics*, 2003.

[105] D.P. Nicolella, B.H. Thacker, H. Katoozian, and D.T. Davy. The effect of three-dimensional shape optimization on the probabilistic response of a cemented femoral hip prosthesis. *Journal of Biomechanics*, 39(7):1265–1278, 2006.

[106] R. Nomoto and J. F. McCabe. Effect of mixing methods on the compressive strength of glass ionomer cements. *Journal of Dentistry*, 29(3):205–210, 2001.

[107] A. O' Hagan. Bayesian analysis of computer code outputs: A tutorial. *Reliability Engineering & System Safety*, 91(10-11):1290–1300, 2006.

[108] A. G. Ogston and J. E. Stainer. The physiological function of hyaluronic acid in synovial fluid; viscous, elastic and lubricant properties. *Journal of Physiology*, 119(2-3):244–252, 1953.

[109] B. P. O'Hara, J. P. Urban, and A. Maroudas. Influence of cyclic loading on the nutrition of articular cartilage. *Annals of the Rheumatic Diseases*, 49(7):536–539, 1990.

[110] A.M.J. Olsson and G.E. Sandberg. Latin hypercube sampling for stochastic finite element analysis. *Journal of Engineering Mechanics*, 128(1):121–125, 2002.

[111] J. Orlik, A. Zhurov, and J. Middleton. On the secondary stability of coated cementless hip replacement: parameters that affected interface strength. *Medical Engineering & Physics*, 25(10):825–831, 2003.

[112] N. Palastanga, D. Field, and R. Soames. *Anatomy and human movement : structure and function*, volume 5. Elsevier Ltd, 2006.

[113] A. Pancanti, M. Bernakiewicz, and M. Viceconti. The primary stability of a cementless stem varies between subjects as much as between activities. *Journal of biomechanics*, 36(6):777–785, 2003.

[114] G. Papachristou, P. Hatzigrigoris, K. Panousis, S. Plessas, J. Sourlas, C. Levidiotis, and E. Chronopoulos. Total hip arthroplasty for developmental hip dysplasia. *International Orthopaedics*, 30:21–25, 2006.

[115] M.S. Park, B.W. Choi, S.J. Kim, and J.H. Park. Plasma spray-coated ti femoral component for cementless total hip arthroplasty. *Journal of Arthroplasty*, 18(5): 626–630, 2003.

[116] Y. Park, H. Shin, D. Choi, C. Albert, and Y. S. Yoon. Primary stability of cementless stem in tha improved with reduced interfacial gaps. *Journal of Biomechanical Engineering*, 130(2):021008, 2008.

[117] M. Peacock, K.A. Buckwalter, S. Persohn, T.N. Hangartner, M.J. Econs, and S. Hui. Race and sex differences in bone mineral density and geometry at the femur. *Bone*, In Press, Uncorrected Proof, 2009.

[118] S. H. Pettersen, T. S. Wik, and B. Skallerud. Subject specific finite element analysis of implant stability for a cementless femoral stem. *Clinical Biomechanics*, 24(6):480–487, 2009.

[119] R.M. Pilliar, J.M. Lee, and C. Maniatopoulos. Observations on the effect of movement on bone ingrowth into porous-surfaced implants. *Clin Orthop Rel*, 208:108–113, 1986.

[120] M. H. Pope and J. O. Outwater. Mechanical properties of bone as a function of position and orientation. *Journal of Biomechanics*, 7(1):61–66, 1974.

[121] W. Pospula. Total hip replacement: past, present and future. *Kuwait Medical Journal*, 2004.

[122] R. Poss, F. C. Ewald, W. H. Thomas, and C. B. Sledge. Complications of total hip-replacement arthorplasty in patients with rheumatoid arthritis. *Journal of Bone and Joint Surgery Am*, 58(8):1130–1133, 1976.

[123] P. J. Prendergast. *Orthopaedic prosthesis fixation.* Encyclopaedia of medical devices and instrumentation, 2006.

[124] P. K. Puthumanapully. *Simulation of bone ingrowth into porous surfaces and structures.* PhD thesis, University of Southampton - Bioengineering Research Group - School of Engineering Sciences, 2011.

[125] S. S. Rajaratnam, C. Jack, A. Tavakkolizadeh, M. D. George, R. J. Fletcher, M. Hankins, and J. A. N. Shepperd. Long-term results of a hydroxyapatite-coated femoral component in total hip replacement: A 15- to 21-year follow-up study. *Journal of Bone and Joint Surgery - British Volume*, 90-B(1):27–30, 2008.

[126] A. Ramos and J.A. Simões. Tetrahedral versus hexahedral finite elements in numerical modelling of the proximal femur. *Medical Engineering & Physics*, 28 (9):916 – 924, 2006.

[127] B. Reggiani, L. Cristofolini, E. Varini, and M. Viceconti. Predicting the subject-specific primary stability of cementless implants during pre-operative planning: Preliminary validation of subject-specific finite-element models. *Journal of Biomechanics*, 10(11):2552–2558, 2007.

[128] S. N. Sangiorgio, E. Ebramzadeh, D. B. Longjohn, and L. D. Dorr. Effects of dorsal flanges on fixation of a cemented total hip replacement femoral stem. *Journal of Bone and Joint Surgery Am*, 86(4):813–820, 2004.

[129] E. Schileo, Taddei F., A. Malandrino, L. Cristofolini, and M. Viceconti. Subject-specific finite element models can accurately predict strain levels in long bones. *Journal of Biomechanics*, 40(13):2982 – 2989, 2007.

[130] T. P. Schmalzried and J. Callaghan. Current concepts review - wear in total hip and knee replacements. *Journal of Bone and Joint Surgery Am*, 81(1):115–136, 1999.

[131] N.N. Shah, A.J. Edge, and D.W. Clark. Hydroxyapatite-ceramic-coated femoral components in young patients followed-up for 16 to 19 years. *Journal of Bone and Joint Surgery Ű British Volume*, 91(B):865–869, 2009.

[132] D. J. Simpson, C. J. Brown, A. L. Yettram, P. Procter, and G. J. Andrew. Finite element analysis of intramedullary devices: the effect of the gap between the implant and the bone. *Proceedings of the Institution of Mechanical Engineers, Part H: Journal of Engineering in Medicine*, 222(3):333–345, 2008.

[133] D. J. Simpson, B. J. L. Kendrick, M. Hughes, S. Glyn-Jones, H. S. Gill, G. F. Rushforth, and D. W. Murray. The migration patterns of two versions of the furlong cementless femoral stem: a randomised, controlled trial using radiostereometric analysis. *Journal of Bone and Joint Surgery - British Volume*, 92-B(10): 1356–1362, 2010.

[134] J. Soyer, J. Avedikian, P. Pries, and J.P. Clarac. Long-term outcome of charnleyŠs femoral implant. a review of 309 cases with follow-up of minimum 20. *Revue de chirurgie orthopedique et reparatrice de l'appareil moteur*, 84(5):416–422, 1997.

[135] A. D. Speirs, M. A. Slomczykowski, T. E. Orr, K. Siebenrock, and L. P. Nolte. Three-dimensional measurement of cemented femoral stem stability: an in vitro cadaver study. *Clinical Biomechanics*, 15(4):248–255, 2000.

[136] A. D. Speirs, M. O. Heller, G. N. Duda, and W. R. Taylor. Physiologically based boundary conditions in finite element modelling. *Journal of Biomechanics*, 40 (10):2318 – 2323, 2007.

[137] E. Steen-Hansen, B. Hove, and J. Andresen. Bone mass in patients with rheumatoid arthritis. *Skeletal Radiology*, 16:556–559, 1987.

[138] B. Stickles, L. Phillips, W.T. Brox, B. Owens, and W.L. Lanzer. Defining the relationship between obesity and total joint arthroplasty. *Obesity*, 9(3):219–223, 2001.

[139] J. Stolk, N. Verdonschot, and R. Huiskes. Hip-joint and abductor-muscle forces adequately represent in vivo loading of a cemented total hip reconstruction. *Journal of Biomechanics*, 34(7):917 – 926, 2001.

[140] J. Stolk, N. Verdonschot, L. Cristofolini, A. Toni, and R. Huiskes. Finite element and experimental models of cemented hip joint reconstructions can produce similar bone and cement strains in pre-clinical tests. *Journal of Biomechanics*, 35 (4):499–510, 2002.

[141] P. Sztefek, M. Vanleene, R. Olsson, R. Collinson, A. A. Pitsillides, and S. Shefelbine. Using digital image correlation to determine bone surface strains during loading and after adaptation of the mouse tibia. *Journal of biomechanics*, 43(4): 599–605, 2007.

[142] F. Taddei, A. Pancanti, and M. Viceconti. An improved method for the automatic mapping of computed tomography numbers onto finite element models. *Medical Engineering & Physics*, 26(1):61–69, 2004.

[143] K. Tamari, P. Tinley, K. Briffa, and K. Aoyagi. Ethnic-, gender-, and age-related differences in femorotibial angle, femoral antetorsion, and tibiofibular torsion: Cross-sectional study among healthy japanese and australian caucasians. *Clinical Anatomy*, 19:59–67, 2006.

[144] C.J. Taunt, H. Finn, and P. Baumann. Immediate weight bearing after cementless total hip arthroplasty. *Orthopedics*, 31(3):223, 2008.

[145] S. Tepper and M. C. Hochberg. Factors associated with hip osteoarthritis: Data from the first national health and nutrition examination survey (nhanes-1). *American Journal of Epidemiology*.

[146] M. S. Thompson, H. Schell, J. Lienau, and G. N. Duda. Digital image correlation: a technique for determining local mechanical conditions within early bone callus. *Medical Engineering & Physics*, 29(7):820–823, 2007.

[147] M. Tryba, I. Linde, G. Voshage, and M. Zenz. Histamine release and cardiovascular reactions to implantation of bone cement during total hip replacement. *Anaesthesist*, 40(1):25–32, 1991.

[148] N. Umeda, M. Saito, N. Sugano, K. Ohzono, T. Nishii, T. Sakai, H. Yoshikawa, D. Ikeda, and A. Murakami. Correlation between femoral neck version and strain on the femur after insertion of femoral prosthesis. *Journal of Orthopaedic Science*, 8(3):381–386, 2003.

[149] M. Van Boekel, E. Vossenaar, F. Van Den Hoogen, and W. Van Venrooij. Autoantibody systems in rheumatoid arthritis: specificity, sensitivity and diagnostic value. *Arthritis Research & Therapy*, 4(2):87–93, 2002.

[150] T. P. Van Staa, H. G. Leufkens, L. Abenhaim, B. Zhang, and C. Cooper. Use of oral corticosteroids and risk of fractures. *Journal of Bone and Mineral Research*, 15:993–1000, 2000.

[151] N. Verdonschot, M. Barink, J. Stolk, J. W. M. Gardeniers, and B. W. Schreurs. Do unloading periods affect migration characteristics of cemented femoral components? an in vitro evalutation with the exeter stem. *Acta Orthopaedica Belgica*, 68(4):348–355, 2002.

[152] M. Viceconti, R. Muccini, M. Bernakiewicz, M. Baleani, and L. Cristofolini. Large-sliding contact elements accurately predict levels of bone-implant micromotion relevant to osseointegration. *Journal of Biomechanics*, 33(12):1611–1618, 2000.

[153] M. Viceconti, L. Monti, R. Muccini, M. Bernakiewicz, and A. Toni. Even a thin layer of soft tissue may compromise the primary stability of cementless hip stems. *Clinical Biomechanics*, 16(9):765–775, 2001.

[154] M. Viceconti, S. Ricci, A. Pancanti, and A. Capello. Numerical model to predict the long-term mechanical stability of cementless orthopaedic implants. *Medical & biological engineering & computing*, 42(6):747–753, 2004.

[155] S. Vidyadhara and S.K. Rao. Uncemented primary press-fit total hip arthroplasty: a 3 to 6 years of experience. *Journal of Orthopaedic Surgery*, 15(1): 50–55, 2007.

[156] E.J. Vresilovic, W.J. Hozack, and R.H. Rothman. Radiographic assessment of cementless femoral components: Correlation with intraoperative mechanical stability. *Journal of Arthroplasty*, 9(2):137–141, 1994.

[157] F.M. Westphal, N. Bishop, M. Honl, E. Hille, K. Püschel, and M.M. Morlock. Migration and cyclic motion of a new short-stemmed hip prosthesis-a biomechanical in vitro study. *Clinical Biomechanics*, 21(8):834–840, 2006.

[158] T. O. White and T. W. Dougall. Arthroplasty of the hip: Leg length is not important. *Journal of Bone and Joint Surgery - British Volume*, 84-B(3):335–338, 2002.

[159] L. A. Whiteside and J. C. Easley. The effect of collar and distal stem fixation on micromotion of the femoral stem in uncemented total hip arthroplasty. *Clinical Orthopaedics and Related Research*, 239:145–153, 1989.

[160] G. Woo. *The mathematics of natural catastrophes*. Imperial College Press, 1999.

[161] X. Yuan, L. Ryd, and R. Huiskes. Wear particle diffusion and tissue differentiation in tka implant fibrous interfaces. *Journal of Biomechanics*, 33(10):1279 – 1286, 2000.